Title
DNA Mediated Assembly of Protein Heterodimers on Membrane Surfaces

Author
Coyle, Michael Patrick

Publication Date
2013

Peer reviewed|Thesis/dissertation

DNA-mediated Assembly of Protein Heterodimers on Membrane Surfaces

By

Michael Patrick Coyle

A dissertation submitted in partial satisfaction of the
requirements for the degree of
Doctor of Philosophy
in
Chemistry
in the
Graduate Division
of the
University of California, Berkeley

Committee in charge:
Professor Matthew B. Francis, Co-chair
Professor Jay T. Groves, Co-chair
Professor Gerard Marriott

Spring 2013

DNA-Mediated Assembly of Protein Heterodimers on Membrane Surfaces

By Michael Patrick Coyle

Abstract

DNA-mediated Assembly of Protein Heterodimers on Membrane Surfaces

by

Michael Patrick Coyle

Doctor of Philosophy in Chemistry

University of California, Berkeley

Professors Matthew B. Francis, and Jay T. Groves, Co-chairs

Signal transduction at cell-cell junctions is critical for many biological processes, such as the development of multicellular organisms and the recognition of damaged or infected cells. Such interfaces can be reconstituted *in vitro* by synthetically coupling cell surface ligands to supported membranes, which can be interfaced directly with live cells. The lateral fluidity of these membranes allows ligand receptor complexes to assemble into oligomers and higher order clusters. This type of higher order clustering has been shown to play a role in the regulation and function of various cell membrane receptors. In order to study complex, multicomponent signaling assemblies, I have extended the use of supported membranes and DNA-based protein assembly to form heterodimers of signaling molecules. Characterization of these structures was performed by fluorescence cross-correlation spectroscopy, which confirmed their lateral mobility and the formation of specific heterodimers. I have additionally demonstrated the interaction of these structures with live cells and the modulation of signaling cluster content in these cells. DNA based assembly was also used for the precise positioning of fluorophores at a fixed distance from a gold nanoparticle encased in a viral capsid. These fluorophores were protected from contact quenching, and their fluorescence was enhanced by their proximity to the gold nanoparticle. Together these studies demonstrate the use of DNA hybridization in directing the formation of functional nanoscale assemblies.

Table of Contents

Acknowledgements

There are so many people to thank for helping me get through graduate school in various ways, both in lab and out of lab. In helping with bigger picture advice, Jay and Matt are both terrific advisors. From both, I learned how to think about science, how to write well, and how to present results. Also, perhaps most importantly, they fill their labs with great people with diverse perspectives and knowledge. I'm very grateful that they hired me to work on this project and supported it throughout my time here. I am also grateful to Dave Wemmer and Jan Liphardt, for being great rotation advisers, and to my qualifying exam and thesis committees, which included Carolyn Bertozzi, Jon Ellman, Jamie Cate, and Gerard Marriott. You all provided great feedback, and helped me develop as a scientist.

In lab, I had so much to learn about optics and spectroscopy, and for this I specifically thank Sara, Adam, Chris, Sam Lord, Lee and Wan-chen for helping me learn these skills. Additionally, the other members of the Eph team, Liz and Adrienne, were so helpful with providing experimental advice and help with cell culture. I was also lucky in my second and third years to have a great undergrad, Samantha, work with me. She is very hard working, and picked up knowledge and skills quickly, and I'm sure she's going to be great at being a dentist or dental researcher, or both. I also thank Michel for showing Samantha many cloning and molecular biology techniques while I was preparing for my qualifying exam.

In addition, there were many people with whom I collaborated on various projects. Theo was willing to work together with me in adapting DNA hybridization to functionalize membrane embedded gold nanoparticles, even though the system still had some kinks. Liz and I spent a lot of time studying interactions between EGFR and EphA2, and doing early "designer cluster" experiments. She's a great person to work with and is a great experimentalist. Also, Kanwal, who rotated in the Groves lab, and did a great job working with the HER2 antibody. Thanks also to Jelly for providing us with the plasmid for making this antibody. Meimei, who is a second year, has become the new DNA expert in the lab moved into the West Wing of the Groves lab with me, and is a welcome addition to the Eph project. Finally, Geoff, Rafal, and Jenny have been great to work with in starting up my post-doc work in the Groves lab.

Working with Stacy on the capsid imaging was a great experience. It was a really interesting project, and Stacy is great to work with. I really enjoyed discussing our results, and solving our (many) experimental issues with that system with her. Additionally, I thank the various people in other labs in Stanley who I constantly asked for help. In particular, Mary Anne Kidwell from the Doudna lab was instrumental in solving the mystery of the incomplete heterodimer formation, by pouring several PAGE gels for those experiments. Nick Endres in the Kuriyan lab provided constructs, antibodies and advice for EGFR experiments. Additionally, the Dernberg and Krantz labs on the 4th floor of Stanley provided molecular biology reagents and equipment. Also, the Dernberg lab's sharing of their espresso machine was much appreciated. For synthetic chemistry advice, I thank Leah, Allie, Chris, Adel, and Dan, who always were really willing to share their knowledge. Thanks also to Sonny and the others who laid the foundation of using DNA as an assembly motif. I thank Sonny especially, though, since he helped me with choosing reagents and sequences for the use in the studies presented and directly helped with the Jurkat cell immobilization.

In both groups, I was in large cohorts. In the Francis group, Allie, Amy, Anna, Troy, Dan, Kris-

ten and I joined. In the Groves lab, I was joined by Geoff, Hsiung-Lin, Nicole, Lee and Chris. We went through many grad school milestones together and they provided useful discussion and help with many of them, including thesis writing. I also have to thank many of my lab-mates for being great friends as well. I have some great memories both in and out of lab with Kanna, Amy, Michelle, Allie, Leah, Chris, Gary, Pradeep, Theo, Adrienne, Nicole, Troy, Eulanca, Kate and Geoff.

Outside of the lab I was fortunate to have the best girlfriend I could ever imagine, Abby. She makes me happy every day and is so supportive in every aspect of my life. I was also lucky to have great house-mates during my time here. Back in Jackson House, the first group I lived with, Ryan, Jeff, Tony, Joe, and our neighbor Natalie were great people to live with and helped me get used to life in Berkeley. I appreciate that Joe still is nice enough to cook for Tony and me occasionally, but living in the same house is definitely something I miss. After moving out of Jackson house, I had another great set of house-mates on Rose Street. The first group consisted of Adam, Bill, Dana, Robyn and me. At the time especially, I really appreciated having all of them in my life, and was excited to come home every day. Ashlee, Tony (same one as above) and Emily, who moved in later, are also great friends and housemates. Especially when being so far away from my family, it was really important to have so many friendly and caring people to live with. In addition to my housemates, I'd like to thank John, Sara, Troy, and Ben for being great friends and sharing great times, even when the great times involve camping, which I generally do not like.

My family has been so supportive of me moving so far away from home to pursue my degree. My parents, John and Linda, have been caring and supportive of my education for my entire life, and invested a lot of time, effort, and money into making sure I had a good education, so I definitely would not have been here without them. Monica, my sister, is much younger than me, but was old enough to play tennis with me during trips home and share music with me, so thanks for that, and being the best sister I could hope for.

Francis group tradition dictates that I thank everyone I overlapped with in some way, so thank you Nick, Aaron, Henrik, Kristen, Kareem, Katherine, Jeff, Praveena, Jake, Ioana, Jim, and Richard. Even though I didn't mention you specifically above, I appreciated all of you in individual ways, and you're all great to work with.

Finally, for administrative help, I thank Laurie, Chona, Adele, and Carisa. Especially Laurie, who most directly deals with my orders, travel, and salary, is so helpful to me, and I'm really appreciative of how well she does her job and keeps the lab running.

Chapter 1: Introduction

Section 1.1: Signaling at cell-cell junctions and reconstituting these junctions with supported membranes

Multicellular eukaryotic organisms can contain trillions of cells and an even greater number of cell-cell junctions. These junctions are critical to animal development,[1–5] the recognition of infected or damaged cells,[6–8] and can be misregulated during cancer progression.[9] Because cell-cell interfaces are poorly mixed and heterogenous, they are difficult to study by classical biochemical techniques and difficult to evaluate quantitatively assuming only solution phase reactions. Despite these challenges, the molecular mechanisms and biochemical characterization of these systems have, in many cases, been thoroughly deciphered. Significant effort is now directed toward connecting these biochemical events to cellular function. In the case of immune recognition, the T-cell receptor (TCR) is sensitive to very low numbers of antigenic peptide,[10,11] which leads to the acquired immune response despite the weak binding constants and fast dissociation kinetics of the molecules involved.[12] Eph receptors have well-defined roles in development and are overexpressed in a variety of tumor types. Still, their role in cancer progression is puzzling, since they have both oncogenic and tumor suppressing properties.[9,13] This suggests that the cellular or environmental context is particular important to the biological outcome of their function.

Recent progress has been made in understanding these systems through the use of supported phospholipid membranes, which can facilitate the reconstitution and manipulation these juxtacrine signaling junctions.[10,12,14–22] With this technique, protein ligands present on a cell surface are synthetically linked to the supported membrane. The lateral mobility of the membrane mimics that of the cell surface and allows the ligands to engage their receptors and assemble into functional clusters. The glass substrates and bilayers can be modified by a variety of means to alter the nature of the ligands presented to cells. For instance, lithographically defined diffusion barriers[23] disrupt pattern formation at the hybrid substrate-cell junction,[15,17] restricting the size of ligand-receptor clusters,[10,24] and frustrating directed transport of receptors.[18,25] The mobility of membrane anchored ligands can be altered by varying the lipid composition used to form the membrane.[17,26,27]

These studies have allowed researchers to understand the important parameters that govern biochemical behavior at these interfaces. Early studies of TCR activation from supported membranes reproduced formation of the "immunological synapse," a bulls-eye like pattern with TCR at the center and adhesion molecules in the surrounding area.[7,14] The synapse was thought to be critical for sustained signaling from TCR and lymphocyte activation.[14] However, further studies revealed that the synapse actually downregulated TCR activation, since diffusion barriers that prevented its formation resulted in sustained calcium signaling.[15]

TCR activation is a rare example of a system that has been extensively investigated by a variety of research groups using supported membranes. Studies of other systems include EphA2-ephrinA1 signaling and activation of cells in the immune system. In the EphA2 system, both actin morphology and downstream signaling were measured to be affected by diffusion barriers in the ephrinA1-bearing supported membrane.[17,28] Mast cells were found to be efficiently stimulated by membrane bound epitopes, even though these same monomeric epitopes would not stimulate these cells when presented in solution.[29] Studies of membrane anchored soluble ligands have also been performed, mostly in the case of epidermal growth factor receptor (EGFR) signaling. Even though the term "juxtacrine" was coined in reference to pro-TGF-α stimulation of EGFR,[30] EGFR stimulation studies are typically performed by stimulation with the soluble ligand, epidermal growth factor (EGF),[31–35] which functions in autocrine or paracrine signaling. Investigators have probed certain mechanistic questions using supported membranes, specifically focusing on the force generated by the cell when interacting with surface bound EGF,[36] the effect of cluster/oligomer size on EGFR phosphorylation,[24] and the effect of bilayer mobility and kinase activity on EGF mediated adhesion.[26]

Section 1.2: Oligomerization in signal transduction

Signal transduction in the systems mentioned above and many others is propagated by receptor binding events, which directly cause conformational changes in the receptor protein. These changes can lead to oligomerization and/or receptor phosphorylation. The phosphorylated receptor can recruit additional molecules to form complexes that propagate signal transduction. Many examples demonstrate that oligomerization is sufficient to trigger downstream signaling in a variety of systems. For example, antibody crosslinking of the TCR ζ-chain stimulates TCR downstream signaling,[37–40] while Fab fragment binding does not.[12,41] Fusing a membrane-linked CD3-ζ chain to a protein that binds strongly to the small molecule FK506 allows downstream activation to proceed upon stimulation by FK1012, which is essentially a dimer of FK506 and cross-links the engineered ζ-chain.[42] Eph receptors are often reported to require preclustered ligand for stimulation in solution,[43] and some extracellular domain antibodies can stimulate tyrosine phosphorylation of the receptors.[44,45] (It should be noted that some controversy exists over the necessity of preclustering from recent studies,[46,47] but the stimulation by antibody crosslinking demonstrates that oligomerization plays at least some role in the function of the receptors.) EGFR family receptors undergo ligand induced dimerization,[48–50] but the increase in local concentration from overexpression in cells[31] or vesicle tethering of the kinase domain *in vitro*[51] increases activation. Additionally, chemical aggregating agents or antibodies that target the EGFR kinase or juxtamembrane domain can induce kinase activity *in vitro*.[52]

These observations suggest that oligomerization can play a role in regulation of signal transduction. The mechanism by which this regulation occurs is unclear, however, and it is likely not conserved among all signaling pathways. In eukaryotic MAP kinase signaling, scaffold proteins provide both allosteric stimulation of kinases and induce proximity in kinases therefore directing their specificity.[53] Bacterial histidine kinases, however, exhibit high substrate specificity for their protein targets and are not likely to require such mechanisms.[54]

Recent work suggests that membrane proteins may employ mechanisms similar to those in MAPK signaling. Human epidermal growth factor family (HER) receptors are often reported

to heterodimerize,[55] which can result in cross-activation of receptors with purified kinase domains *in vitro* and allows signal propagation from the kinase-dead receptor HER3.[56] Observations of heterodimerization between GPCRs have led to hypotheses that they provide additional levels of regulation and potential roles for "orphan" GPCRs (which do not have known agonists).[57] Eph receptors have been observed to interact functionally with EGFR family receptors,[58–60] other members in the Eph family,[61] and other membrane receptors.[62,63] Additionally, EphA receptors recruit a transmembrane metalloprotease upon kinase stimulation,[64–66] a process that is possibly mechanosensitive.[17]

Section 1.3: Biomolecule conjugation to supported membranes

Various bioconjugation methods have been used to link proteins and other biomolecules to supported membranes.[22] The natural ability of cells to lipidate proteins can be exploited by GPI-tagging of proteins with glycophosphatidylinositol (GPI) during recombinant expression, which can incorporate into liposomes. These proteoliposomes can be used to form protein functionalized supported membranes, but these membranes often suffer from a high density of defects and the presence of unruptured vesicles.[22] Acylation of lysine residues with biotin allows a wide variety of molecules to be linked.[17,24,26,27] Michael addition to maleimide groups can be used for site selective covalent conjugation of proteins with a surface accessible cysteine to membranes displaying maleimides.[22,67] Nickel chelation is very commonly used as an alternative, since transition metal-chelating decahistidine tags can be genetically introduced into most proteins.[68]

For proteins of commercial origin, the biotin-streptavidin interaction is especially useful since it does not require genetic modification of the proteins of interest, but lysine acylation with amine reactive biotin moieties does not permit proteins to be anchored with defined orientation. Biotin can be introduced site selectively by conjugation to genetically introduced cysteine residues, but a protein with a reactive cysteine could easily be conjugated to maleimide phospholipids directly. Exploring enzyme-based site selective techniques to introduce biotin[69] would be beneficial and this technique has been used for surface immobilization,[70] but has not been explored for use with membranes. Nickel chelation allows functionalization of a membrane with proteins of interest in a defined orientation over a wide range of surface densities,[68] even with sub-micromolar protein incubation concentrations.

More exotic site selective bioconjugation approaches have been sparsely explored. Alkylation of tyrosine residues with π-alkyl palladium complexes resulted in successful incorporation of conjugates into liposomes,[71] but the high abundance of tyrosine on the surface of proteins limits this approach's applicability to larger proteins. Ligation of GPI tails to intein fusion proteins has been demonstrated,[72] but only for proteins expressed in bacteria. Many cell surface proteins contain posttranslational modifications and are expressed with maximal retention of function and solubility in eukaryotic systems. Expression in these systems results in exposure of the protein to physiological temperatures and thiol containing molecules for several days, which could result in cleavage of the intein moiety. These potential issues initially directed researchers away from these approaches, but recent studies employed native chemical ligation to fuse the intra- and extracellular domains of the EphA4 receptor.[73,74] The extraceullar domain contains post-translational modifications and was expressed as a secreted protein from both a baculovirus/Sf9 cell expression system and HEK293T expression

system. The yield, purity and reactivity of proteins expressed in the insect cell system was reported to be considerably higher, but optimization of the intein to prevent disulfide scrambling was still required.[74,75]

DNA molecules have been introduced into liposomes and supported membranes by various chemical methods. Disulfide exchange has been used to link thiol-DNA to thiolate bearing liposomes, but with low yield.[76] Linking DNA to long alkyl chains during solid phase DNA synthesis allows higher yield incorporation.[77,78] This synthetic approach has been used for studies of DNA mediated vesicle fusion,[78–80] the formation of tethered membranes,[78,81–83] and the incorporation of DNA into live cell membranes.[84]

We saw these studies as promising for the functionalization of supported membranes with proteins as well. Despite the considerable synthetic challenge of site selective attachment of proteins to other macromolecules (such as DNA oligonucleotides), a variety of approaches have been developed for this purpose. Cysteine-maleimide addition has been employed linking enhanced yellow fluorescent protein (YFP) to DNA,[85] but this method would be of limited applicability due to the difficulty of introducing reactive cysteines into secreted proteins.

We identified several new approaches as especially promising, since both applications required reactions to proceed at very low concentrations. An artificial amino acid based approach has been used for the attachment of DNA aptamers to viral capsid based carriers.[86] Expressed protein ligation of intein fusion proteins with cysteine bearing oligonucleotides has been used for microarray immobilization.[87] Single turnover enzyme tag approaches have been demonstrated for the immobilization of proteins[70] and the assembly of proteins on DNA origami structures.[88]

Section 1.4: Methods to direct protein oligomerization

Several methods have been reported and used in the literature to direct or manipulate the oligomeric state of proteins. For directing homotypic interactions, antibodies (which have two binding sites per molecule) have often been employed. As mentioned above, antibody-induced crosslinking of EGFR kinase domains resulted in *trans*-phosphorylation *in vitro*.[52] Treating live T-cells with cross-linking antibodies that bind membrane receptors has offered evidence that cluster size is a mechanism by which molecules are sorted into the immunological synapse.[16] While bivalent antibodies could be used to direct heterotypic interactions, they have scarcely been employed for this purpose. When they have,[89–91] they are typically employed for the purpose of therapeutic benefit to recruit immune cells to cancer biomarkers or to target tumor cells with multiple biomarkers.[92–94] Still, the effect of oligomeric state of protein targets has, in many of these cases, not been evaluated, and these systems have not been used to investigate the effect of oligomeric state on downstream signaling.

Small molecule approaches have been more widely used. As mentioned above, the small molecule FK506 is cell permeable and binds its cellular target, FKBP, with high affinity.[95] The domain of this protein that binds the small molecule can be fused with a protein of interest so that a bifunctional small molecule, FK1012, will trigger oligomerization. This approach has demonstrated that cross-linking in such a way can bypass extracellular activation.[42] Hetero-oligomeric interactions have been induced using similar approaches. The most common uses rapamycin, a small molecule that can bind two targets, or rapamycin derivatives that

link fusion proteins engineered with rapamycin binding sites.[96,97] These approaches have been successful in providing a route to chemically inducible control of heterodimerization.

While small molecule mediated methods allow the rapid and controllable induction of dimerization, optical triggering promises the addition of spatial control as well. Several methods to this end have been reported, mostly based on light sensitive proteins in plants. One example uses proteins from *Arabidopsis thaliana* that can be directed to interact or dissociate by different wavelengths of infrared light. When engineered into the cytoskeleton controlling Rho-family GTPase network in mammalian cells, this system can be used to direct cell morphology.[98]

Section 1.5: Motivation for DNA based assembly of heterodimers on supported membranes

We are primarily interested in studying signaling systems that are naturally found at cell-cell interfaces. As mentioned above, receptors that function at these junctions often are found in higher order oligomers upon activation by ligand.[99–101] Studies in EGFR[48,55,56,102] and Eph[61,62,103,104] families of receptor tyrosine kinases suggest that dimerization can exert additional layers of regulation or perhaps lead to additional receptor functions.

Increasing numbers of therapeutic bispecific antibodies under development and entering clinical trials[92,93] suggest that it may be possible to modulate signaling cluster content with therapeutic benefit. To study complex, multicomponent signaling clusters, we intended to extend the use of supported membranes and DNA based protein assembly.[88,105–110]

Section 1.6: Chapter 1 references

(1) Irvine, K. D.; Rauskolb, C. *Annual review of cell and developmental biology* **2001**, *17*, 189–214.
(2) Brachmann, R.; Lindquist, P. B.; Nagashima, M.; Kohr, W.; Lipari, T.; Napier, M.; Derynck, R. *Cell* **1989**, *56*, 691–700.
(3) Flanagan, J.; Vanderhaeghen, P. *Annual Review of Neuroscience* **1998**, *21*, 309–345.
(4) Wilkinson, D. G. *Nature reviews. Neuroscience* **2001**, *2*, 155–64.
(5) Anklesaria, P.; Teixidó, J.; Laiho, M.; Pierce, J. H.; Greenberger, J. S.; Massagué, J. *Proceedings of the National Academy of Sciences of the United States of America* **1990**, *87*, 3289–93.
(6) Watts, T. H.; Gaub, H. E.; McConnell, H. M. *Nature* **1986**, *320*, 179–81.
(7) Monks, C. R.; Freiberg, B. A.; Kupfer, H.; Sciaky, N.; Kupfer, A. *Nature* **1998**, *395*, 82–6.
(8) Dustin, M. L.; Groves, J. T. *Annual review of biophysics* **2012**, *41*, 543–56.
(9) Pasquale, E. B. *Nature reviews. Cancer* **2010**, *10*, 165–80.
(10) Manz, B. N.; Jackson, B. L.; Petit, R. S.; Dustin, M. L.; Groves, J. T. *Proceedings of the National Academy of Sciences of the United States of America* **2011**, *108*, 9089–94.
(11) Sykulev, Y.; Joo, M.; Vturina, I.; Tsomides, T. J.; Eisen, H. N. *Immunity* **1996**, *4*, 565–71.
(12) Huppa, J. B.; Axmann, M.; Mörtelmaier, M. A.; Lillemeier, B. F.; Newell, E. W.; Brameshuber, M.; Klein, L. O.; Schütz, G. J.; Davis, M. M. *Nature* **2010**, *463*, 963–7.
(13) Kaenel, P.; Mosimann, M.; Andres, A.-C. *Cell Adhesion & Migration* **2012**, *6*, 138–147.

(14) Grakoui, A.; Bromley, S. K.; Sumen, C.; Davis, M. M.; Shaw, A. S.; Allen, P. M.; Dustin, M. L. *Science* **1999**, *285*, 221–7.
(15) Mossman, K. D.; Campi, G.; Groves, J. T.; Dustin, M. L. *Science* **2005**, *310*, 1191–3.
(16) Hartman, N. C.; Nye, J. A.; Groves, J. T. *Proceedings of the National Academy of Sciences of the United States of America* **2009**, *106*, 12729–34.
(17) Salaita, K.; Nair, P. M.; Petit, R. S.; Neve, R. M.; Das, D.; Gray, J. W.; Groves, J. T. *Science* **2010**, *327*, 1380–5.
(18) DeMond, A. L.; Mossman, K. D.; Starr, T.; Dustin, M. L.; Groves, J. T. *Biophysical journal* **2008**, *94*, 3286–92.
(19) Dustin, M. L. *Journal of structural biology* **2009**, *168*, 152–60.
(20) Yu, Y.; Fay, N. C.; Smoligovets, A. A.; Wu, H.-J.; Groves, J. T. *PLoS ONE* **2012**, *7*, e30704.
(21) Cemerski, S.; Das, J.; Giurisato, E.; Markiewicz, M. a; Allen, P. M.; Chakraborty, A. K.; Shaw, A. S. *Immunity* **2008**, *29*, 414–22.
(22) Lin, W. C.; Yu, C.; Triffo, S.; Groves, J. T. *Current Protocols in Chemical Biology* **2010**, *2*, 235–269.
(23) Groves, J. T.; Boxer, S. G. *Accounts of chemical research* **2002**, *35*, 149–57.
(24) Stabley, D.; Retterer, S.; Marshall, S.; Salaita, K. *Integrative biology* **2013**.
(25) Yu, C.; Wu, H.-J.; Kaizuka, Y.; Vale, R. D.; Groves, J. T. *PLoS ONE* **2010**, *5*, e11878.
(26) Nam, J.-M.; Nair, P. M.; Neve, R. M.; Gray, J. W.; Groves, J. T. *ChemBioChem* **2006**, *7*, 436–40.
(27) Hsu, C.-J.; Hsieh, W.-T.; Waldman, A.; Clarke, F.; Huseby, E. S.; Burkhardt, J. K.; Baumgart, T. *PloS one* **2012**, *7*, e32398.
(28) Xu, Q.; Lin, W.-C.; Petit, R. S.; Groves, J. T. *Biophysical journal* **2011**, *101*, 2731–9.
(29) Carroll-Portillo, A.; Surviladze, Z.; Cambi, A.; Lidke, D. S.; Wilson, B. S. *Frontiers in immunology* **2012**, *3*, 46.
(30) Massague, J. *J Biol Chem* **1990**, *265*, 21393–21396.
(31) Endres, N. F.; Das, R.; Smith, A. W.; Arkhipov, A.; Kovacs, E.; Huang, Y.; Pelton, J. G.; Shan, Y.; Shaw, D. E.; Wemmer, D. E.; Groves, J. T.; Kuriyan, J. *Cell* **2013**, *152*, 543–556.
(32) Chung, I.; Akita, R.; Vandlen, R.; Toomre, D.; Schlessinger, J.; Mellman, I. *Nature* **2010**, *464*, 783–787.
(33) Saffarian, S.; Li, Y.; Elson, E. L.; Pike, L. J. *Biophysical journal* **2007**, *93*, 1021–31.
(34) Macdonald, J. L.; Pike, L. J. *Proceedings of the National Academy of Sciences of the United States of America* **2008**, *105*, 112–7.
(35) Ozcan, F.; Klein, P.; Lemmon, M. a; Lax, I.; Schlessinger, J. *Proceedings of the National Academy of Sciences of the United States of America* **2006**, *103*, 5735–40.
(36) Stabley, D. R.; Jurchenko, C.; Marshall, S. S.; Salaita, K. S. *Nature methods* **2012**, *9*, 64–7.
(37) Romeo, C.; Seed, B. *Cell* **1991**, *64*, 1037–1046.
(38) Irving, B. A.; Weiss, A. *Cell* **1991**, *64*, 891–901.
(39) Letourneur, F.; Klausner, R. D. *Proceedings of the National Academy of Sciences of the United States of America* **1991**, *88*, 8905–9.
(40) Kubo, R.; Born, W.; Kappler, J.; Marrack, P.; Pigeon, M. *J. Immunol.* **1989**, *142*, 2736–2742.
(41) Johnson, K. G.; Bromley, S. K.; Dustin, M. L.; Thomas, M. L. *Proceedings of the National Academy of Sciences* **2000**, *97*, 10138–10143.
(42) Spencer, D. M.; Wandless, T. J.; Schreiber, S. L.; Crabtree, G. R. *Science* **1993**, *262*,

1019–1024.
(43) Davis, S.; Gale, N. W.; Aldrich, T. H.; Maisonpierre, P. C.; Pawson, T.; Goldfarb, M.; Yancopoulos, G. D. *Science* **1994**, *266*, 816–819.
(44) Carles-Kinch, K.; Kilpatrick, K. E.; Stewart, J. C.; Kinch, M. S. *Cancer Res.* **2002**, *62*, 2840–2847.
(45) Vearing, C.; Lee, F.-T.; Wimmer-Kleikamp, S.; Spirkoska, V.; To, C.; Stylianou, C.; Spanevello, M.; Brechbiel, M.; Boyd, A. W.; Scott, A. M.; Lackmann, M. *Cancer research* **2005**, *65*, 6745–54.
(46) Wykosky, J.; Palma, E.; Gibo, D. M.; Ringler, S.; Turner, C. P.; Debinski, W. *Oncogene* **2008**, *27*, 7260–73.
(47) Lema Tomé, C. M.; Palma, E.; Ferluga, S.; Lowther, W. T.; Hantgan, R.; Wykosky, J.; Debinski, W. *The Journal of biological chemistry* **2012**, *287*, 14012–22.
(48) Lemmon, M. A. *Experimental cell research* **2009**, *315*, 638–48.
(49) Lemmon, M. A.; Schlessinger, J. *Cell* **2010**, *141*, 1117–34.
(50) Yarden, Y.; Schlessinger, J. *Biochemistry* **1987**, *26*, 1443–1451.
(51) Zhang, X.; Gureasko, J.; Shen, K.; Cole, P. A.; Kuriyan, J. *Cell* **2006**, *125*, 1137–49.
(52) Mohammadi, M.; Honegger, A.; Sorokin, A.; Ullrich, A.; Schlessinger, J.; Hurwitz, D. R. *Biochemistry* **1993**, *32*, 8742–8748.
(53) Won, A. P.; Garbarino, J. E.; Lim, W. A. *Proceedings of the National Academy of Sciences of the United States of America* **2011**, *108*, 9809–14.
(54) Laub, M. T.; Goulian, M. *Annual review of genetics* **2007**, *41*, 121–45.
(55) Yarden, Y.; Sliwkowski, M. X. *Nature Reviews Molecular Cell Biology* **2001**, *2*, 127–37.
(56) Jura, N.; Shan, Y.; Cao, X.; Shaw, D. E.; Kuriyan, J. *Proceedings of the National Academy of Sciences of the United States of America* **2009**, *106*, 21608–13.
(57) Levoye, A.; Dam, J.; Ayoub, M. A.; Guillaume, J.-L.; Jockers, R. *EMBO reports* **2006**, *7*, 1094–8.
(58) Larsen, A. B.; Pedersen, M. W.; Stockhausen, M.-T.; Grandal, M. V.; Van Deurs, B.; Poulsen, H. S. *Molecular cancer research* **2007**, *5*, 283–93.
(59) Zhuang, G.; Brantley-Sieders, D. M.; Vaught, D.; Yu, J.; Xie, L.; Wells, S.; Jackson, D.; Muraoka-Cook, R.; Arteaga, C.; Chen, J. *Cancer research* **2010**, *70*, 299–308.
(60) Brantley-Sieders, D. M.; Zhuang, G.; Hicks, D.; Fang, W. Bin; Hwang, Y.; Cates, J. M. M.; Coffman, K.; Jackson, D.; Bruckheimer, E.; Muraoka-Cook, R. S.; Chen, J. *The Journal of clinical investigation* **2008**, *118*, 64–78.
(61) Janes, P. W.; Griesshaber, B.; Atapattu, L.; Nievergall, E.; Hii, L. L.; Mensinga, A.; Chheang, C.; Day, B. W.; Boyd, A. W.; Bastiaens, P. I.; Jørgensen, C.; Pawson, T.; Lackmann, M. *The Journal of cell biology* **2011**, *195*, 1033–45.
(62) Janes, P. W.; Nievergall, E.; Lackmann, M. *Seminars in cell & developmental biology* **2012**, *23*, 43–50.
(63) Yokote, H. *Proceedings of the National Academy of Sciences* **2005**, *102*, 18866–18871.
(64) Janes, P. W.; Saha, N.; Barton, W. A.; Kolev, M. V.; Wimmer-Kleikamp, S. H.; Nievergall, E.; Blobel, C. P.; Himanen, J.-P.; Lackmann, M.; Nikolov, D. B. *Cell* **2005**, *123*, 291–304.
(65) Janes, P. W.; Wimmer-Kleikamp, S. H.; Frangakis, A. S.; Treble, K.; Griesshaber, B.; Sabet, O.; Grabenbauer, M.; Ting, A. Y.; Saftig, P.; Bastiaens, P. I.; Lackmann, M. *PLoS biology* **2009**, *7*, e1000215.
(66) Hattori, M.; Osterfield, M.; Flanagan, J. *Science Signaling* **2000**, *289*, 1360–1365.

(67) Gureasko, J.; Galush, W. J.; Boykevisch, S.; Sondermann, H.; Bar-Sagi, D.; Groves, J. T.; Kuriyan, J. *Nature structural & molecular biology* **2008**, *15*, 452–61.
(68) Nye, J. A.; Groves, J. T. *Langmuir* **2008**, *24*, 4145–9.
(69) Duffy, S.; Tsao, K. L.; Waugh, D. S. *Analytical biochemistry* **1998**, *262*, 122–8.
(70) Jongsma, M. A.; Litjens, R. H. G. M. *Proteomics* **2006**, *6*, 2650–5.
(71) Tilley, S. D.; Francis, M. B. *Journal of the American Chemical Society* **2006**, *128*, 1080–1.
(72) Paulick, M. G.; Wise, A. R.; Forstner, M. B.; Groves, J. T.; Bertozzi, C. R. *Journal of the American Chemical Society* **2007**, *129*, 11543–50.
(73) Singla, N.; Erdjument-Bromage, H.; Himanen, J. P.; Muir, T. W.; Nikolov, D. B. *Chemistry & biology* **2011**, *18*, 361–71.
(74) Singla, N.; Himanen, J. P.; Muir, T. W.; Nikolov, D. B. *Protein science : a publication of the Protein Society* **2008**, *17*, 1740–7.
(75) Cui, C.; Zhao, W.; Chen, J.; Wang, J.; Li, Q. *Protein expression and purification* **2006**, *50*, 74–81.
(76) Yoshina-Ishii, C.; Boxer, S. G. *Journal of the American Chemical Society* **2003**, *125*, 3696–7.
(77) Yoshina-Ishii, C.; Miller, G. P.; Kraft, M. L.; Kool, E. T.; Boxer, S. G. *Journal of the American Chemical Society* **2005**, *127*, 1356–7.
(78) Chung, M.; Lowe, R. D.; Chan, Y.-H. M.; Ganesan, P. V; Boxer, S. G. *Journal of structural biology* **2009**, *168*, 190–9.
(79) Van Lengerich, B.; Rawle, R. J.; Boxer, S. G. *Langmuir* **2010**.
(80) Chan, Y.-H. M.; Van Lengerich, B.; Boxer, S. G. *Proceedings of the National Academy of Sciences of the United States of America* **2009**, *106*, 979–84.
(81) Ajo-Franklin, C. M.; Yoshina-Ishii, C.; Boxer, S. G. *Langmuir* **2005**, *21*, 4976–4983.
(82) Chung, M.; Boxer, S. G. *Langmuir* **2011**, *27*, 5492–7.
(83) Rawle, R. J.; Van Lengerich, B.; Chung, M.; Bendix, P. M.; Boxer, S. G. *Biophysical journal* **2011**, *101*, L37–9.
(84) Selden, N. S.; Todhunter, M. E.; Jee, N. Y.; Liu, J. S.; Broaders, K. E.; Gartner, Z. J. *Journal of the American Chemical Society* **2012**, *134*, 765–8.
(85) Kukolka, F.; Niemeyer, C. M. *Organic & biomolecular chemistry* **2004**, *2*, 2203–6.
(86) Tong, G. J.; Hsiao, S. C.; Carrico, Z. M.; Francis, M. B. *Journal of the American Chemical Society* **2009**, *131*, 11174–8.
(87) Lovrinovic, M.; Spengler, M.; Deutsch, C.; Niemeyer, C. M. *Molecular Biosystems* **2005**, *1*, 64–9.
(88) Saccà, B.; Meyer, R.; Erkelenz, M.; Kiko, K.; Arndt, A.; Schroeder, H.; Rabe, K. S.; Niemeyer, C. M. *Angewandte Chemie (International ed. in English)* **2010**, 9378–9383.
(89) Brennan, M.; Davison, P. F.; Paulus, H. *Science* **1985**, *229*, 81–83.
(90) Robinson, M. K.; Hodge, K. M.; Horak, E.; Sundberg, A. L.; Russeva, M.; Shaller, C. C.; Von Mehren, M.; Shchaveleva, I.; Simmons, H. H.; Marks, J. D.; Adams, G. P. *British journal of cancer* **2008**, *99*, 1415–25.
(91) McDonagh, C. F.; Huhalov, A.; Harms, B. D.; Adams, S.; Paragas, V.; Oyama, S.; Zhang, B.; Luus, L.; Overland, R.; Nguyen, S.; Gu, J.; Kohli, N.; Wallace, M.; Feldhaus, M. J.; Kudla, A. J.; Schoeberl, B.; Nielsen, U. B. *Molecular cancer therapeutics* **2012**, *11*, 582–93.
(92) Cochran, J. R. *Science translational medicine* **2010**, *2*, 17ps5.
(93) Holmes, D. *Nature Reviews Drug Discovery* **2011**, *10*, 798–800.

(94) Bostrom, J.; Yu, S.-F.; Kan, D.; Appleton, B. A.; Lee, C. V; Billeci, K.; Man, W.; Peale, F.; Ross, S.; Wiesmann, C.; Fuh, G. *Science* **2009**, *323*, 1610–4.
(95) Harding, M. W.; Galat, A.; Uehling, D. E.; Schreiber, S. L. *Nature* **1989**, *341*, 758–60.
(96) Bayle, J. H.; Grimley, J. S.; Stankunas, K.; Gestwicki, J. E.; Wandless, T. J.; Crabtree, G. R. *Chemistry & biology* **2006**, *13*, 99–107.
(97) Inoue, T.; Heo, W. D.; Grimley, J. S.; Wandless, T. J.; Meyer, T. *Nature Methods* **2005**, *2*, 415–418.
(98) Levskaya, A.; Weiner, O. D.; Lim, W. A.; Voigt, C. A. *Nature* **2009**, *461*, 997–1001.
(99) Hartman, N. C.; Groves, J. T. *Current opinion in cell biology* **2011**, *23*, 370–6.
(100) Bethani, I.; Skånland, S. S.; Dikic, I.; Acker-Palmer, A. *The EMBO Journal* **2010**, *29*, 2677–2688.
(101) Li, P.; Banjade, S.; Cheng, H.-C.; Kim, S.; Chen, B.; Guo, L.; Llaguno, M.; Hollingsworth, J. V; King, D. S.; Banani, S. F.; Russo, P. S.; Jiang, Q.-X.; Nixon, B. T.; Rosen, M. K. *Nature* **2012**, *483*, 336–340.
(102) Olayioye, M. A.; Neve, R. M.; Lane, H. A.; Hynes, N. E. *The EMBO journal* **2000**, *19*, 3159–67.
(103) Freywald, A.; Sharfe, N.; Roifman, C. M. *The Journal of biological chemistry* **2002**, *277*, 3823–8.
(104) Truitt, L.; Freywald, T.; DeCoteau, J.; Sharfe, N.; Freywald, A. *Cancer research* **2010**, *70*, 1141–53.
(105) Tepper, A. W. J. W. *Journal of the American Chemical Society* **2010**, *132*, 6550–7.
(106) Niemeyer, C. M.; Koehler, J.; Wuerdemann, C. *ChemBioChem* **2002**, *3*, 242–5.
(107) You, M.; Wang, R.-W.; Zhang, X.; Chen, Y.; Wang, K.; Peng, L.; Tan, W. *ACS Nano* **2011**, *5*, 10090–5.
(108) Erkelenz, M.; Kuo, C.-H.; Niemeyer, C. M. *Journal of the American Chemical Society* **2011**, *133*, 16111–16118.
(109) Yan, H.; Park, S. H.; Finkelstein, G.; Reif, J. H.; LaBean, T. H. *Science* **2003**, *301*, 1882–4.
(110) Stephanopoulos, N.; Liu, M.; Tong, G. J.; Li, Z.; Liu, Y.; Yan, H.; Francis, M. B. *Nano letters* **2010**, *10*, 2714–20.

Chapter 2

Section 2.1: Functionalization of supported membranes with DNA oligonucleotides

We use supported membranes functionalized with DNA oligonucleotides to direct the assembly of heterooligomeric complexes. DNA functionalized membranes have been used extensively to study vesicle fusion[1,2] and to prepare tethered membranes.[3] These studies used oligonucleotides that were synthesized and doubly acylated with fatty acids by solid phase DNA synthesis.[4–6] Despite the success of this strategy, applicability is limited because of the requirement that the lipidated DNA be produced by solid phase synthesis and that the DNA is incorporated into vesicles instead of directly into supported membranes. A strategy employing commercially available reagents would be preferable, such as that shown in Figure 2.1a using Michael addition to maleimide phospholipids.

Small unilamellar vesicles (SUVs) consisting of 1:20 molar ratio of maleimide functionalized DOPE to DOPC (see experimental section for more details and full chemical names of phospholipids used) were prepared by sonication, as were SUVs containing only DOPC. These vesicles were used to prepare supported membranes on glass. Coupling of 6-carboxyfluorescein (6-FAM) labeled ssDNA by Michael addition was evaluated by fluorescence microscopy (Figure 2.1b). Fluorescence recovery after photobleaching (FRAP) verified the lateral mobility of the DNA linked to the membrane (Figure 2.1c).

To determine the surface density of the DNA coupled to the membrane, the fluorescence intensity measured from the DNA functionalized membrane was compared with fluorescence intensity measured from supported membranes with known concentrations of fluorescent molecules.[7] To determine the relationship between surface density of the known standards and fluorescence intensity, a dilution series was made in which the fluorescent lipid vesicles were mixed with non-fluorescent vesicles and bilayers were formed from these mixtures (Figure 2.2a). Measured fluorescence intensity of known standards increased linearly with respect to expected surface density. To determine the difference in molar brightness between the phospholipid anchored fluorophore and that used to label the DNA, the solution fluorescence intensity of a dilution series was measured for both the vesicles and the fluorescent DNA itself.

Initial results from these experiments using 6-FAM labeled DNA suggested that the surface density of the DNA was very low (< 1000 strands/μm^2). However, the measured density did not scale predictably with the concentration added. Additionally, a longer incubation of thiolated 6-FAM-labeled DNA, which should increase surface density, resulted in lower observed fluorescence intensity. These observations can be explained by the tendency of carboxyfluorescein to self-quench.[8] When these experiments were repeated with the fluorophores

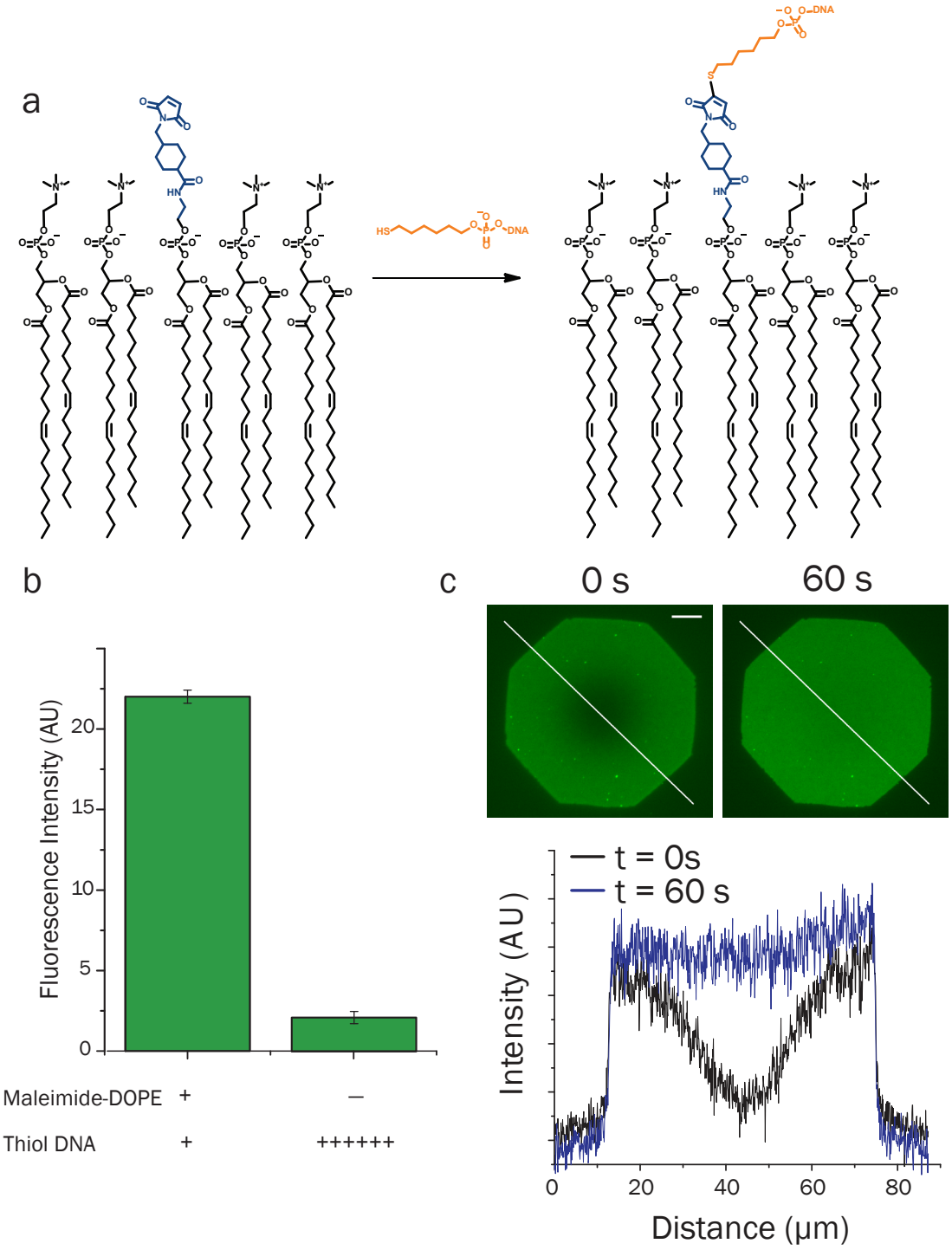

Figure 2.1. Conjugation of ssDNA to supported membranes. (a) Scheme depicting conjugation of thiol ssDNA to maleimide functionalized phospholipid membranes. (b) Fluorescence microscopy characterization of fluorescently labeled thiol ssDNA treated maleimide membranes demonstrates specific conjugation of the DNA to the maleimide headgroup. (c) Representative FRAP characterization of a membrane treated with fluorescently labeled thiol ssDNA demonstrates the lateral fluidity of the DNA. The diagonal white line shows the region shown in the intensity profile. The scale bar represents 10 μm.

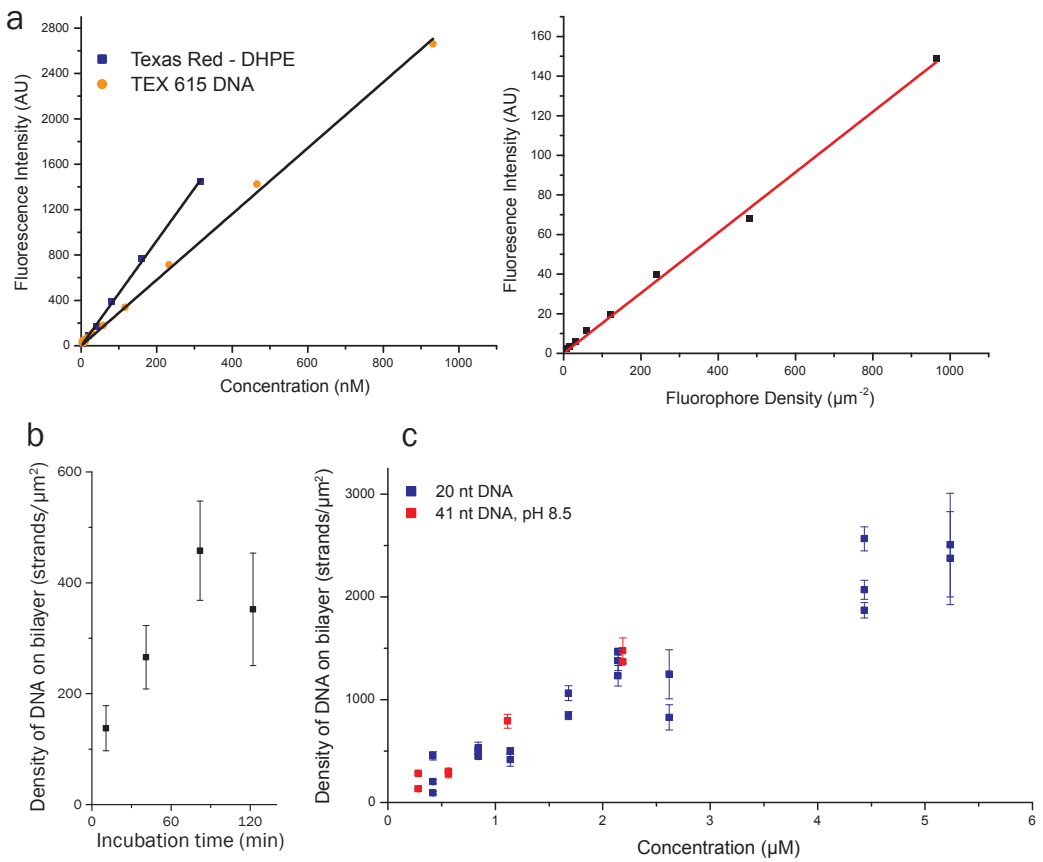

Figure 2.2. Quantification of DNA surface density on supported membranes. (a) *Left.* A representative comparison of molecular brightness of lipid fluorophores compared to DNA fluorophores is shown. Linear functions fitting the data are shown in black. *Right.* Relationship of surface density of fluorophore to pixel grayscale values. A linear function fitting the data is shown in red. (b) Measurement of the surface density of hybridized fluorescently labeled DNA on supported membranes that had been treated with 20mer thiol ssDNA for the indicated times. (c) The surface density of coupled DNA can be varied over a large concentration range. The error bars represent the standard error of the mean of duplicate images.

TEX615 and Alexa Fluor 488, we observed higher surface densities that scaled as expected with the parameters of incubation time and the concentration of added thiol DNA.

Upon treating DNA with 20 nt DNA strands and varying the incubation time, increases in surface density were observed as a function of incubation time until a maximum was reached at approximately 80 min (Figure 2.2b). Varying the incubation concentration of thiol-DNA was also observed to change the measured surface density proportionally (Figure 2.2c). These measurements over a range of thiol-DNA incubation concentrations are shown in Figure 2.2c. With incubation concentrations of DNA in the low micromolar range, surface densities in the range of 0 to 3000 strands/μm^2 were observed. The density of many cell surface proteins is <3000 molecules/μm^2.[9–13] The addition of thiol DNA in concentrations above 6 μM resulted in further increases in measured surface density, but larger variations between identical samples were observed, and the relationship between surface density and incubation concentration became nonlinear. A 41 nt ssDNA coupled to the supported membrane

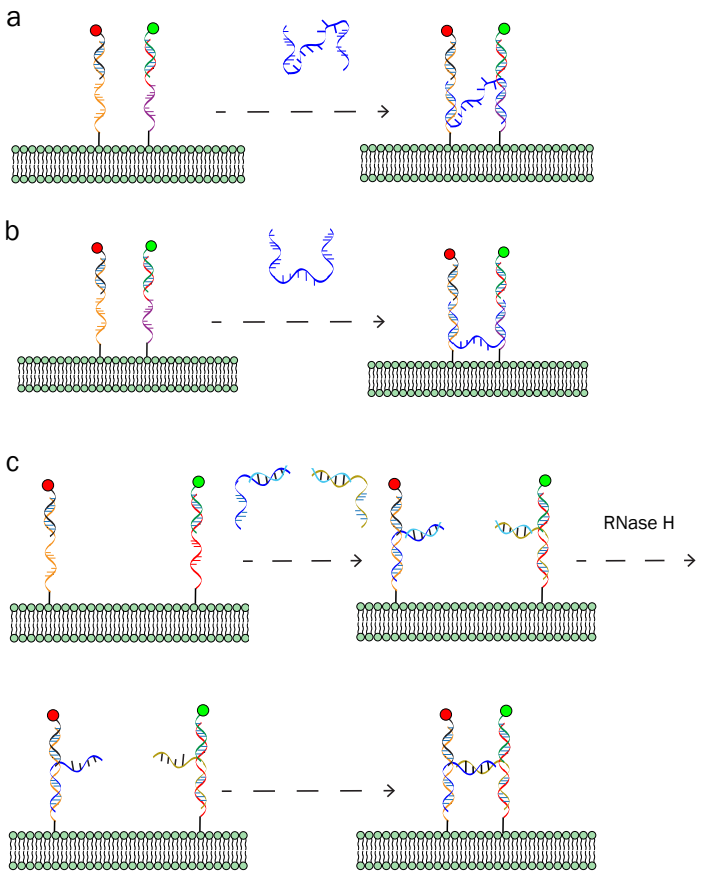

Figure 2.3. Triggerable dimerization schemes that failed to show cross-correlation. (a) Both strands are linked to the bilayer with their 5' end and an "N" shaped crosslinking strand is added. (b) One strand is linked by 5' and the other by 3' end, allowing a U-shaped strand to link them. (c) DNA-RNA hybrids with overhangs complementary to the supported membrane functionalized strands were added. RNase H was then added to remove the protecting RNA.

less efficiently than a 20 nt ssDNA using the same buffer conditions (PBS, pH 7.4), but the use of pH 8.5 borate buffered saline (BBS, 10 mM borate, 150 mM NaCl) as a higher pH buffer yielded surface densities of a 41 nt ssDNA that were very similar to those of a 20 nt ssDNA coupled at lower pH.

Section 2.2: Formation and characterization of DNA based heterodimers

For the assembly of more complex structures, we designed DNA heterodimers using previously published assembly sequences.[14–16] Several strand configurations, shown in Figure 2.3, were evaluated. Of these, a particularly successful strategy for the formation of four-strand "Y"-shaped structures was selected.

The two arms of the branched structures were labeled with green and red fluorophores, as shown in Figure 2.4b, allowing characterization by two-color fluorescence cross-correlation spectroscopy (FCCS)[17] with pulsed interleaved excitation (PIE,[18] see Figure 2.4a for experimental diagram). In FCCS, the fluorescence emission from a confocal spot is measured as a

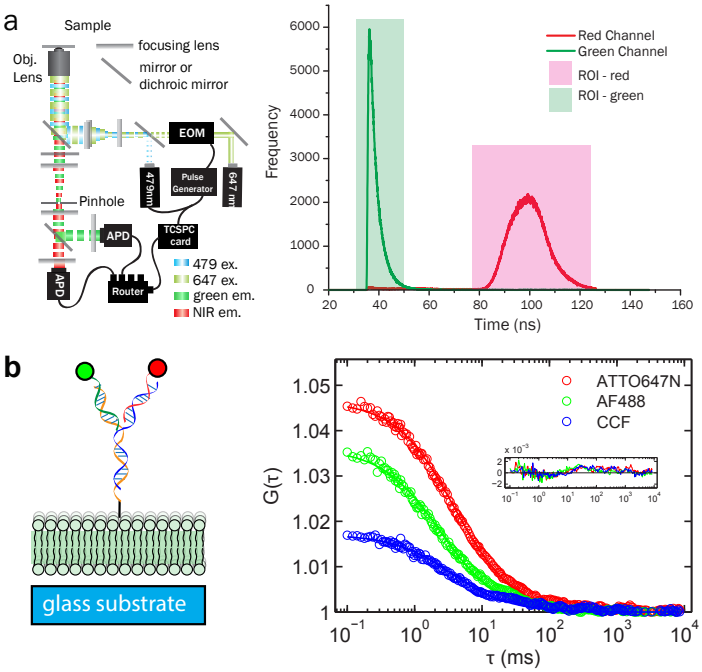

c

Sample	$G(0)_x/\min(G(0)_r, G(0)_g)$
Heterodimer	0.46 - 0.48
Negative control	0.00 - 0.03
Dual labeled ssDNA	0.80 - 0.88

Figure 2.4. Analysis of fluorophore heterodimers with FCCS. (a) A diagram is shown for a PIE-FCCS experiment. Excitation light is interleaved to allow time resolved data collection, as shown in the graph, and thus removal of the contribution of fluorescence signal bleedthrough to cross-correlation. (b) FCCS analysis indicated the co-diffusion of the DNA-bound fluorophores, suggesting that they had formed a heterodimer. Fits to the data are shown as solid lines. Fit residuals are shown in the inset in the corresponding colors. (c) The table compares the relative cross-correlation amplitudes to the lower of the two autocorrelation amplitudes, including positive and negative control samples (shown as Figure 2.4).

function of time. Fluctuations in intensity are assumed to result from the diffusion of fluorophores through the illuminated spot. Autocorrelation of the intensity function of each channel allows determination of the number of molecules in the illuminated spot and the diffusion coefficient. The cross-correlation function determines the same parameters for species in which the fluorescent dyes are diffusing together.

FCCS experiments have characterized the binding properties of biomolecules,[19,20] measured enzymatic activity,[21] and quantified clustering in cell membranes.[22] PIE eliminates artifactual cross-correlation from fluorescence spectral bleed-through by exciting the sample with interleaved laser pulses. The red peak is broad in our experiment since pulsing is achieved through electro-optic modulation of a continuous wave KrAr laser. The amplitude of the cross-correlation function is proportional to the concentration of dual-labeled species. Measurement of this parameter can be obscured by a variety of artifacts that can both raise or lower the measured cross-correlation amplitude.[23,24] Using control samples that establish

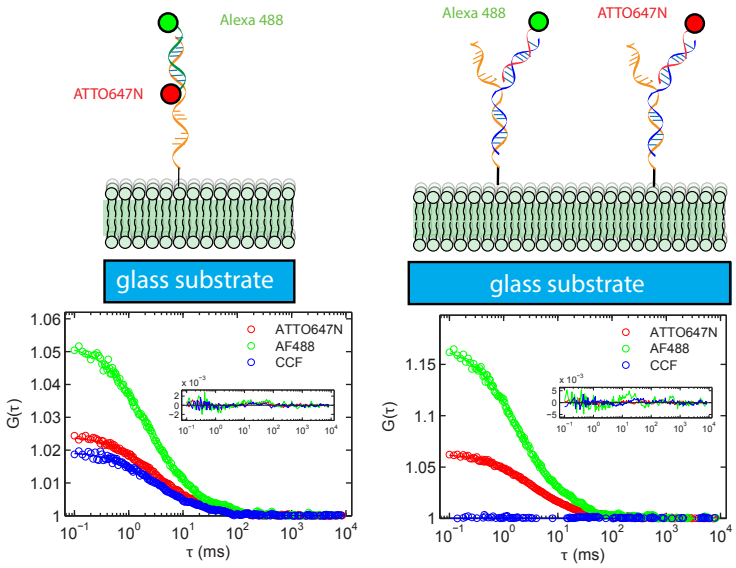

Figure 2.5. FCCS control samples. FCCS analysis of positive and negative controls is shown for the experiment described in figure 2.3. Interpretation and data analysis are described in the text.

the upper and lower bounds of the cross-correlation measurement enables calibration of the cross-correlation signal and quantification of the amount of heterodimer formed (Figure 2.4c).[20]

To establish the upper bound of cross-correlation, a doubly modified oligonucleotide was used that contained ATTO647N conjugated by amine acylation and Alexa 488 conjugated by maleimide addition. UV-vis spectroscopy showed that the molecule was labeled to near completion with both dyes, with a ratio of 1.0:1.0:0.84 (AF488:DNA:ATTO647N). FCCS analysis yielded a high cross-correlation measurement of 0.80-0.88 (Figure 2.4 and 2.5). While this number is coincidentally similar to the labeling ratio measured by UV-vis, it takes into account a different measured concentration of the two dyes. Analysis of the autocorrelation functions show Ng = 19 and Nr = 41-44. These observations suggest that optical effects, such as the offset of the point spread functions of the two lasers and the chromatic aberration, are predominant factors in decreasing measured cross-correlation. Additionally, the calculation of F_{CC} used here divides by the lower of the two amplitudes,[20,22] normalizing for differences in detected concentration of the two species. Therefore, we interpret this measurement to be representative of the maximum observable cross-correlation by our instrument.

To ensure that PIE is successful in removing cross-correlation artifacts, single DNA strands with the same nucleotide sequence were hybridized with membrane anchored strands. These diffused independently and no cross-correlation was observed (Figure 2.5). The dimer structure was analyzed by FCCS (Figure 2.4). Comparing the cross-correlation measurement of this sample to that of the positive control provides an estimate of 52-60% yield of assembled heterodimer.

The formation of protein heterodimers was demonstrated by assembling complexes of Fab' fragment-DNA conjugates, effectively reconstructing membrane-bound antibodies. Fab'

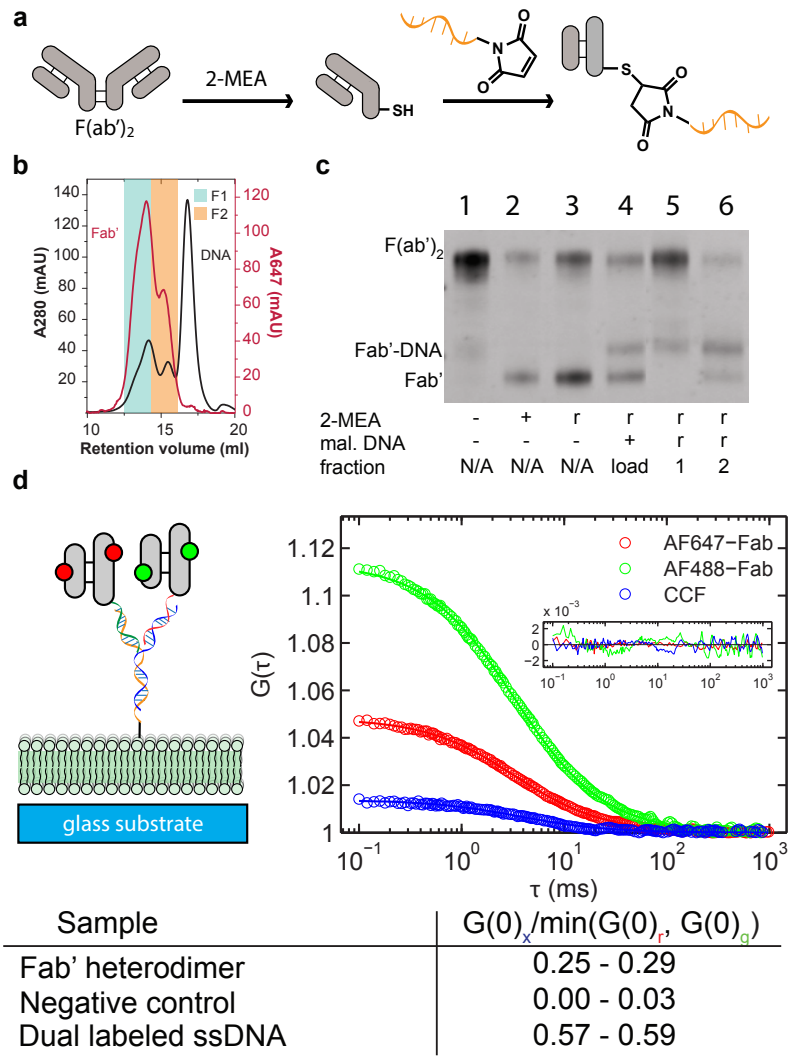

Sample	$G(0)_x/\min(G(0)_r, G(0)_g)$
Fab' heterodimer	0.25 - 0.29
Negative control	0.00 - 0.03
Dual labeled ssDNA	0.57 - 0.59

Figure 2.6. Dimerization of Fab'-DNA conjugates on supported membranes. (a) A scheme is shown for Fab'-DNA conjugate synthesis. (b) SEC separations were performed for AF647 labeled Fab-DNA conjugates. (c) An SDS-PAGE gel of 1) $F(ab')_2$, 2) Fab' before removal of the 2-MEA reducing agent, 3) Fab' after removal of the 2-MEA reducing agent, (4) Fab' treated with maleimide DNA, (5) the highest molecular weight peak from SEC chromatography (blue shading), and (6) the intermediate molecular weight peak from SEC (orange shading). The entry "r" in the table indicates that the reagent has been removed. (d) FCCS analysis confirmed formation of a Fab' heterodimer using the pooled fractions. Fits to the data are shown as solid lines. Fit residuals are shown in the inset.

fragments can be generated from IgG antibodies, which are readily obtained against many proteins. For this study, $F(ab')_2$ fragments generated from polyclonal donkey anti-mouse antibodies were obtained from a commercial source, labeled with fluorophores, and partially reduced with 2-mercaptoethylamine (2-MEA) to produce Fab' fragments with free thiol groups at the C-terminal regions, Figure 2.6a.[25,26]

The products were desalted and treated with maleimide functionalized 20 nt ssDNA. The conjugates were purified by size exclusion chromatography (Figure 2.6b) and analyzed by gel electrophoresis (SDS-PAGE, Figure 2.6c). Separation of the proteins from free ssDNA is

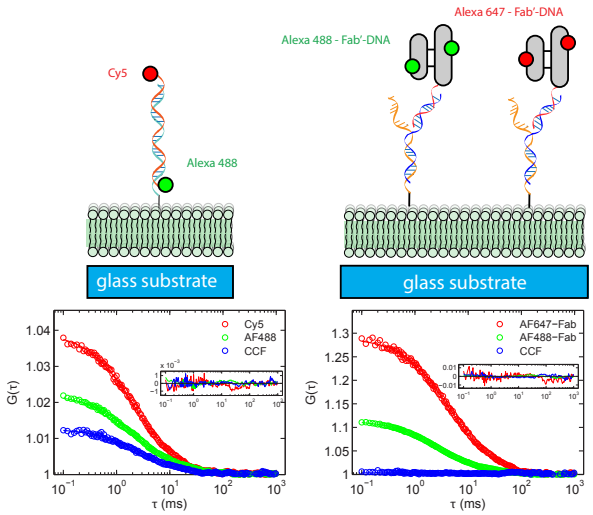

Figure 2.7. FCCS control samples. FCCS analysis of positive and negative controls is shown for the experiment described in figure 2.5. Interpretation and data analysis are described in the text.

shown in the chromatogram (Figure 2.6b). After treating the Fab' fragments with maleimide DNA, gel electrophoresis analysis indicated the presence of a species with higher molecular weight compared to the unmodified Fab' fragments (Figure 2.6c). These conjugates were prepared with different sequences of DNA and labeled with distinct fluorophores so that a heterodimer could be prepared on DNA functionalized supported membranes, as shown in Figure 2.6d. The resulting structure was then analyzed by FCCS to measure heterodimerization (Figure 2.6d). By comparing the cross correlation amplitude to that of a doubly-labeled control sample (Figure 2.7), we determined that a 42-44% assembly yield was obtained for the heterodimeric structure. When expanded to antibody fragments with different specificities this technique provides a way to colocalize two different receptors using a convenient synthetic protocol.

Section 2.3: Chapter 2 experimental

Materials

DNA oligonucleotides were purchased from Integrated DNA Technologies (Coralville, IA), or when noted from Eurofins MWG operon (Huntsville, AL). Thiolated DNA was purchased with C6 Thiol Modifier on the 5' end of the strand or the C3 thiol modifier at the 3' end of the strand. Alexa Fluor 488-NHS ester and TEX615 modifications were also added to the 5' end by the manufacturer and these strands were HPLC purified by the manufacturer.

Alexa Fluor 647 carboxylic acid, succinimidyl ester was purchased from Invitrogen (Carlsbad, CA). ATTO647 NHS ester was purchased from Sigma-Aldrich (St. Louis, MO). Succinimidyl 3-(2-Pyridyldithio)propionate (SPDP) and NHS-PEO_6-maleimide were purchased from Pierce (Rockford, IL). Maleimide-NTA was purchased from Dojindo Molecular Technologies (Kumamoto, Japan).

The phospholipids 1,2-dioleoyl-s*n*-glycero-3-phosphocholine (DOPC),1,2-dipalmitoyl-s*n*-glyc-

ero-3-phosphoethanolamine-*N*-[4-(p-maleimidomethyl)cyclohexane-carboxamide] (MCC-DHPE), 1,2-dioleoyl-sn-glycero-3-phosphoethanolamine-*N*-[4-(*p*-maleimidomethyl)cyclohexane-carboxamide] (MCC-DOPE), 1,2-dioleoyl-s*n*-glycero-3-[(*N*-(5-amino-1-carboxypentyl) iminodiacetic acid)succinyl] (DOGS-NTA), and 1,2-dioleoyl-s*n*-glycero-3-phospho-L-serine (DOPS) were purchased from Avanti Polar Lipids (Alabaster, AL). The fluorescent lipid probes Texas Red 1,2-dihexadecanoyl-s*n*-glycero-3-phosphoethanolamine and *N*-(4,4-difluoro-5,7-dimethyl-4-bora-3a,4a-diaza-s-indacene-3-propionyl)-1,2-dihexadecanoyl-s*n*-glycero-3-phosphoethanolamine were purchased from Invitrogen (Carlsbad, CA).

Micro Bio-Spin 6 and 30 Chromatography columns were obtained from Bio-Rad (Hercules, CA). NAP-5 columns and Vivaspin concentrators were obtained from GE Healthcare (Piscataway, NJ).

DNA sequences used

We used the following sequences, also used for orthogonal DNA surface functionalization in other studies.[14–16]

```
1 : 5′– GTA ACG ATC CAG CTG TCA CT – 3′
1’: 5′– AGT GAC AGC TGG ATC GTT AC – 3′
2 : 5′– TCA TAC GAC TCA CTC TAG GG – 3′
2’: 5′– CCC TAG AGT GAG TCG TAT GA – 3′
3 : 5′– ACT GAC TGA CTG ACT GAC TG – 3′
3’: 5′– CAG TCA GTC AGT CAG TCA GT – 3′
```

Fluorophore labeling of oligonucleotides

Amine modified (5’-C6 amine modifier) strands were ethanol precipitated before use. To a solution of boric acid buffer (adjusted to pH 9 with NaOH), were added 0.1 mg of oligonucleotide and 0.25 mg of Alexa Fluor 647 carboxylic acid, succinimidyl ester. This reaction proceeded overnight. The DNA was ethanol precipitated to remove most of the unreacted dye, then resuspended in water and injected onto a PROTO C18 reverse phase HPLC column (Higgens analytical), equilibrated with 93% 0.1M triethylamine acetate (TEAA), pH 7 and 7% acetonitrile. A flow rate of 0.5 mL/min with a gradual increase in acetonitrile concentration separated the modified and unmodified oligonucleotides. Fractions were collected when the UV-vis monitor detected both fluorophore absorbance and absorbance of DNA. The solvent was removed under reduced pressure. The ATTO647N oligonucleotide used for heterodimerization and for negative controls was prepared in a similar manner. However, in this case, the fractions were pooled, desalted in a Nap-5 column, and the product was ethanol precipitated.

Vesicle preparations

The appropriate lipid mixture was transferred into a clean round bottom flask. The solvent (chloroform) was evaporated under reduced pressure at 37-42 ºC for at least 15 minutes. The lipid film was then stored under nitrogen until ready. Lipid films were resuspended in ddH_2O. Maleimide containing vesicles, to be used for thiol-DNA coupling, were resuspended to 0.5 mg/mL total lipid concentration and sonicated. Vesicles made for the purpose of

quantitative fluorescence microscopy standards were resuspended to 1 mg/mL in water then extruded through a 100 nm track etch membrane (Whatman, Kent, UK) eleven times.

Supported lipid bilayer preparation

Surface density measurements were performed in glass bottom 96-well plates. These were cleaned by incubation with 0.5 M NaOH for 1 hour, and then rinsed with water. The water was aspirated immediately before deposition of vesicles. Vesicle suspensions were mixed 1:1 (v/v) with phosphate buffered saline (PBS, 10 mM phosphate buffer, 150 mM NaCl, diluted from 10X PBS, Cellgro) and deposited on the clean glass surface. The membrane was rinsed with 12-15 mL of PBS. For linking 41 nt DNA to the membrane, borate buffered saline (BBS, 10 mM boric acid, 150 mM NaCl, pH adjusted to 8.5 with NaOH) was used in place of PBS.

FCCS experiments were performed using piranha cleaned Fisher Brand circular microscope cover glass or Werner number 1.5 thickness coverslips. All were 22 mm in diameter and we did not notice significant differences between the two brands of coverslips. First, these cover slips were cleaned in a bath sonicator with a 1:1 (v/v) solution of 2-propanol and ddH_2O. Then, they were treated with 3:1 (v/v) concentrated sulfuric acid and 30% hydrogen peroxide solution for 5 minutes and rinsed extensively with water before use. As above, the vesicle suspension was mixed 1:1 (v/v) with PBS or BBS and deposited on a plastic Petri dish. A dried cover slip was then placed on this drop and submerged in a bath of PBS or BBS. The sample was assembled and rinsed with 15 mL of buffer.

Alternatively, deposition of the SUV/buffer mixture was found to result in bilayers of comparable quality. In this procedure, the SUV and buffer mixture was added to a dry coverslip secured in an assembled sample holder and then incubated for at least 5 minutes before rinsing.

Supported lipid bilayer functionalization

Thiolated oligonucleotides, except those mentioned later, were stored in 0.5X TE buffer (5 mM Tris, 0.5 mM EDTA, pH 8), with 1-10 mM tris(2-carboxyethyl)phosphine (TCEP). Within an hour before use, they were filtered through two Bio-spin 6 or Bio-spin 30 columns (Bio-rad, Hercules, CA). While a previous study used these conditions to store oligonucleotides,[14] we noticed eventual oxidation and decrease of reactivity over time. For this reason, newer batches of thiol ssDNA were alternatively dissolved in TE buffer to 5 mg/mL and diluted to 1 mg/mL aliquots. Both the stock solution and the dilution were stored frozen. TCEP solution was diluted from an unbuffered stock solution to a 10 mM solution buffered with 100 mM 4-(2-hydroxyethyl)-1-piperazineethanesulfonic acid buffer (HEPES), pH 8. The buffered solution of TCEP was added to the DNA yielding a 1-2 mM final concentration of the reducing agent and incubated at room temperature for at least 30 min. Then the solution was filtered as above. Some samples were found not to be completely reduced under these conditions. In this case, we added TCEP to 2 mM final concentration and incubated at 37 ºC for 90 minutes before filtering. We also found some batches of DNA (especially those more recently acquired) to achieve more reliable coupling to membranes if they were first ethanol precipitated before aliquoting and TCEP reduction.

After bilayer formation, desalted ssDNA was added to an appropriate concentration and incubated for 80 minutes. After this time, the excess ssDNA was washed with excess buffer (15-30 mL).

Fluorescence Microscopy

FRAP and surface density measurements were performed on a Nikon TE-300 inverted fluorescence microscope using 40X 0.75NA Plan Fluor or 100X Plan Fluor NA 0.5-1.3 objectives (Nikon, Tokyo, Japan). A super high pressure mercury arc lamp (Nikon, Tokyo, Japan) provided illumination for fluorescence images. Images were recorded on a Coolsnap HQ camera (Photometrics, Tuscon, AZ).

Measurement of DNA surface density on supported membranes

To determine the relationship between thiol ssDNA incubated with supported membranes and the resulting surface density, we converted the observed fluorescence to surface density of fluorophore-ssDNA conjugates by comparing the fluorescence of DNA-supported membrane samples to membranes formed with fluorophores of known surface density as described in the literature.[7] We first prepared these standard membranes of known surface density using vesicles composed of 5% DOPS, a small percentage of fluorescent lipid (for comparisons with TEX 615, we used Texas Red-DHPE and for comparisons with AF488 we used BODIPY-DHPE), and the remaining percentage DOPC. To obtain a serial dilution of the fluorophore, vesicle suspensions were mixed with unlabeled vesicles of the following composition: 98 mol % DOPC and 2 mol % DOGS-NTA. Vesicles and supported membranes were prepared as described in the appropriate section above.

The brightness ratio of the lipid and DNA conjugated fluorophores was determined by measuring the fluorescence intensity of fluorescent vesicles or fluorescent DNA in solution, as shown in Figure 2.2. A representative standard curve relating measured fluorescence intensity to surface density is shown in Figure 2.2. Using this information and the relation of fluorescence intensity to surface density, we could determine the surface density of DNA from the measured fluorescence intensity.

Fluorescence cross-correlation spectroscopy

FCCS experiments were conducted with a home-built setup shown in Figure 2.4. Two lasers are joined into a fiber launcher. The beams are expanded and directed to a dichroic mirror in the body of a Nikon TE2000 microscope and directed through a Nikon 100X TIRF NA 1.49 objective lens onto the sample. Fluorescence light returns through the same path, but passes through the dichroic mirror and is focused onto a 50 μm confocal pinhole. The beam is recollimated and passes through another dichroic mirror, splitting the two channels onto two avalanche photodiode detectors (APDs). Before the APDs, the light is filtered by bandpass filters appropriate for the fluorophores used.

In FCCS, the fluorescence intensity of a confocal spot is measured as a function of time. Fluctuations in intensity are assumed to result from diffusion of fluorophores through the illuminated spot. Autocorrelation of the intensity function of each channel allows determi-

nation of the number of molecules in the illuminated spot and the diffusion coefficient. The cross-correlation function determines the same parameters for species in which the fluorescent dyes are diffusing together. The co-diffusing species must be persistent relative to the timescale of diffusion through the illuminated area (a few milliseconds). Fluorescence signal bleedthrough, which can cause positive cross-correlation artifact, was minimal, due to the large spectral separation between fluorophores. Still, the use of pulsed interleaved excitation and time-correlated single photon counting (TCSPC) completely removed any remaining contribution. A representative histogram is shown in Figure 2.4. The shaded areas show the time filters and correlation function calculations use only photons in these regions. The red curve is broad since the KrAr laser is pulsed by an electro-optic modulator, which creates an excitation function of similar profile to the modulation. Since the peaks from the two channels are well separated in time, the broadness of this peak does not prevent the use of PIE.

Assembly of heterodimer

Supported membranes were prepared and functionalized with 41 nt (5'-Thiol+seq1+A+seq2-3') or 45 nt (5'-2×A Thiol+seq1+3×A+seq2-3') DNA as described above. After washing, a cross-linking strand was added (5'-seq3+3×A+seq1'-3') to a final concentration of 0.2-1 μM. In the shown Fab' heterodimerization experiments, the lower end of this concentration regime was used. The excess cross-linking strand was washed away with excess buffer (15-50 mL). Then, fluorescent strands (5'-AF488+seq2'-3' or 5'-seq3'-ATTO647N-3') or Fab'-DNA conjugates (same sequences, but with labeled Fab fragments instead of fluorophores) were added to 200 nM final concentration. In the case of the Fab'-DNA conjugates, the actual concentration of the conjugate was likely lower, since the protein concentration (as determined by fluorophore and fluorophore labeling ratio) was used to calculate how much to add and a considerable amount of protein was not conjugated to DNA.

Controls for FCCS

Positive control strands for FCCS were either purchased from IDT (5'-Cy5+seq2'+T+seq1'+AF488-3') or made from doubly modified DNA from Eurofins MWG Operon (5'-Thiol+seq2'+Amine-3'). The commercially obtained strand from IDT was subjected to another round of HPLC purification. For strands modified in house, the DNA was ethanol precipitated before use. The DNA was treated with 0.25 mg of ATTO647N-NHS ester from an ATTO647N protein labeling kit. The reaction was performed in PBS (10 mM PB, 150 mM NaCl) with a supplement of 50 mM bicarbonate (the final pH of this solution was not tested). After the reaction was complete, residual dye was removed with 2 Bio-Spin 6 columns and ethanol precipitation. Analysis of 5'-Cy5+seq2'+T+seq1'+AF488-3' after HPLC purification by UV-vis spectroscopy showed a ratio of 0.92:1:1.3 (Cy5:DNA:AF488). Analysis of 5'-AF488+seq2'+Atto647N-3' by UV-vis gave a ratio of 1.0:1.0:0.84 (AF488:DNA:ATTO647N). Readings of more than 1 dye per DNA molecule are likely the result of unexpected changes in the extinction coefficient of either the dye or the DNA or deviation of the actual DNA extinction coefficient from the calculated one.

Interpretation of FCCS data

The correlation functions were calculated using homebuilt scripts in Matlab using a multi-tau strategy[27] and fit to a standard model of 2-D diffusion.

$$G(\tau) = \frac{1}{N}\left(1 + \frac{\tau}{\tau_D}\right) + 1$$

The parameter N refers to the average number of molecules in the collection volume. The independent variable τ refers to the lag time, and τ_D is the midpoint of the correlation decay. To calculate the degree of cross correlation, we first compared the ratio of the cross-correlation amplitude, which refers to G(0).

$$F_{CC} = \frac{G(0)_x - 1}{\min\left(G(0)_r, G(0)_g\right) - 1}$$

This fraction was calculated for the heterodimer sample, the positive control sample, and the negative control sample (FCCS curves for positive and negative control samples are shown in Figures 2.5 and 2.7). The F_{CC} values (shown in Figure 2.4 and Figure 2.6) of the heterodimer are then divided by the F_{CC} values of the positive control to give an estimation of the yield of the heterodimer.

Maleimide DNA preparation

Amine modified DNA (C6 amino modifier, IDT) was ethanol precipitated and 200 µg were added to a microcentrifuge tube in PBS buffer. NHS-PEO_6-maleimide was added to a final concentration of 1.6 mM. Half was added immediately and half was added after the reaction had proceeded for 30 min. Characterization by MALDI-TOF mass spectrometry typically showed complete conversion under these conditions. The sample was then desalted with a NAP-5 column according to the manufacturer's direction for a 0.1 mL sample volume. The eluent was divided into various tubes (with a target of 25-50 µg/tube) and ethanol precipitated. The pellet was dried under reduced pressure at room temperature or in a nitrogen charged dry box at room temperature and stored dry at -80 °C. Representative data from MALDI characterization are shown in Figure 2.6.

Fab'-DNA conjugate preparation

$F(ab')_2$ fragments were buffer exchanged into PBS using a Vivaspin 500 10 kDa molecular weight cut-off (MWCO, GE healthcare) or an Amicon ultra 10 kDa MWCO (Millipore) spin concentrator. Sodium bicarbonate was added to 0.1 M and the solution was transferred to one vial of a monoclonal antibody labeling kit (Invitrogen) or a protein labeling kit (Invitrogen). The reaction was performed according to the manufacturer's direction, but purification was not. Unconjugated dye was removed with a NAP-5 column equilibrated with PBS (GE healthcare) according to the manufacturer's direction for a 0.1 mL sample volume. The sample

was concentrated with a Vivaspin 500 10 kDa MWCO spin concentrator, cysteamine-HCl was added to 1.7 mM, and this reaction was incubated at room temperature for 1 hour. After incubation, the reaction was desalted with a NAP-5 column equilibrated with PBS and 1 mM EDTA. This sample was concentrated in a Vivaspin 500 10 kDa MWCO concentrator and added to 2-5 equivalents of maleimide DNA. The reaction was incubated for approximately 3 hours at room temperature and stored at 4°C until purification on a Superdex 200 column (GE healthcare).

Section 2.4: Chapter 2 references

(1) Chan, Y.-H. M.; Van Lengerich, B.; Boxer, S. G. *Proceedings of the National Academy of Sciences of the United States of America* **2009**, *106*, 979–84.
(2) Van Lengerich, B.; Rawle, R. J.; Boxer, S. G. *Langmuir* **2010**.
(3) Chung, M.; Lowe, R. D.; Chan, Y.-H. M.; Ganesan, P. V; Boxer, S. G. *Journal of structural biology* **2009**, *168*, 190–9.
(4) Czolkos, I.; Hannestad, J. K.; Jesorka, A.; Kumar, R.; Brown, T.; Albinsson, B.; Orwar, O. *Nano letters* **2009**, *9*, 2482–6.
(5) Yoshina-Ishii, C.; Miller, G. P.; Kraft, M. L.; Kool, E. T.; Boxer, S. G. *Journal of the American Chemical Society* **2005**, *127*, 1356–7.
(6) Selden, N. S.; Todhunter, M. E.; Jee, N. Y.; Liu, J. S.; Broaders, K. E.; Gartner, Z. J. *Journal of the American Chemical Society* **2012**, *134*, 765–8.
(7) Galush, W. J.; Nye, J. A.; Groves, J. T. *Biophysical journal* **2008**, *95*, 2512–9.
(8) Chen, R. F.; Knutson, J. R. *Analytical biochemistry* **1988**, *172*, 61–77.
(9) Chen, Y.; Munteanu, A. C.; Huang, Y.-F.; Phillips, J.; Zhu, Z.; Mavros, M.; Tan, W. *Chemistry- A European Journal* **2009**, *15*, 5327–36.
(10) Salaita, K.; Nair, P. M.; Petit, R. S.; Neve, R. M.; Das, D.; Gray, J. W.; Groves, J. T. *Science* **2010**, *327*, 1380–5.
(11) Swift, J. L.; Godin, A. G.; Doré, K.; Freland, L.; Bouchard, N.; Nimmo, C.; Sergeev, M.; De Koninck, Y.; Wiseman, P. W.; Beaulieu, J.-M. *Proceedings of the National Academy of Sciences of the United States of America* **2011**, *108*, 7016–21.
(12) Kempiak, S. J.; Yip, S.-C.; Backer, J. M.; Segall, J. E. *The Journal of cell biology* **2003**, *162*, 781–7.
(13) Plunkett, M.; Springer, T. *The Journal of Immunology* **1986**, *136*, 4181–4187.
(14) Hsiao, S. C.; Shum, B. J.; Onoe, H.; Douglas, E. S.; Gartner, Z. J.; Mathies, R. A.; Bertozzi, C. R.; Francis, M. B. *Langmuir* **2009**, *25*, 6985–91.
(15) Twite, A. A.; Hsiao, S. C.; Onoe, H.; Mathies, R. A.; Francis, M. B. *Advanced materials* **2012**, *24*, 2380–5.
(16) Onoe, H.; Hsiao, S. C.; Douglas, E. S.; Gartner, Z. J.; Bertozzi, C. R.; Francis, M. B.; Mathies, R. A. *Langmuir* **2012**, *28*, 8120–6.
(17) Bacia, K.; Schwille, P. *Nature protocols* **2007**, *2*, 2842–56.
(18) Müller, B. K.; Zaychikov, E.; Bräuchle, C.; Lamb, D. C. *Biophysical journal* **2005**, *89*, 3508–22.
(19) Chen, J.; Nag, S.; Vidi, P.-A.; Irudayaraj, J. *PLoS ONE* **2011**, *6*, e17991.
(20) Slaughter, B. D.; Schwartz, J. W.; Li, R. *Proceedings of the National Academy of Sciences of the United States of America* **2007**, *104*, 20320–5.
(21) Kettling, U.; Koltermann, A.; Schwille, P.; Eigen, M. *Proceedings of the National Academy of Sciences of the United States of America* **1998**, *95*, 1416–20.

(22) Triffo, S. B.; Huang, H. H.; Smith, A. W.; Chou, E. T.; Groves, J. T. *Journal of the American Chemical Society* **2012**, *134*, 10833–42.
(23) Weidemann, T.; Wachsmuth, M. *Single Molecules* **2002**, *3*, 49–61.
(24) Foo, Y. H.; Naredi-Rainer, N.; Lamb, D. C.; Ahmed, S.; Wohland, T. *Biophysical Journal* **2012**, *102*, 1174–1183.
(25) Chaudri, Z.; Bartlet-Jones, M.; Panayotou, G. *FEBS letters* **1999**, *450*, 23–26.
(26) Brennan, M.; Davison, P. F.; Paulus, H. *Science* **1985**, *229*, 81–83.
(27) Wohland, T.; Rigler, R.; Vogel, H. *Biophysical journal* **2001**, *80*, 2987–99.

Chapter 3

Section 3.1: Evaluation of cell interactions with membranes bearing DNA or DNA anchored proteins

Evaluation of non-specific interactions between DNA functionalized membranes and living cells and accessibility of the DNA to presented cells was performed by modification of live Jurkat T-cells with surface ssDNA, as described previously.[1] Cells were incubated with membranes functionalized with ssDNA sequences that were either complementary or non-complementary to the cell surface ssDNA or a membrane of identical composition, but with no DNA functionalization as a negative control. Upon washing, cells bound only to the membranes functionalized with complementary ssDNA, confirming specificity of the interaction by

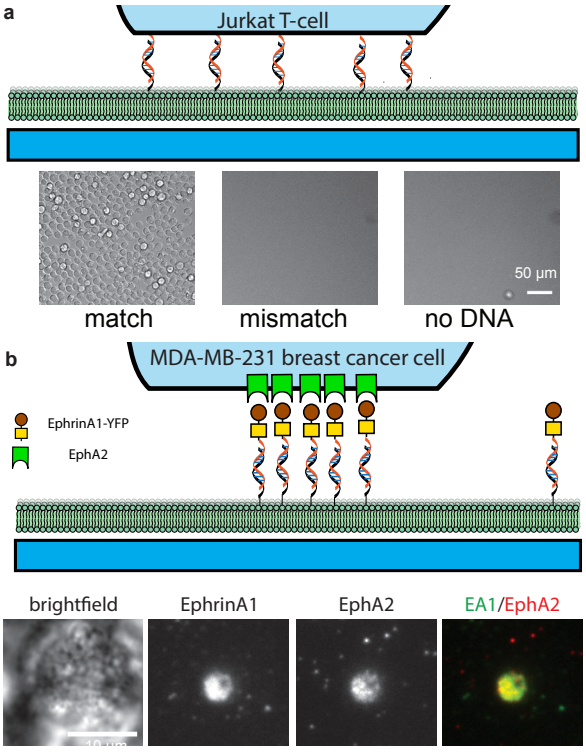

Figure 3.1. DNA directed ligand display. a) Non-adherent Jurkat T-cells functionalized with ssDNA attached only to membranes functionalized with complementary DNA strands. Few bound cells were observed on a maleimide-capped sample that lacked DNA. The scale bar represents 50 µm. (b) The DNA anchored Ephrin-A1-YFP construct stimulated MDA-MB-231 cells. In these images, EphA2 was stained with an antibody after cell permeabilization and imaged with TIRF microscopy. The scale bar represents 10 µm.

DNA hybridization (Figure 3.1). In addition, only one layer of cells was visible on the sample containing complementary DNA, while out-of-focus cells were visible in all samples before rinsing.

Presentation of a functional ligand for a cell surface receptor confirmed the utility of membrane anchored DNA for protein presentation to cells. EphrinA1-YFP-His_{10}, which stimulates the EphA2 receptor when presented from a supported membrane,[2] was linked to NTA_3-DNA.[3] This conjugate was subsequently hybridized to a supported membrane functionalized with complementary DNA. Fluorescence signal from the YFP portion of the protein-DNA conjugate confirmed the membrane bound presence of the protein and FRAP analysis confirmed lateral mobility of the anchored protein. MDA-MB-231 cells were incubated with the EphrinA1-functionalized bilayers for 1 h, fixed with paraformaldehyde solution, and stained with an anti-EphA2 antibody. Analysis by total internal reflection fluorescence (TIRF) microscopy, which illuminates only the interface between the cell and the substrate, showed colocalization of the membrane-bound EphA2 receptors with EphrinA1 (Figure 3.1), as expected from previous reports using biotin-streptavidin interactions or metal chelation.[2,4]

Section 3.2: Epidermal growth factor conjugation strategies

Epidermal growth factor (EGF) is a small protein with several disulfide bonds that can be expressed recombinantly in *E. coli*. It is commercially available in milligram quantities and can also be purchased with small molecule modifications specific to the N-terminus, according to the manufacturer. Site specific conjugation to PEG by reductive amination has been reported,[5] but required long reaction times and very high concentrations of substrate. The N-terminus is an attractive target for binding, since the N-terminus is distant from the receptor binding domain and selective modification of the N-terminus with a macromolecule has been shown to have little effect on biological activity.[6]

Site selective labeling of N-termini is plausible on small proteins with few lysines, since the pKa of lysine differs greatly from that of the N-terminus. Still, the value of the pKa of a given lysine on a protein is difficult to predict, it may be influenced by other nearby residues on the folded protein. To evaluate the success of this strategy, we added varying numbers of equivalents of an NHS-maleimide crosslinker to EGF, quenched the reaction with β-mercaptoethanol, and characterized the product by MALDI-TOF MS (Figure 3.2). In order to take advantage of the difference in pKa of the two species most effectively, various pH conditions for the reaction were explored. When treating EGF with the NHS reagent at pH 8, little specificity was observed. Adding 0.5 equivalents of the reagent yielded one modification, but increasing the number of equivalents to 2.5 resulted in multiple modifications of the protein. In phosphate buffer at pH 6.5, a similar lack of specificity was observed. Upon addition of one equivalent of the reagent, unmodified, singly, and doubly modified proteins could be observed. Adding five equivalents resulted in very little unmodified or singly modified protein, and most had two or three reagent adducts, suggesting that little to no specificity can be obtained by exploiting the difference in pKa between the N-terminus and the lysine residues on EGF. Still, acylation was effective in allowing DNA conjugation to EGF, which seemed to retain at least some activity. Additionally, other researchers have also used membrane anchored EGF with multiple amine group modifications.[7,8]

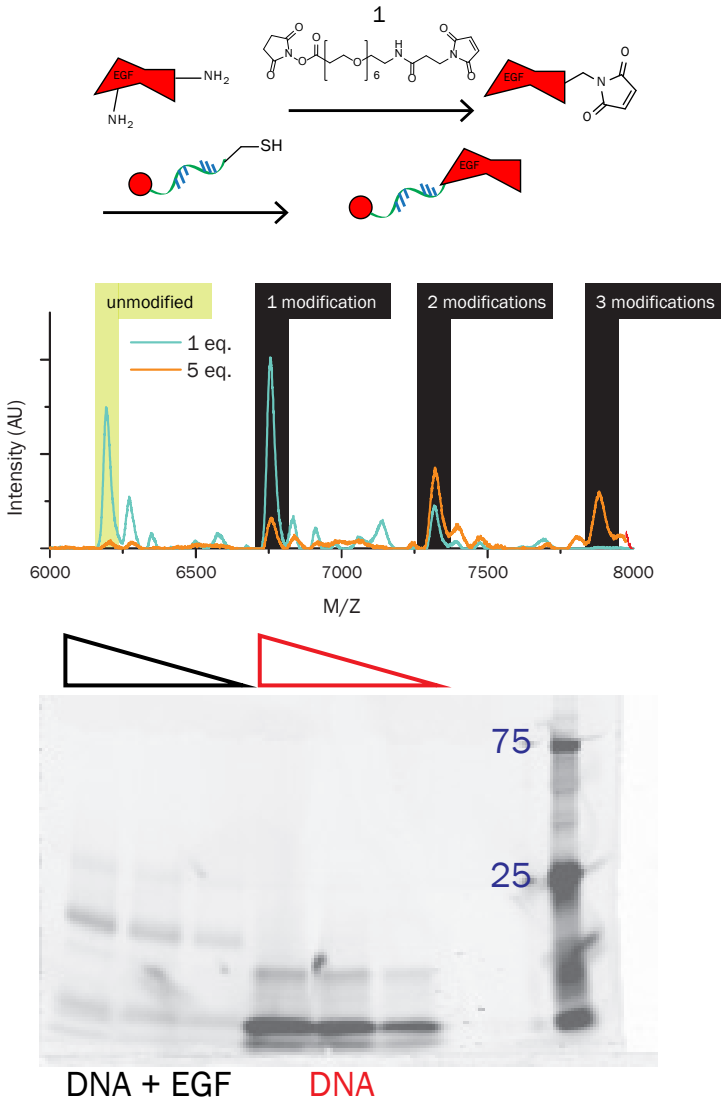

Figure 3.2. Modification of EGF with NHS-maleimide cross-linker. (a) Schematic of DNA conjugation using an NHS-maleimide cross-linker and fluorescently labeled thiol-DNA. (b) MALDI-TOF analysis shows that EGF treated with 1 (blue) or 5 (orange trace) the NHS-maleimide cross-linker (1) at pH 6.5 is not likely to be modified preferentially at the N-terminus, and that even at this low pH, all of the lysine residues can be acylated (c) Serial dilutions of reduced, thiol terminated, Cy3 labeled DNA that was treated with or without EGF-maleimide.

In order to explore the possibility of modifying the N-terminus of EGF site selectively, we evaluated transamination strategies using pyridoxal-5'-phosphate (PLP)[9,10] and *N*-methylpyridinium carboxaldehyde (*N*-PyC, also referred to as "Rapoport's salt").[11] For preliminary evaluation of the efficiency of these strategies, incubation with PLP or *N*-PyC was immediately followed with addition of a large excess of *O*-benzylhydroxylamine (Bn-ONH_2), and incubated overnight. Analysis of the reaction was performed by MALDI-TOF mass spectrometry (Figure 3.3).

Initial observations using PLP were promising, but the conversion observed seemed to reach

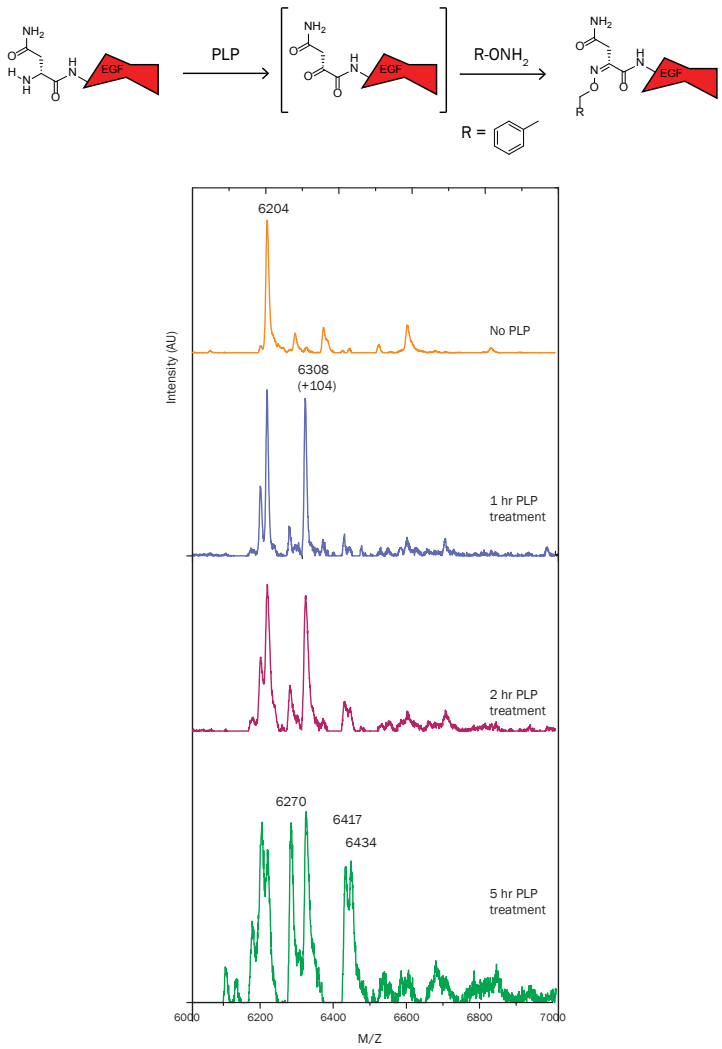

Figure 3.3. PLP mediated transamination of EGF. MALDI-TOF analysis of EGF treated with PLP for indicated times and then treated with Bn-ONH_2, which results in the +104 mass shift.

a maximum level of less than 50%, and optimization of the reaction time with the transamination reagent failed to increase the yield. Reaction conversion was evaluated by treating EGF with PLP for the time indicated, and then treating the mixture with Bn-ONH_2 (Figure 3.3). Increasing reaction time to two hours from one hour showed no increase in the final yield of reactive material, as measured by conversion of the starting material to the product of condensation with Bn-ONH_2. Increasing the reaction time further resulted in formation of at least one side product and still no observable increase in the final yield of product.

Transamination with *N*-PyC resulted in higher conversion, as measured by a similar MALDI-TOF MS assay of addition of Bn-ONH_2 mass (Figure 3.4). Side product formation with *N*-PyC was minimal when transamination time was limited to 1 h. Upon overnight incubation (> 12 h) however, several additions of the reagent were observed by MS. These likely corresponded to imine formation with the N-terminus of the protein and the lysine residues. Curiously, a mass reduction corresponded to the loss of the first amino acid of EGF (Asn) was also observed, even during short exposure to *N*-PyC. Relatively higher conversion to this

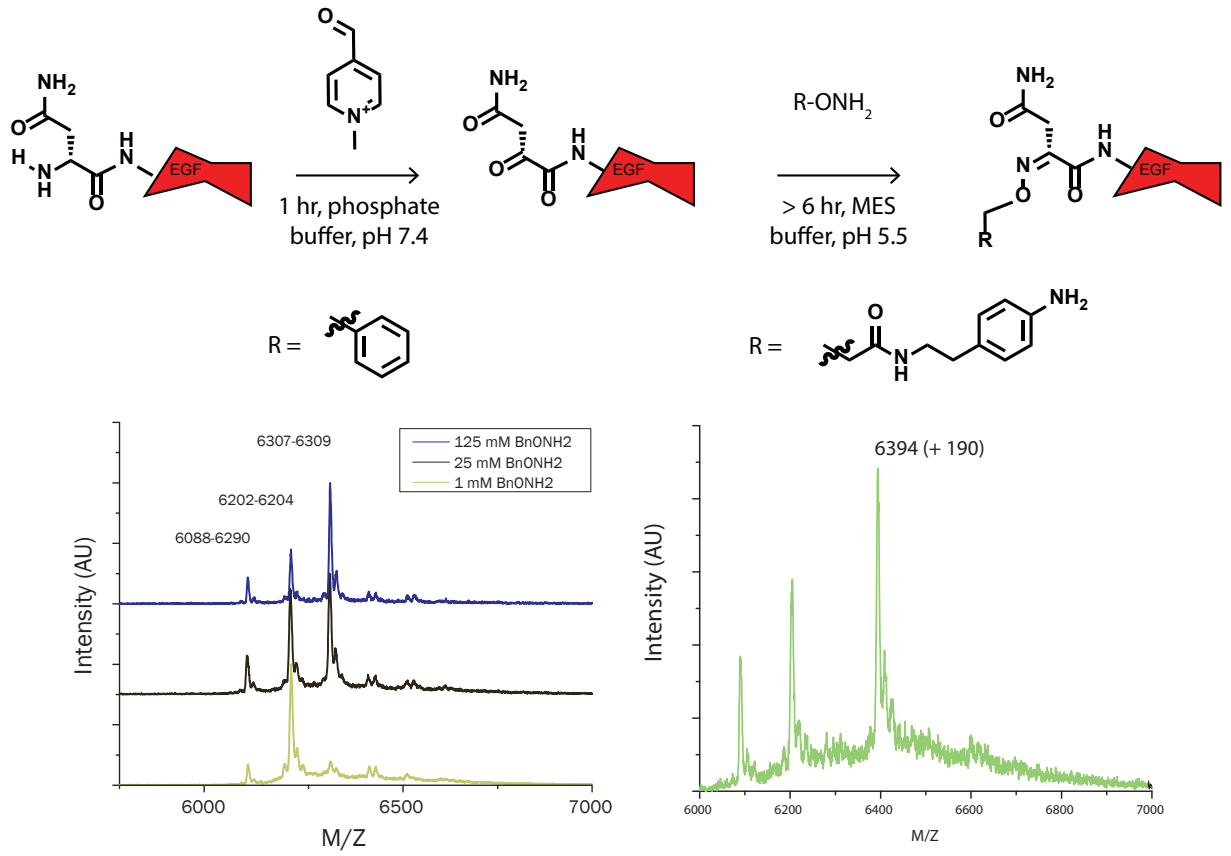

Figure 3.4. Scheme depicting transamination with and oxime formation with *N*-PyC ("Rapoport's salt"). Treatment of transaminated EGF with (left) Bn-ONH_2 and aniline-ONH_2 resulted in formation of product, as determined by MALDI-TOF MS.

side product was observed during longer incubation times with the transamination reagent. These adducts were, disturbingly, identical in mass difference to the desired oxime adduct. Several pieces of evidence suggested that the mass adduct corresponded to desired product, such as the dependence of conversion on concentration of Bn-ONH_2 and the lack of any adduct after short incubation times. To confirm, the transaminated protein was incubated with the alkoxyamine reagent (1) shown in Figure 3.4. The product of this reaction was observed to have a higher mass (+ 190), corresponding to the higher mass of the hydroxylamine reagent.

This work demonstrates that the transamination of EGF may be a promising way to site allow site selective conjugation of DNA to this protein. Still, this strategy is still under development and the non-site selective strategy described above (Figure 3.2) was used for further studies.

Section 3.3: Directing signal cluster composition with heterodimeric structures

The ability to direct molecules into signaling clusters was demonstrated using epidermal growth factor (EGF) presented to MDA-MB-231 cells. While EGF is a soluble ligand, presentation to cells from a membrane surface results in visible clustering of the ligand.[8,12] Upon

conjugation to Cy3-labeled DNA (Figure 3.2), hybridization of the conjugate to DNA functionalized membranes, and presentation to MDA-MB-231 cells, clustering of EGF and phosphorylation of EGFR were observed (Figure 3.5). A Fab' fragment that has no binding target on the cell membrane was not observed to undergo any change in localization caused by the cell. Presentation of a heterodimer of these molecules resulted in clustering of both, and no evidence of disruption of receptor phosphorylation was observed. These observations demonstrate that colocalization between anchored molecules can be directed independently of any inherent propensity of these molecules to colocalize.

We plan to use this system to investigate proximity effects on receptor tyrosine kinase signaling, specifically in the EphA2 and EGFR signaling pathways. To provide extra stability to the EphrinA1-DNA conjugate, we designed, expressed, and purified an EphrinA1-SNAPtag fusion and conjugated this molecule to DNA (Figure 3.6), similar to strategies used in other studies.[13,14] EGF and EphrinA1 DNA conjugates were presented to MDA-MB-231 cells, which express both EGFR and EphA2 (Figure 3.7). While the size of a DNA heterodimer is well below the diffraction limit, differences in colocalization between samples containing monomeric ligands and samples containing dimeric ligands could be observed (Figure 3.7), suggesting that differences in receptor colocalization could be observed using immunofluorescence.

These cells were fixed, permeabilized and stained for pTyr-1173 on EGFR. Analysis of fixed cells showed a difference in colocalization (Figure 3.7) between monomer and heterodimer presented samples. Since variations in the ligand distribution could be seen, we also expected to see differences in receptor distribution between cells presented with monomeric ligand and those presented with dimeric ligand. Upon staining the cells with an antibody against phosphotyrosine 1173 (pY-EGFR) on the EGFR receptor, both colocalization measurements

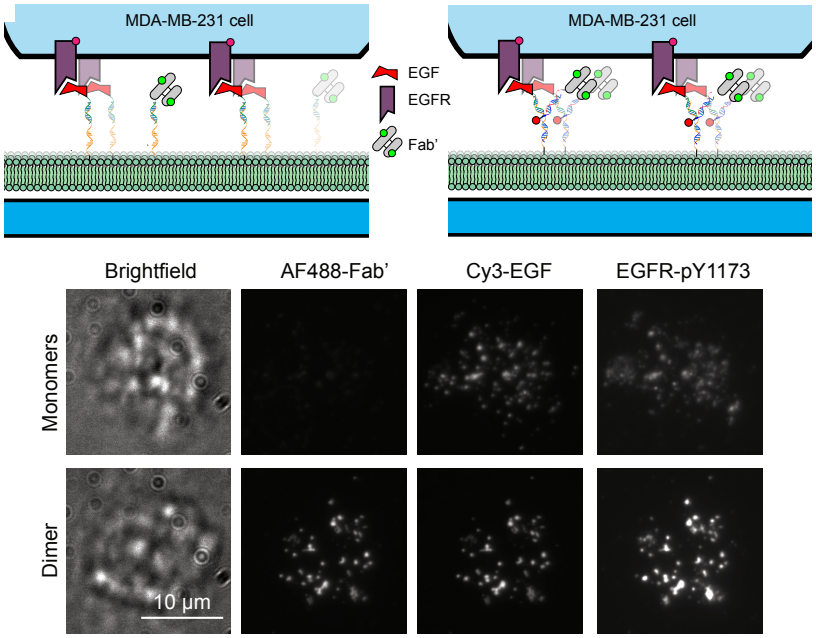

Figure 3.5. Heterodimeric protein complexes of EGF and an inert Fab' fragment remain intact during interaction with MDA-MB-231 cells. Phosphorylation of the EGFR receptor is observed in both cases. The scale bar represents 10 µm.

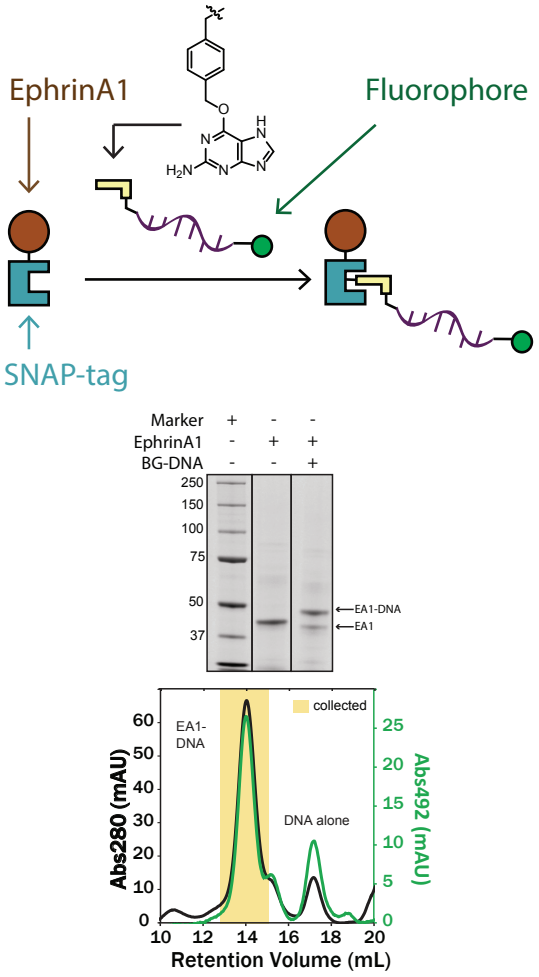

Figure 3.6. Conjugation of benzyl guanine modified DNA to EphrinA1-SNAP tag fusion protein. The results of the reaction were analyzed by SDS-PAGE gel electrophoresis and stained with Sypro Ruby stain. Black lines enclose gel lanes that were not adjacent in the original image of the gel. The molecular weight of the markers in kD is indicated by the numbers to the left of the marker bands. Gel lanes show EphrinA1-SNAP tag conjugate before and after treatment with benzylguanine (BG) DNA. The intended product was purified by size exclusion chromatography and the shaded area was collected.

decreased, which was likely caused by incomplete antigen staining and some amount of nonspecific binding. Colocalization between the EphrinA1 ligand and the EGFR receptor was considerably increased for cells presented with a heterodimer, demonstrating that the EGFR is binding ligand and recruiting the EphrinA1 molecule. This observation suggests that the heterodimer is able to interact with the EGFR receptor and that ligand-receptor binding is preserved. A similar experiment measuring the colocalization of EGF with EphA2 demonstrated that the EphrinA1 ligand is also capable to bind its receptor (Figure 3.8). A diagram of the data analysis steps performed using Matlab and CellProfiler[15] is shown in Figure 3.9.

These experiments demonstrate the ability to change the composition of large signaling clusters, but do not provide sufficient evidence to conclude that both ligands on a single heterodimer can, non-exclusively, bind their target receptors. Answering this question definitively by immunofluorescence is unlikely, since incomplete or mutually exclusive antibody binding would artifactually decrease colocalization measurements. Additionally, the resolution of this technique is too low to resolve individual dimers. In order to address this possibility more definitively, future work will measure FRET between fluorescent protein fusions of these RTKs in response to heterodimers at varying surface densities and with different linker flexibilities.

Section 3.4: Chapter 3 experimental

Synthesis of tris-NTA-modified Oligonucleotides

We prepared tris-NTA-modified DNA strands as described in the literature.[6] DNA with three amino groups at the 5' end was obtained from IDT or Eurofins MWG operon. The 5' end was modified with two Uni-link amino modifiers

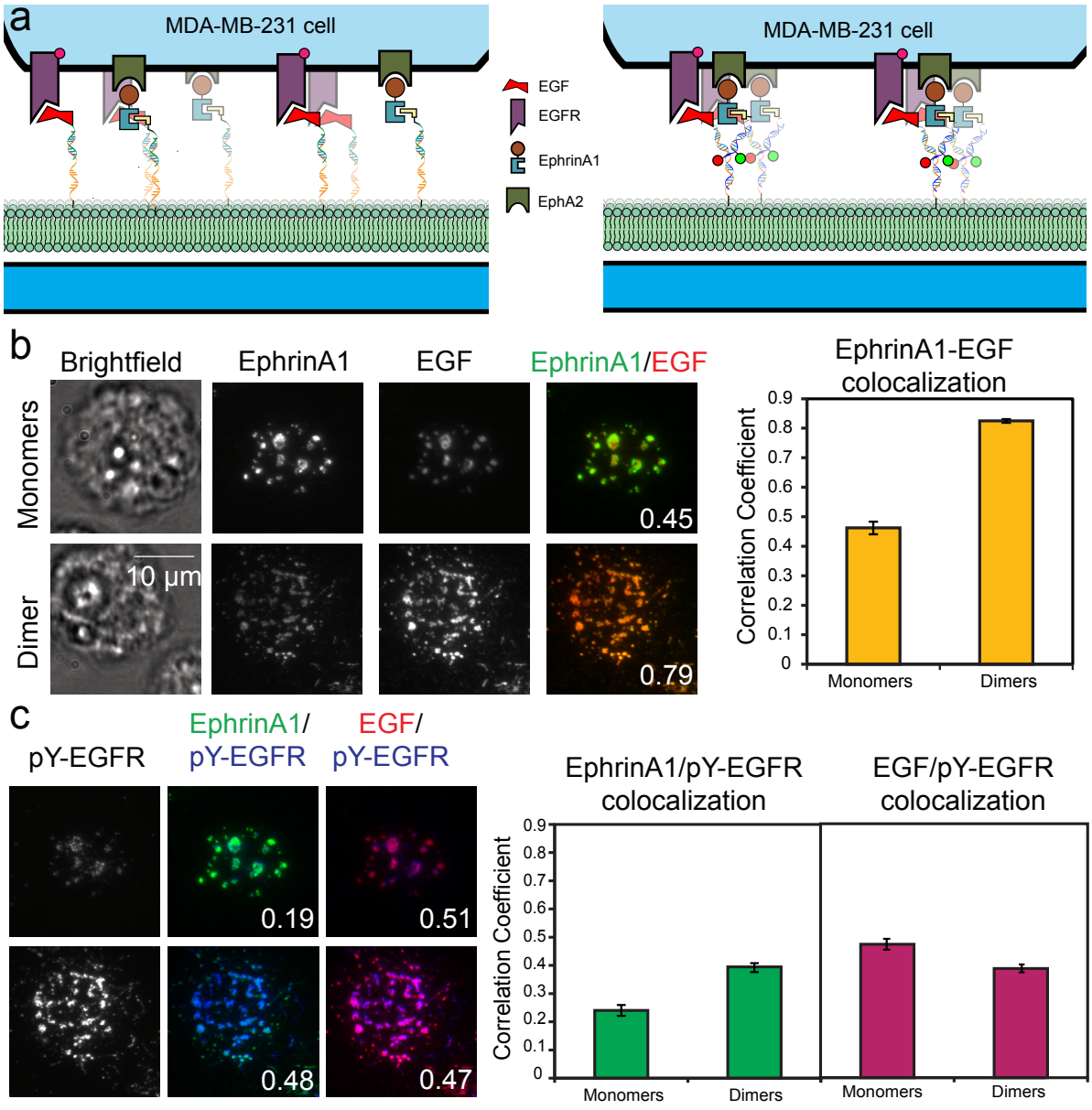

Figure 3.7. Alteration of receptor localization in cells. (a) MDA-MB-231 cells were deposited on supported membranes containing DNA bearing monomeric or dimeric ligand. (b) TIRF microscopy analysis demonstrates that the ligands appear segregated when presented as monomers but colocalized when presented as dimers. Colocalization was measured as the correlation coefficient in the EphrinA1 clusters, and is described in more detail in the Supporting Information. (c) Immunofluorescence staining of pTyr1173 residue on EGFR of the cells in (b) shows that the receptor localization is altered by presentation of these ligands. The scale bar represents 10 μm and the error bars depict the standard error of the mean. (monomers: N_{cells} = 87, dimer: N_{cells} = 137. Numbers inset in the example images denote the actual correlation coefficient of the two channels shown in that particular image.

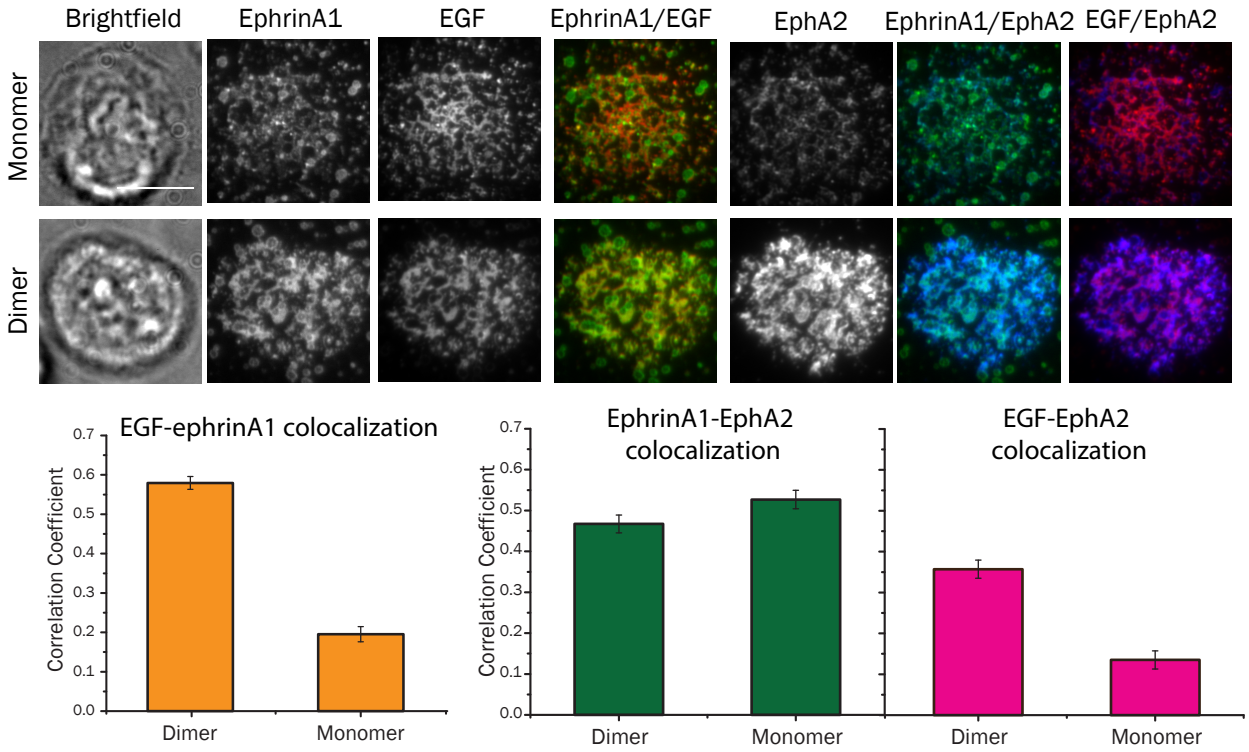

Figure 3.8. EphrinA1-EphA2 binding in heterodimers. A similar experiment to that described in Figure 3.7 was performed to evaluate the ability of EphrinA1 to bind EphA2. (a) Ligand heterodimerization is evinced by the overlay of fluorescence intensity EphrinA1 and EGF. The correlation coefficient was determined for a population of cells. These values for monomer and dimer treated cells are compared on the graph. The scale bar represents 10 μm. (b) Staining for receptor demonstrates localization of EGF with EphA2 only when the EGF is presented as a heterodimer with EphrinA1, suggesting that the EphrinA1 ligand is binding its cognate receptor. Colocalization was analyzed over a population of cells (dimer, N_{cells} = 62; monomers, N_{cells} = 97) as the correlation coefficient, shown on the graph. Error bars represent the standard error of the mean. Large EphrinA1 aggregates can be seen in both channels and do not seem to bind receptors on the cell, as deduced from lack of colocalization with regions of EphA2 staining. These regions were excluded from colocalization analysis.

and one C6-amino modifier. It was dissolved in water to 0.2 mM. 50 μL of this solution was filtered through a Micro Bio-Spin 6 column that was equilibrated with phosphate buffer (100 mM sodium phosphate, 100 mM NaCl, pH 7.3). 50 μL of the filtered tris-amine DNA was incubated with 12.5 μL of 50 mM SPDP that was freshly dissolved in DMSO for one hour at room temperature. A second Micro Bio-Spin 6 column was used to filter the sample of DNA product to remove excess SPDP. The eluent was treated with 6.25 μL of 100 mM TCEP for fifteen minutes at room temperature to reduce the disulfide bonds, resulting in a DNA product with three thiol groups at the 5' end. This product was treated with 7 μL of 50 mg/mL maleimide-NTA dissolved in phosphate buffer and incubated at room temperature for one hour. The resulting tris-NTA-modified DNA was filtered with a Micro Bio-spin 6 column and frozen. The resulting DNA product was purified by reverse phase liquid chromatography and HPLC under similar conditions to those described for the fluorophore conjugates. Crude and purified products were characterized by MALDI-TOF mass spectrometry. Similar results were

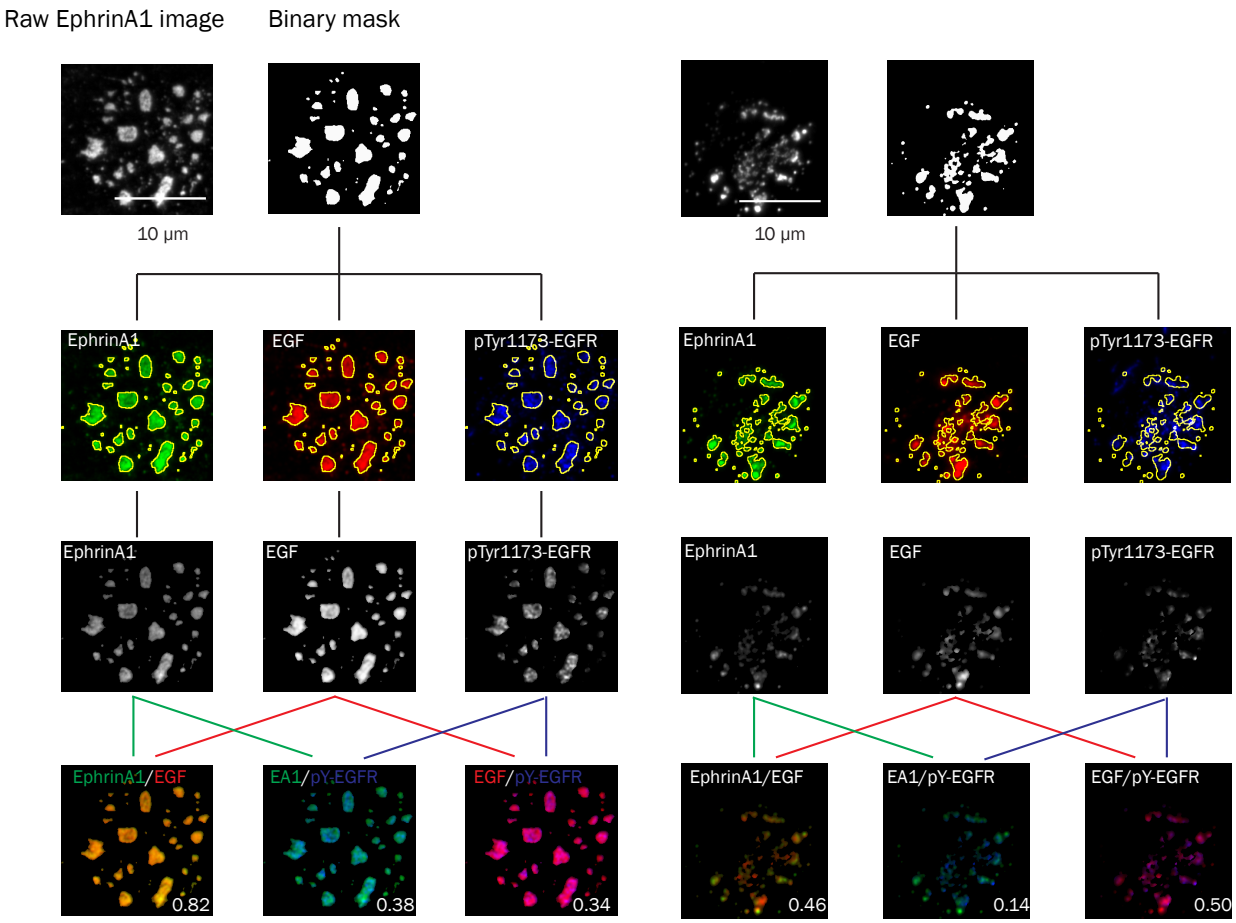

Figure 3.9. Data analysis scheme for colocalization calculation in Figures 3.7 and 3.8. EphrinA1 images were used to determine the positions of clusters by automatic thresholding to create a binary mask. The mask was applied to the raw images (yellow outline on color image, row 2) so that all intensity outside the mask was deleted, leaving the masked images in row 3. The colocalization analysis was done between these images. Overlays of these representative images (representative images are chosen for close similarity in their correlation coefficient scores to that of the cell population means in all channels) are shown in row 4. The overlays in the figures are of minimally processed unmasked images.

also obtained if ethanol precipitation was used to desalt samples instead of using the gel filtration spin columns.

Jurkat cell immobilization

Jurkat cells were grown in RPMI-1640 medium with 10% fetal bovine serum and 1% penicillin/streptomycin. Supported membranes were prepared as described above in 96 well plates with 20mer DNA either complementary (sequence 1 + FAM) or non-complementary (sequence 3) to the DNA that would be functionalized on the Jurkat cells. Other bilayers were also left unmodified.

NHS-DNA was prepared as described in a previous study.[1] Briefly, thiol modified DNA (5'- Thi-

ol-seq1') that was reduced and stored in the presence of TCEP was desalted in a PBS equilibrated NAP-5 column. NHS-PEO_6-maleimide was added to a final concentration of 330 μM and incubated for 5 minutes. This reaction was also desalted in a PBS equilibrated NAP-5 column. Media was removed from cells and they were rinsed with PBS. The cells were resuspended with the DNA reaction mixture and incubated for 30 min. They were then centrifuged and resuspended in medium. Micrographs of these cells were acquired on an Axiovert 200 M (Carl Zeiss, Thornwood, NY).

EGF transamination

With PLP: EGF was buffer exchanged into 50 mM phosphate buffer + 150 mM NaCl, pH 6.5 and treated with 100 mM PLP for the indicated time. Then, the solution was treated with 125 mM Bn-ONH_2 and analyzed by MALDI-TOF.

With *N*-pyridinium carboxaldehyde: EGF was buffer exchanged into 50 mM phosphate buffer, pH 7.4 with a 3 kDa molecular weight cutoff spin concentrator. *N*-PyC was added to 100 mM and the solution incubated at 37 °C for one hour, at which time the solution was observed to have a yellow color. The sample was then desalted with a NAP-5 column (the yellow color was removed upon desalting), concentrated, passed through another NAP-5 column, concentrated again, then treated with hydroxylamine compounds indicated in 2-(*N*-morpholino) ethanesulfonic acid buffer (MES), pH 5.5, and analyzed by MALDI-TOF.

MDA-MB-231 cell culture and activation

MDA-MB-231 human breast cancer epithelial cells were obtained from the ATCC (Manassas, VA). Those shown in Figure 3.1 were cultured in DMEM media supplemented with 10% fetal bovine serum, L-glutamine, and penicillin/streptomycin (Invitrogen, Carlsbad, CA). Prior to deposition on supported lipid bilayers, the cells were grown to 90% confluence, treated with 0.25% trypsin-EDTA (Invitrogen, Carlsbad, CA), centrifuged, counted, and added to each cell chamber. Cells in other figures were grown in the absence of antibiotics and dissociated with CellStripper (Mediatech, Manassas, VA) instead of trypsin.

For the activation of EphA2, the cells were prepared as above. Supported membranes were also prepared and functionalized as described in the section above, with the following differences: BBS was used instead of PBS to ensure compatibility of this higher pH buffer with cell experiments. After functionalization with DNA, excess maleimides were quenched with 5 mM β-mercaptoethanol for 5 min and blocked with 0.1% BSA for 30 min. Before cells were added, the buffer was exchanged with cell media. EphrinA1-YFP-His_{10} was linked to NTA_3-DNA (sequence 3) by mixing protein (final concentration ~5 μM), DNA (final concentration ~1.5 μM) and Ni^{2+} (final concentration 1 mM). EphrinA1-YFP-His_{10} was prepared as described in a previous study. Briefly, it was produced in HEK-293T cells transiently transfected with a plasmid encoding the gene for this protein.[2] The protein was isolated from the supernatant of the transfected cells after four days and purified by immobilized metal affinity chromatography with a Ni-NTA resin.

Cells were incubated for 1 hour, fixed with 4% paraformaldehyde and permeabilized with 0.1% Triton-X. A polyclonal rabbit anti-EphA2 antibody (Santa Cruz Biotechnology, Santa Cruz,

CA) and an Alexa Fluor 647 anti-rabbit secondary antibody (Invitrogen, Carlsbad, CA) were used to visualize the receptor. A similar procedure was used for the cells analyzed in Figure 3.7, but the primary antibody used for staining targeted a phosphopeptide of the EGFR protein (ab5652, Abcam). Alexa Fluor 568 conjugated secondary antibody was used to stain the samples shown. The cells in Figure 3.8 were stained with a monoclonal mouse anti-EphA2 antibody (clone D7). Similar results were obtained with the antibody described above as well.

EprhinA1-SNAP-tag expression and purification

The gene encoding the EphrinA1 ectodomain was cloned into a pFastBac vector containing the SNAPtag and His10 sequences and introduced into the bac-to-bac insect cell/baculovirus based expression system (Invitrogen) according to manufacturer's direction and standard cloning procedures. The protein was secreted from infected Sf9 cells and captured on Ni-NTA resin (Qiagen). The resin was washed and the protein was eluted using an imidazole gradient.

Synthesis of benzylguanine/fluorophore tagged DNA and EphrinA1-SNAPtag-DNA conjugates

The following sequences were purchased from IDT:

5'– Thiol – seq2' – Amine – 3'
5' – Amine – seq3' – Thiol – 3'

The solutions were dissolved in TE buffer and before use were ethanol precipitated, then redissolved in water. Both samples were diluted to 0.54 – 0.55 mM in PBS buffer with 50 mM sodium bicarbonate added. Alexa Fluor 488 Carboxylic Acid, 2,3,5,6-Tetrafluorophenyl Ester was added to 10 fold excess and incubated overnight at room temperature. Most of the free dye was removed by ethanol precipitation, the samples were resuspended in 5 mM TCEP in 100 mM HEPES buffer, and incubated for 90 minutes at 37 ºC. The samples were desalted with a Biospin 6 column equilibrated in 50 mM phosphate buffer with 150 mM NaCl, pH 7.4. Benzyl-guanine maleimide (New England Biolabs, Ipswich, MA) that had been dissolved in anhydrous *N,N'*-dimethylformamide (Solulink) was added to 10-fold excess. Excess maleimide reagent was removed by desalting in a NAP-5 column and the eluent was ethanol precipitated, then resuspended in TE buffer.

EphrinA1-SNAP tag protein frozen aliquots were thawed and buffer exchanged into PBS with 1 mM cysteine-HCl. Benzyl guanine-fluorophore oligonucleotides prepared as described above were added to 1-2 molar equivalents and incubated for 60-120 min at 37 ºC. The samples were then typically stored at 4 ºC overnight, which may have increased the yield, but this possibility was not thoroughly investigated. The reactions were filtered through a 0.22 µm filter and injected on a Superdex 200 size exclusion column. Representative chromatography and SDS-PAGE analyses are shown in Figure 3.6.

EGF-DNA synthesis

Doubly modified 5'-C6 thiol and 3'-C6 amine DNA was labeled with Cy3 or Cy5 NHS ester (GE

healthcare), desalted with a NAP-5 column, and ethanol precipitated. Conversion was measured by fluorophore absorbance compared to the expected absorbance of the DNA. The DNA was treated with 2 mM TCEP for 90 minutes at 37 °C. Recombinant human EGF (Invitrogen) was dissolved in PBS with 10% glycerol and stored in the freezer. Before use it was thawed and buffer exchanged into PBS and treated 2 equivalents of NHS-PEO_6-maleimide (Pierce). The reaction proceeded for 1 hour and the sample was desalted with a NAP-5 column. The reduced thiol DNA was also desalted in a NAP-5 column and all were concentrated in Amicon 3 kDa MWCO concentrators (Millipore). The samples were mixed and incubated for 3 hours at room temperature, then stored at 4 °C. The samples were analyzed by SDS-PAGE under reducing conditions, as shown in Figure 3.5.

Image analysis

Images in figure 5 were analyzed for colocalization within defined regions of interest. Colocalization analysis was otherwise affected by the general enrichment of labels under the cell and low correlation in other regions, giving artifactually high correlation between all pairs. Using home-written scripts in MATLAB, cells were chosen using the brightfield images in a given dataset and images in the fluorescence channels were cropped according to this region of interest. Additionally, the full images were loaded, and background was found and removed using morphological filtering (strel, using the “disk” operator). Objects were found by automatic threshold selection then by creating a binary mask for regions above the threshold (Figure 3.9). These masks were saved and used by CellProfiler[15] to mask all fluorescence channels, which excluded other regions of the image from further analysis. Colocalization analysis was performed using the Pearson’s correlation module in CellProfiler (MeasureCorrelation). The mean of these measurements ± SEM for the indicated cell populations are shown in Figure 3.7 and 3.8.

Section 3.4: Chapter 3 references

(1) Hsiao, S. C.; Shum, B. J.; Onoe, H.; Douglas, E. S.; Gartner, Z. J.; Mathies, R. A.; Bertozzi, C. R.; Francis, M. B. *Langmuir* **2009**, *25*, 6985–91.
(2) Xu, Q.; Lin, W.-C.; Petit, R. S.; Groves, J. T. *Biophysical journal* **2011**, *101*, 2731–9.
(3) Goodman, R. P.; Erben, C. M.; Malo, J.; Ho, W. M.; McKee, M. L.; Kapanidis, A. N.; Turberfield, A. J. *ChemBioChem* **2009**, *10*, 1551–7.
(4) Salaita, K.; Nair, P. M.; Petit, R. S.; Neve, R. M.; Das, D.; Gray, J. W.; Groves, J. T. *Science* **2010**, *327*, 1380–5.
(5) Lee, H.; Jang, I. H.; Ryu, S. H.; Park, T. G. *Pharmaceutical Research* **2003**, *20*, 818–825.
(6) Lee, H.; Park, T. *Pharmaceutical research* **2002**, *19*, 845–851.
(7) Stabley, D. R.; Jurchenko, C.; Marshall, S. S.; Salaita, K. S. *Nature methods* **2012**, *9*, 64–7.
(8) Stabley, D.; Retterer, S.; Marshall, S.; Salaita, K. *Integrative biology* **2013**.
(9) Scheck, R. a; Francis, M. B. *ACS chemical biology* **2007**, *2*, 247–51.
(10) Witus, L. S.; Moore, T.; Thuronyi, B. W.; Esser-kahn, A. P.; Scheck, R. A.; Iavarone, A. T.; Francis, M. B. *Journal of the American Chemical Society* **2010**, 16812–16817.
(11) Witus, L. S. Optimization Of Protein Bioconjugation Reactions Using Combinatorial

Peptide Libraries, University of California, Berkeley, 2012.
(12) Nam, J.-M.; Nair, P. M.; Neve, R. M.; Gray, J. W.; Groves, J. T. *ChemBioChem* **2006**, *7*, 436–40.
(13) Jongsma, M. A.; Litjens, R. H. G. M. *Proteomics* **2006**, *6*, 2650–5.
(14) Saccà, B.; Meyer, R.; Erkelenz, M.; Kiko, K.; Arndt, A.; Schroeder, H.; Rabe, K. S.; Niemeyer, C. M. *Angewandte Chemie (International ed. in English)* **2010**, 9378–9383.
(15) Kamentsky, L.; Jones, T. R.; Fraser, A.; Bray, M.-A.; Logan, D. J.; Madden, K. L.; Ljosa, V.; Rueden, C.; Eliceiri, K. W.; Carpenter, A. E. *Bioinformatics* **2011**, *27*, 1179–80.

Chapter 4

Section 4.1: Introduction

Protein based viral capsids have been recognized as attractive scaffolds for nanoscale assembly[1–4] since they are made from nanometer sized monomers that assemble into functional units that range in size from tens of nanometers to microns. The individual monomers can be chemically modified in specific locations,[5] adding further functionality and enabling the incorporation of these structures with synthetic molecules and materials. These hybrid materials enjoy the benefits of both the precise nanoscale architecture of biomolecules, and the diverse functionalities afforded by small molecules and inorganic nanoparticles.

Metal nanoparticles have been used extensively in modulating the photophysical properties of organic fluorophores. Gold nanoparticles of various sizes have been implicated in quenching fluorophores, both as a function of distance and through contact quenching.[6–9] Larger (>30 nm) gold nanoparticles can enhance the brightness of an organic fluorophore[10,11] by enhancing the radiative decay rate of the excited fluorophore. Experimental studies at intermediate size regimes, though, have demonstrated mixed results, with some studies reporting quenching,[12,13] and some reporting enhancement.[14–16]

We believe that some of the reasons for these discrepancies result from the difficulty of maintaining a fluorophore in close proximity to an AuNP while preventing contact of that fluorophore with the nanoparticle surface. Additionally, the measurement of small enhancement value is technically challenging in bulk since gold nanoparticles, which have considerably higher molar extinction coefficients than organic fluorophores, absorb both excitation and emission light. We address these challenges by assembling a hollow viral capsid around 10 nm gold nanoparticles, spacing organic fluorophores from the outside of the capsid with DNA oligonucleotides, and measuring fluorescence enhancement of single viral capsids using total internal reflection fluorescence (TIRF) microscopy.

Section 4.2: Encapsulation of AuNPs with the MS2 bacteriophage and conjugation of DNA strands

This work described in this section was entirely performed by Stacy Capehart and Jeff Glasgow, but I will describe it here briefly.

Disassembly and reassembly of MS2 has been demonstrated by other groups,[17,18] and our group has developed an osmolyte based method for protein encapsulation.[19] This approach was adapted for the reassembly of AuNPs, and was found to encapsulate AuNPs 5-20 nm in

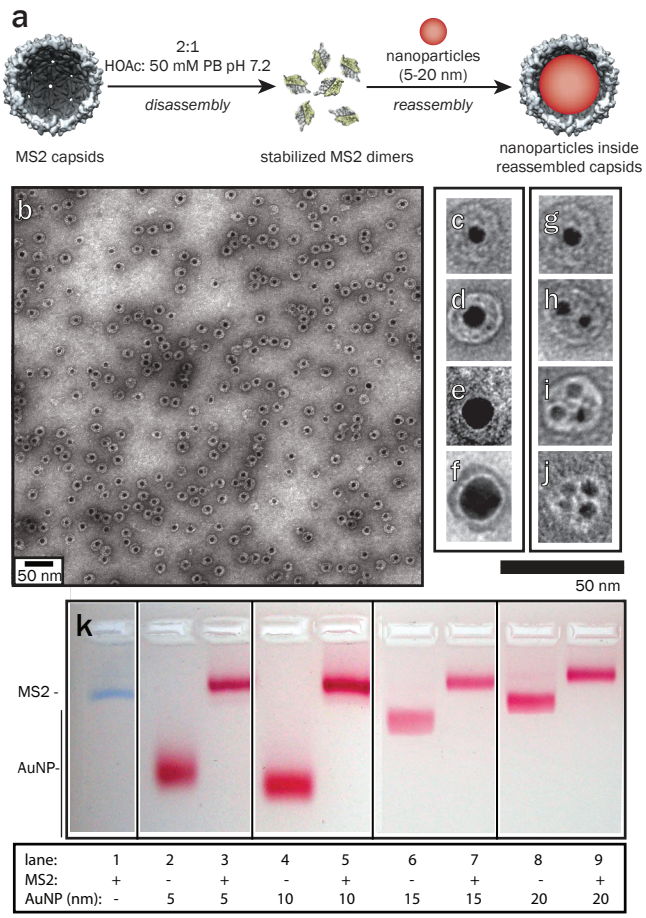

Figure 4.1. (a) T19pAF MS2 subjected to reassembly conditions in the presence of different sizes and concentrations of AuNPs. Transmission electron micrograph images of T19pAF MS2 reassembled around (b) 10 nm AuNPs, (c) 5 nm AuNPs, (d) 10 nm AuNPs, (e) 15 nm AuNPs, (f) 20 nm AuNPs, (g) one 5 nm AuNP, (h) two 5 nm AuNPs, (i) three 5 nm AuNPs, and (j) four 5 nm AuNPs. The native gel shown in (k) demonstrates similar electrophoretic mobility for MS2 reassembled around different size AuNPs (lanes 3, 5, 7, and 9) as particle-free MS2 (lane 1). The electrophoretic mobilities of the reassembled samples are different than their corresponding free AuNPs (lanes 2, 4, 6, and 8, respectively).

diameter as shown by transmission electron microscopy (TEM, Figure 4.1). Additionally, multiple AuNPs that were 5 nm in diameter could be incorporated into a single capsid. Native agarose gel electrophoresis could be used to monitor the assembly of encapsulation by their electrophoretic mobility.

For our initial studies involving fluorophores, MS2 capsids containing 10 nm AuNPs were selected. As reported by another group using a similar viral capsid system, 10 nm AuNPs encapsulated most efficiently, resulting in the fewest unencapsulated AuNPs and empty viral capsids. DNA strands were conjugated to *p*-amino-phenylalanine residues on the exterior surface of the MS2 capsid by a previously characterized oxidative coupling reaction[5,20–22] with aminophenol terminal DNA. This artificial amino acid was incorporated into the MS2 coat protein by amber stop codon suppression.[5,23] The preserved structure of the capsid was confirmed by TEM, dynamic light scattering and fluorescence correlation spectroscopy (Figure 4.2c). TEM analysis was used to determine the percentage of viral capsids containing AuNPs after reassembly and modification with DNA. Most of the assemblies consisted of capsids containing a single nanoparticle (77.2%), while capsids without AuNPs accounted for a few of the observed structures (2.7%). Unencapsulated AuNPs (6.6%) and potentially malformed capsids (13.5%) comprised the remaining particles.

Modification of the capsid proteins was quantified by SDS-PAGE (Figure 4.2b) and showed identical modification of the AuNP containing capsids when compared with their counterparts lacking AuNPs. The DNA modification was determined by optical densitometry to be ~60 strands per capsid (33%), ~45 strands per capsid (25%), and ~34 strands (19%) for 3, 12, and 24 bp hairpin sequences, respectively. Modification by different length DNA did not proceed to identical levels of modification, meaning that comparisons between samples with different lengths of DNA should be made cautiously, if at all.

Previous studies have shown that these conditions are compatible with the protein assembly and do not impair the hybridization ability of the DNA strands.[21] No effects were observed for

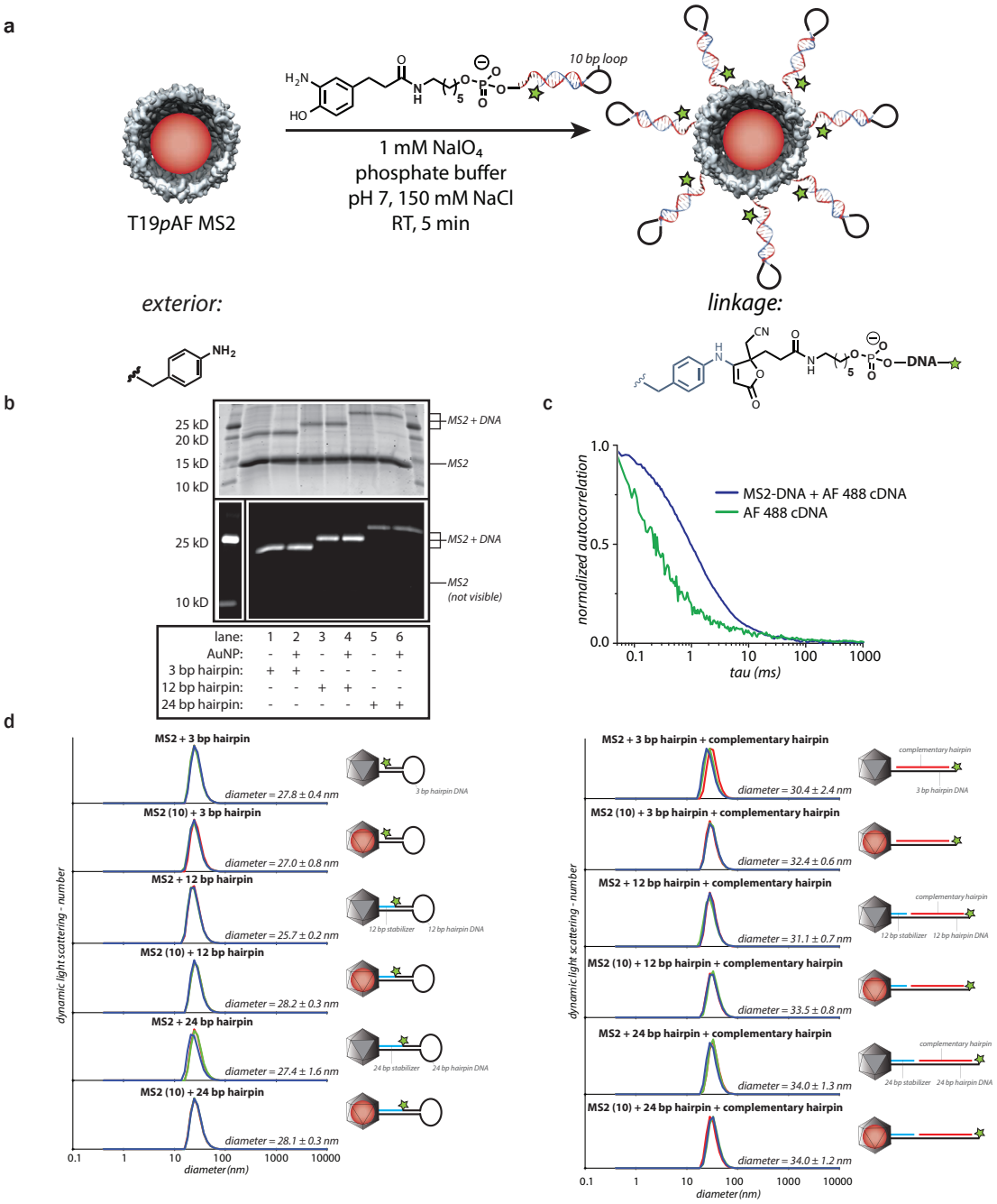

Figure 4.2 (a) Overall synthetic strategy for constructing fluorophore-AuNP conjugates. For exterior surface modification, dye-labeled aminophenol-containing DNA can be attached to exterior anilines on T19pAF MS2 using a $NaIO_4$-mediated oxidative coupling reaction. (b) SDS-PAGE analysis of capsid DNA conjugates. For quantification of modification by densitometry, see text. (c) Fluorescence correlation spectroscopy (FCS) analysis of MS2-DNA plus AF 488 cDNA as well as AF 488 cDNA. The FCS data suggest that the capsids were assembled and that few unhybridized AF 488 DNA strands remained in solution. (d) (*left)* Dynamic light scattering by number data for 3 bp hairpin MS2, 3 bp hairpin MS2 plus gold 12 bp hairpin MS2, 12 bp hairpin MS2 plus gold, 24 bp hairpin MS2, and 24 bp hairpin MS2 plus gold. (*right*) Dynamic light scattering by number for MS2 samples incubated with a complementary sequence that opened the hairpin for the constructs analyzed on the left.

the AuNPs as well, as judged by the retention of their surface plasmon band centered at 520 nm. The percent DNA modification of MS2 was quantified by SDS-PAGE gel electrophoresis using optical densitometry (Figure 4.2b), indicating similar modification levels for capsids with and without gold inside. Previous work exploring single silver nanoprisms indicated that maximum fluorescence enhancement occurs with a dye that has a fluorescence emission slightly red-shifted from their surface plasmon band.[24] The emission spectrum of AF488 directly overlaps with the surface plasmon resonance peak for 10 nm AuNPs, providing a close fit to this criterion. Excess fluorescently-labeled DNA was removed through successive centrifugal filtrations with multiple 100 kDa molecular weight cutoff spin filters and non-denaturing agarose gel electrophoresis. Fluorescence correlation spectroscopy (FCS, Figure 4.2c) and dynamic light scattering (DLS, Figure 4.2d) were used to characterize the resulting constructs. Each of these techniques suggested that the MS2 capsids were assembled, fluorescently labeled, and accompanied by few if any unattached fluorescently labeled DNA strands.

Section 4.3: Fluorescence enhancement from capsid encapsulated nanoparticles

To explore the distance dependence of the enhancement, the synthetic procedure was used with different fluorophore-DNA sequences to position the dyes 3 bp from the capsid (1 nm from protein, 9.5 nm from the AuNP), 12 bp from the capsid (4 nm from the protein, 12.5 nm from the AuNP), and 24 bp from the capsid (8 nm from the protein, 16.5 nm from the AuNP). For the 12 bp and 24 bp distances, additional stabilizing strands were included to ensure that rigid double stranded DNA separated the fluorophores from the surfaces. Stabilizing strands were not included for the 3 bp distance.[25]

Total internal reflection fluorescence (TIRF) microscopy was used to measure the fluorescence intensity of the individual capsids in the six resulting samples (three distances with one set containing gold and another set without gold). The MS2-AuNP-fluorophore samples were incubated with glass slides bearing DNA strands that were complementary to those attached to the capsids, leading to the capture of the particles. The TIRF microscopy setup and surface modification is described in detail in the experimental section. Once a reasonable surface density was reached, a set of TIRF images was collected for each sample. Images for samples with and without gold particles are shown in Figure 4.3, using identical scaling and acquisition parameters.

Each set of images was analyzed separately, and the results are shown in Figure 4.3. A distribution of intensities was anticipated due to the differences in the levels of fluorescence labeling between individual capsids. The data are represented as mean intensity histograms, allowing the average brightness per particle to be compared in the presence and absence of gold particles.

The data plotted in Figure 4.3 indicate a 2.2-fold enhancement for a 3 bp separation, a 1.2-fold enhancement for a 12 bp separation, and no effect was observed for a 24 bp separation when the gold particles were added to the capsids. Images were also collected using confocal microscopy. The confocal microscopy results agreed with the TIRF microscopy results and are shown in Figure 4.3.

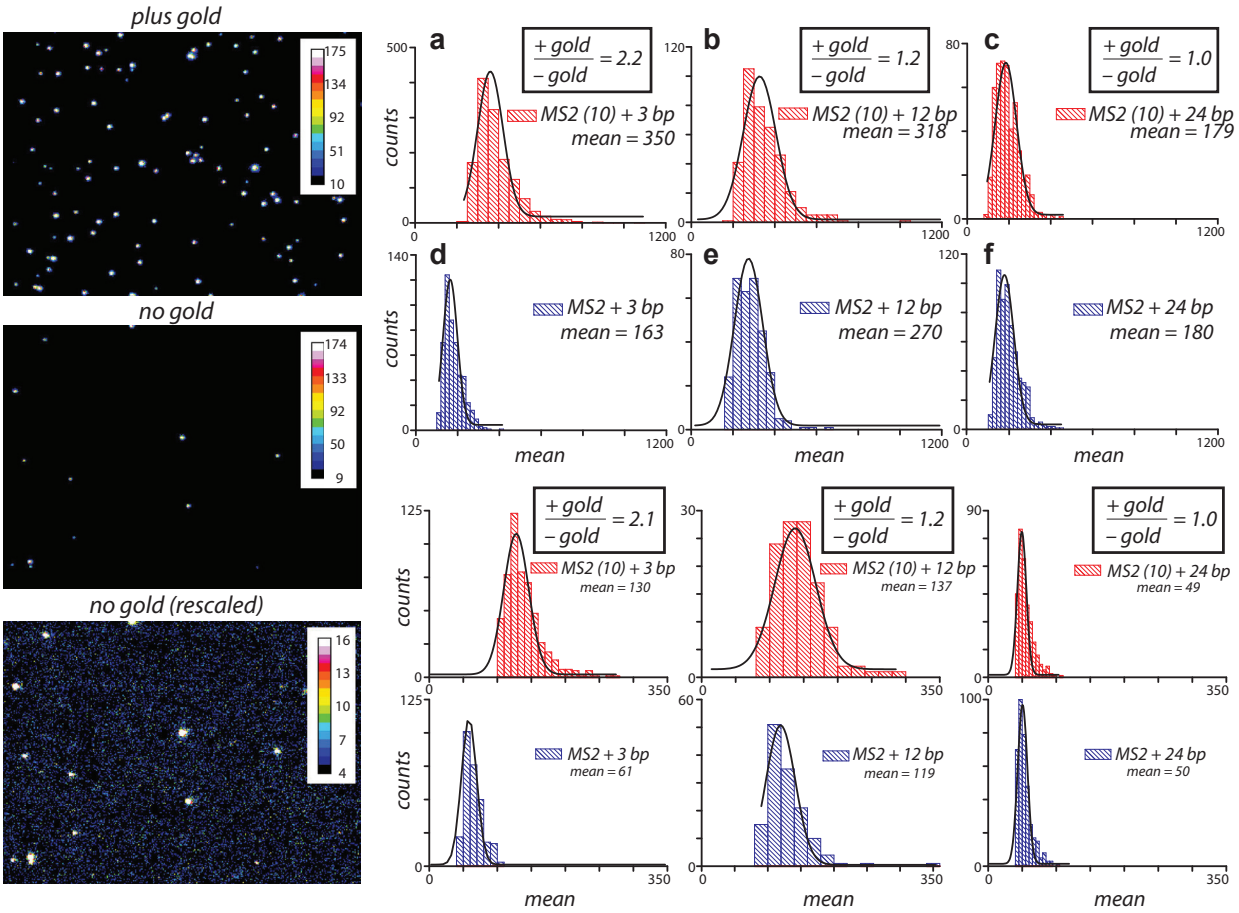

Figure 4.3 (top) Mean intensity histograms determined from TIRF microscopy images for (a) 3 bp hairpin, (b) 12 bp hairpin, and (c) 24 bp hairpin MS2 capsids with gold as well as (d) 3 bp hairpin, (e) 12 bp hairpin, and (f) 24 bp hairpin MS2 capsids without gold samples. The black curves are gaussian fits to the histogram data. (bottom) The same samples were also analyzed by spinning disk confocal microscopy.

Although one might anticipate the fluorophore brightness for each of the three gold-free samples to be identical, we attribute the observed changes in mean intensity among the gold-free samples to differences in fluorescence labeling. Higher modification levels may not necessarily result in increased sample brightness. Interactions between dyes attached to the capsid as well as interactions between the attached dyes and aromatic residues on the protein surface may affect the quantum yield of the fluorophore. Consequently, the most accurate comparisons are drawn only by comparing the samples with and without gold for each separation distance, as both samples have identical numbers of attached chromophores.

TIRF images were collected for multiple sample preparations, as well as a different MS2-DNA-fluorophore construct. Similar trends were observed throughout these sample sets. The results are detailed in Figure 4.4.

Fluorescence lifetime data were also collected for the AF 488 dye, three analogous DNA constructs, three MS2 samples without AuNPs, and three MS2 samples with AuNPs. A representative fluorescence lifetime trace overlaid with the instrument response function is plotted in Figure 4.5. A decrease in fluorescence lifetime was observed when the fluorophores were

	3 bp distance	12 bp distance	24 bp distance
sample 1 *(shown in text)*	2.2	1.2	1.0
sample 2	3.9	3.4	2.0
sample 3*	5.4*	1.8*	3.1*

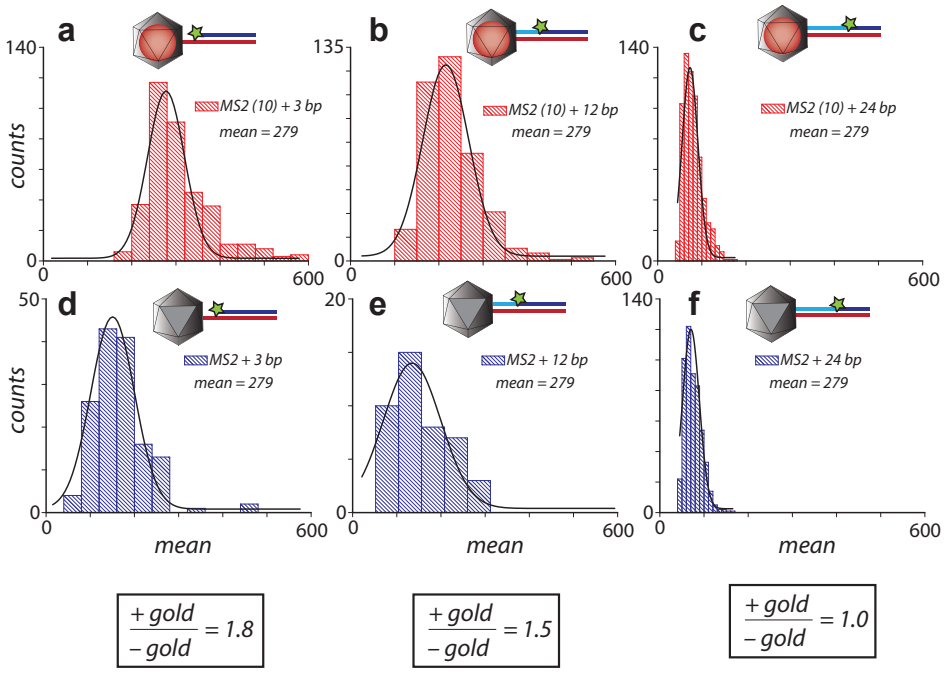

Figure 4.4. *table* TIRF microscopy results of (+gold/−gold) ratios for multiple capsid sample preparations. Samples 1, 2, and 3 shown in the table are different preparations of the hairpin DNA MS2 construct described within the main text. The percent MS2 modifications for sample 1 are ~60 strands per capsid (33%), ~45 strands per capsid (25%), and ~34 strands per capsid (19%), for 3, 12, and 24 bp separation, respectively. The percent MS2 modifications for sample 2 are ~34 strands per capsid (19%), ~9 strands per capsid (5%), and ~ 9 strands per capsid (5%), for 3, 12, and 24 bp separation, respectively. The percent MS2 modifications for sample 3 are ~25 strands per capsid (14%), ~16 strands per capsid (9%), and ~11 strands per capsid (6%) for 3, 12, and 24 bp separation, respectively. The * denotes that the fluorophore DNA hairpin strand was not pre-formed prior to attachment to the capsid. In all cases, fluorescence enhancement is observed. However, these data point to critical parameters in this construct to obtain reproducible intensity enhancements (percent MS2 modification and preformation of the hairpin DNA prior to attachment). *bottom* Mean intensity histograms determined from confocal microscopy images for (a) 3 bp hairpin, (b) 12 bp hairpin, and (c) 24 bp hairpin MS2 capsids with gold as well as (d) 3 bp hairpin, (e) 12 bp hairpin, and (f) 24 bp hairpin MS2 capsids without gold samples. The black curves are gaussian fits to the histogram data. These results are similar to those obtained with TIRF microscopy.

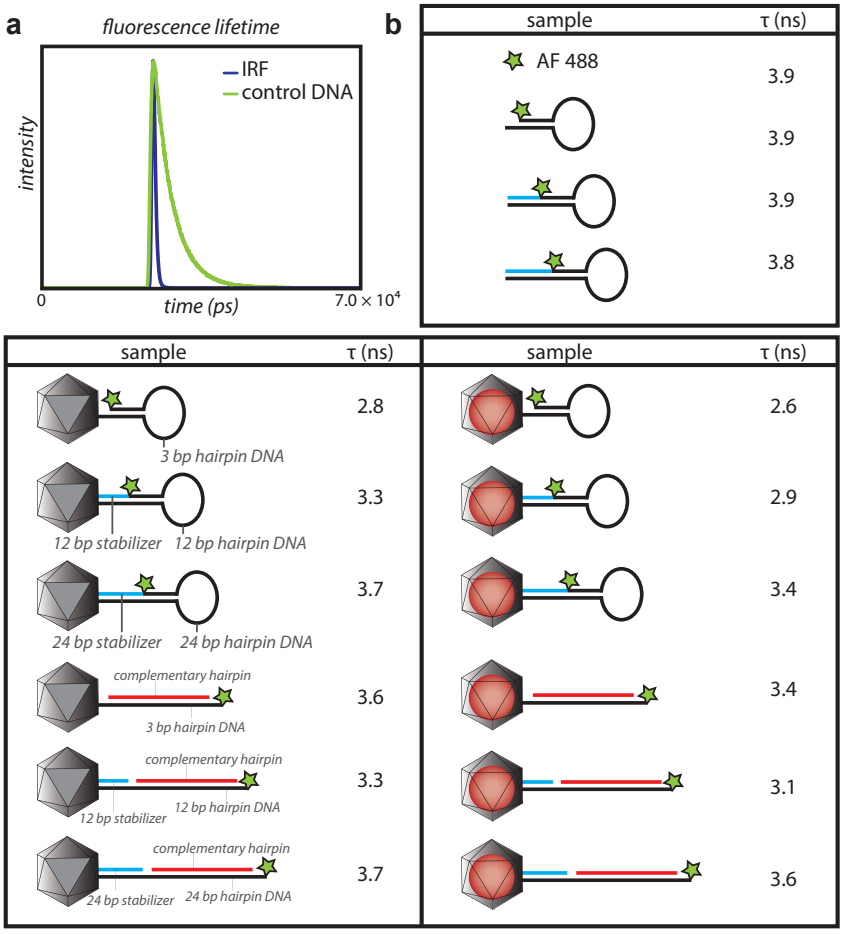

Figure 4.5. Fluorescence lifetime analysis of MS2-DNA conjugates. (a) Representative fluorescence lifetime trace of a control AF 488 DNA sample (green curve) overlaid with the instrument response function (IRF, blue curve). (b) Fluorescence lifetime data are tabulated for free AF 488, three DNA control samples, as well as three MS2 distances with and without gold. Error on lifetime measurements is approximately 0.1 ns. Additionally, lifetime analysis was performed with capsids-DNA hairpin samples that were treated with a DNA strand that hybridizes completely with the hairpin, increasing the distance of the fluorophore from the capsid and the AuNP.

placed close to the gold-free capsid surface, with the shortest lifetime observed for the smallest separation between the fluorophore and protein, as tabulated in Figure 4.5. We attribute this decrease in lifetime to interactions between the AF 488 and either other dyes attached to the capsid or aromatic residues on the capsid. A further decrease in fluorescence lifetime was observed for each of the samples with AuNPs on the interior surface, with the shortest lifetime at the smallest separation. This decrease in lifetime was in accordance with other groups that have reported fluorescence enhancement.[26–32] This effect is likely due to an increased radiative decay rate as a result of the AuNP being in close proximity to the fluorophores.

A control lifetime experiment was conducted with 10 nm AuNPs that were modified with multiple DNA strands, and then incubated with complementary fluorescently-labeled DNA strands.[33] These designs placed fluorophores 9.5 nm, 12.5 nm, and 16.5 nm from the AuNP

surface. We were not able to obtain reasonable fits of fluorescence lifetimes for these data at concentrations similar to those used for capsid samples, due to low photon counts. This suggests the dyes are able to directly contact the surface of the AuNP, quenching their fluorescence. These results have been described in bulk fluorescence measurements for a similar system.[33] This is in sharp contrast to the results we see where the metal nanoparticle is encapsulated in the viral capsid.

Section 4.4: Conclusions

These studies demonstrate the utility of nanoscale protein assemblies for the integration of multiple components into complex systems. The precise dimensions of the viral capsids, in addition to the distinct chemically addressable exterior and interior surfaces, were crucially important for positioning of the dyes without allowing metal surface contact. In ongoing studies, we are using this synthetic system to explore an expanded range of metals, nanocrystal sizes, and fluorophore spectral properties. We are also exploring the use of additional protein scaffolds for the construction of fluorophore-nanoparticle structures with different geometric relationships. In addition to providing experimental tests of metal-enhanced fluorescence, the availability of these systems will provide valuable synthetic routes to access these structures for use in future applications.

Section 4.5: Chapter 4 experimental

Experimental procedures where I had little to no contribution are not described in this section, but rather in the supporting information of the manuscript cited in the Copyright Notice section of this chapter.

Preparation of glass coverslips for TIRF and confocal microscopy

Coverslips were cleaned by sonication in a 50:50 (v/v) mixture of isopropanol and water. They were then dried and further cleaned by plasma treatment for 5 min in a Harrick Plasma PDC-32G plasma cleaner. They were then assembled with an Attofluor cell chamber (Invitrogen, Carlsbad, CA) and 0.25 mL poly-L-lysine PEG with PLK-PEG-biotin (500:3 ratio of the two solutions by volume) was added. After 30 min, the samples were rinsed five times with 5 mL of 1xTAE-Mg^{2+} (40 mM Tris, 20 mM acetic acid, 2 mM EDTA, and 12.5 mM magnesium acetate, pH 8.0) buffer each time. Neutravidin was added to a final concentration of 0.1 mg/mL and incubated for 10 min. Excess neutravidin was rinsed with ten 5 mL rinses with 1xTAE-Mg^{2+} buffer. The sample was incubated for an additional 30 min and then rinsed with five 5 mL portions of 1xTAE-Mg^{2+} buffer. PEG-biotin labeled DNA was added to approximately 10 nM final concentration and incubated for 10 min. Again, excess DNA was rinsed away with five 5 mL portions of 1xTAE-Mg^{2+} buffer.[16] Capsid solutions were added until an appropriate density was achieved.

TIRF image collection

Samples were checked for fluorescence contamination by finding focus using reflection interference contrast microscopy and then examining the sample with the same imaging

conditions as described below. In general, the level of observable particles before adding our capsid sample was very low: most fields of view contained at most 1-2 particles.

TIRF angle was empirically optimized for the first sample we examined on a given day, and kept constant between samples. The angle was adjusted until few diffusing species could be seen during stream acquisition. Since coverslips may differ in thickness (although the observations did not indicate that re-optimization was necessary), images were sometimes collected from the same sample at de-optimized TIRF angles and little difference was observed in molecular brightness. The stage was then moved to a new area and a series of images was collected with an exposure time of 240 ms. The camera was set to bin pixels on chip 2 by 2, providing a pixel size of 0.1284 μm.

These settings provided sufficiently high signal to noise ratio to resolve individual capsids, as described in the image analysis section. Regions of interest were chosen without prior inspection to avoid photobleaching before data collection.

TIRF image analysis

Each image set was analyzed separately using ImageJ software. Images were loaded into the program as a stack, background subtracted, and the threshold range was determined (image\adjust\threshold\default). The threshold range for each stack was set as twenty five percent of the smallest maximum through the largest maximum. Images that contained few or no particles (less than 10) were removed from each stack. The particles were then analyzed by selecting the size as greater than or equal to 3 square pixels and the circularity was selected to be 0.90 – 1.00 (analyze\analyze particles). The area, mean, and integrated intensity were recorded for each particle spot in the stack of images. Mean intensity histograms are shown in Figure 4.3.

Preparation of glass plates for lifetime measurements

Glass bottom 8-well chamber slides were incubated with 0.5 M NaOH for 1 h at rt. The NaOH solution was then removed, and a solution of BSA in phosphate buffered saline was added to the wells. Following overnight incubation at 4 °C, the BSA solution was removed; the plates were rinsed once with 1x TAE-Mg^{2+} buffer, and dried prior to sample addition. All prepared glass plates were used within 3 h of preparation.

Analysis of fluorescence lifetime data

The instrument response function was measured at approximately one nanosecond, while the measured decay curves have lifetimes on the order of a few nanoseconds. Consequently, a simple semi-log plot with linear regression was not sufficient to extract lifetime information. Thus, the decay curves were fit via an iterative non-linear least squares method that takes into account the instrument response function as measured from a colloidal sample. The samples containing AuNPs scattered light strongly, and the signal due to scattering was incorporated into the fitting to correctly account for the signal shape. Measurement error was calculated as the standard deviation between three successive acquisitions. The error of the fitting procedure was also evaluated and included in the stated errors by calculating

the standard deviation of the fitted time constants derived from randomized starting parameters. The following is the fitting function used.

$$f(t) = g(t) * [A \cdot H(t - t_0) \cdot e^{\frac{-(t-t_0)}{\tau}} + B \cdot \delta(t - t_0)]$$

Where g(t) = the measured instrument response function, H(t) = the Heaviside step function that defines t_0 for the fluorescence decay, δ(t) = the Dirac delta function that accounts for the scattered light, A = amplitude of the fluorescence component, t_0 = time zero for the fluorescence decay, τ = decay time for the fluorescence component, B = amplitude of the scattered light, and the * denotes a numerical convolution.

Effect of TIRF evanescent field on brightness measurements

The effect of small differences in the distance of capsids from the surface as a result of gold functionalization was considered in regards to the effect of these differences on measured fluorescence intensity, since the intensity of excitation light decays exponentially as a function of distance from the surface. The following equation relates intensity of the excitation light to the distance from the surface:[34]

$$I(z) = I(0)e^{-z/d}$$

I(z) is the intensity at a given distance from the surface. *I(0)* refers to the intensity at the surface. The distance from the surface is represented as *z*, and the penetration depth is represented by *d*. The penetration depth is given by:[34,35]

$$d = \frac{\lambda}{4\pi}\sqrt{\frac{1}{n_1^2 sin^2(\alpha) - n_2^2}}$$

The critical angle for the glass/water (n_1 = 1.52 n_2 = 1.33) interface is approximately 61°. This gives a penetration depth by the above calculation of 216 nm and would result in a difference of $e^{-1/216}$ or 0.5% in excitation light intensity for a difference in distance of 1 nm. Of course, it has been suggested that the depth of the evanescent field is not the only contribution to the z-selectivity of TIRF microscopy.[34,36] In addition, the collection light efficiency of fluorophores nearer the surface is enhanced if a very high numerical aperture objective (NA > 1.4) is used. This behavior can be approximated using a single exponential with lower penetration depth.[34] In a system similar to ours, but using an objective with a NA of 1.45 (instead of 1.49 in our study), the penetration depth was found to be 125 nm.[36] The resulting difference of intensities between fluorophores separated by 1 nm would be $e^{-1/125}$ or 0.8%. Assuming an even smaller penetration depth of 60 nm, the difference in intensities between the aforementioned fluorophores would be expected to be approximately 1.6%. These differences cannot explain the differences in fluorescence intensity reported in this work.

Section 4.6: Chapter 4 references

(1) Douglas, T.; Young, M. *Nature* **1998**, *393*, 152–155.
(2) Fiedler, J. D.; Brown, S. D.; Lau, J. L.; Finn, M. G. *Angewandte Chemie (International ed. in English)* **2010**, *49*, 9648–51.
(3) Stephanopoulos, N.; Carrico, Z. M.; Francis, M. B. *Angewandte Chemie (International ed. in English)* **2009**, *48*, 9498–502.
(4) Dedeo, M. T.; Duderstadt, K. E.; Berger, J. M.; Francis, M. B. *Nano letters* **2010**, *10*, 181–6.
(5) Carrico, Z. M.; Romanini, D. W.; Mehl, R. A.; Francis, M. B. *Chemical communications (Cambridge, England)* **2008**, 1205–7.
(6) Liu, Y.; Yehl, K.; Narui, Y.; Salaita, K. *Journal of the American Chemical Society* **2013**.
(7) Jennings, T. L.; Singh, M. P.; Strouse, G. F. *Journal of the American Chemical Society* **2006**, *128*, 5462–7.
(8) Singh, M. P.; Strouse, G. F. *Journal of the American Chemical Society* **2010**, *132*, 9383–91.
(9) Yun, C. S.; Javier, A.; Jennings, T.; Fisher, M.; Hira, S.; Peterson, S.; Hopkins, B.; Reich, N. O.; Strouse, G. F. *Journal of the American Chemical Society* **2005**, *127*, 3115–9.
(10) Anger, P.; Bharadwaj, P.; Novotny, L. *Physical Review Letters* **2006**, *96*, 113002.
(11) Acuna, G. P.; Möller, F. M.; Holzmeister, P.; Beater, S.; Lalkens, B.; Tinnefeld, P. *Science (New York, N.Y.)* **2012**, *338*, 506–10.
(12) Acuna, G. P.; Bucher, M.; Stein, I. H.; Steinhauer, C.; Kuzyk, A.; Holzmeister, P.; Schreiber, R.; Moroz, A.; Stefani, F. D.; Liedl, T.; Simmel, F. C.; Tinnefeld, P. *ACS Nano* **2012**, *6*, 3189–95.
(13) Chhabra, R.; Sharma, J.; Wang, H.; Zou, S.; Lin, S.; Yan, H.; Lindsay, S.; Liu, Y. *Nanotechnology* **2009**, *20*, 485201.
(14) Maiti, S.; Dutta, S.; Das, P. K. *Chemistry (Weinheim an der Bergstrasse, Germany)* **2011**, *17*, 7538–48.
(15) Kang, K. A.; Wang, J.; Jasinski, J. B.; Achilefu, S. *Journal of nanobiotechnology* **2011**, *9*, 16.
(16) Chen, J.; Jin, Y.; Fahruddin, N.; Zhao, J. X. *Langmuir : the ACS journal of surfaces and colloids* **2013**, *29*, 1584–91.
(17) Wu, M.; Brown, W. L.; Stockley, P. G. *Bioconjugate Chemistry* **1995**, *6*, 587–595.
(18) Ashley, C. E.; Carnes, E. C.; Phillips, G. K.; Durfee, P. N.; Buley, M. D.; Lino, C. a; Padilla, D. P.; Phillips, B.; Carter, M. B.; Willman, C. L.; Brinker, C. J.; Caldeira, J. D. C.; Chackerian, B.; Wharton, W.; Peabody, D. S. *ACS Nano* **2011**.
(19) Glasgow, J. E.; Capehart, S. L.; Francis, M. B.; Tullman-Ercek, D. *ACS nano* **2012**, *6*, 8658–64.
(20) Hooker, J. M.; Esser-Kahn, A. P.; Francis, M. B. *Journal of the American Chemical Society* **2006**, *128*, 15558–9.
(21) Tong, G. J.; Hsiao, S. C.; Carrico, Z. M.; Francis, M. B. *Journal of the American Chemical Society* **2009**, *131*, 11174–8.
(22) Behrens, C. R.; Hooker, J. M.; Obermeyer, A. C.; Romanini, D. W.; Katz, E. M.; Francis, M. B. *Journal of the American Chemical Society* **2011**, *133*, 16398–401.
(23) Mehl, R. A.; Anderson, J. C.; Santoro, S. W.; Wang, L.; Martin, A. B.; King, D. S.; Horn, D. M.; Schultz, P. G. *Journal of the American Chemical Society* **2003**, *125*, 935–9.
(24) Chen, Y.; Munechika, K.; Ginger, D. S. *Nano letters* **2007**, *7*, 690–6.

(25) Tinland, B.; Pluen, A.; Sturm, J.; Weill, G. *Macromolecules* **1997**, *30*, 5763–5765.
(26) Zhang, Y.; Aslan, K.; Previte, M. J. R.; Geddes, C. D. *Applied Physics Letters* **2007**, *90*, 173116.
(27) Kühn, S.; Håkanson, U.; Rogobete, L.; Sandoghdar, V. *Physical Review Letters* **2006**, *97*, 017402.
(28) Tovmachenko, O. G.; Graf, C.; Van den Heuvel, D. J.; Van Blaaderen, A.; Gerritsen, H. C. *Advanced Materials* **2006**, *18*, 91–95.
(29) Fu, Y.; Zhang, J.; Lakowicz, J. R. *Journal of fluorescence* **2007**, *17*, 811–6.
(30) Ray, K.; Zhang, J.; Lakowicz, J. R. *Analytical chemistry* **2008**, *80*, 7313–8.
(31) Bardhan, R.; Grady, N. K.; Cole, J. R.; Joshi, A.; Halas, N. J. *ACS nano* **2009**, *3*, 744–52.
(32) Fu, Y.; Zhang, J.; Lakowicz, J. R. *Journal of the American Chemical Society* **2010**, *132*, 5540–1.
(33) Zheng, D.; Seferos, D. S.; Giljohann, D. A.; Patel, P. C.; Mirkin, C. A. *Nano letters* **2009**, *9*, 3258–61.
(34) Axelrod, D. In *Methods in Enzymology*; Marriott, G.; Parker, I., Eds.; Academic Press, 2003; Vol. 361, pp. 1–33.
(35) Groves, J. T.; Parthasarathy, R.; Forstner, M. B. *Annual review of biomedical engineering* **2008**, *10*, 311–38.
(36) Mattheyses, A. L.; Axelrod, D. *Journal of Biomedical Optics* **2006**, *11*, 014006.

Chapter 5: Discussion, Conclusions and Future Directions

Section 5.1: Discussion of heterodimer formation results and possible improvements

FCCS analysis of heterodimers (Figures 2.4 and 2.6) suggests that the assembly of the DNA structure is incomplete. To determine if the reaction time used to hybridize strands to those on the membrane achieved saturation, several membranes were prepared and treated with thiol DNA. Fluorescently labeled complementary DNA (cDNA) was added and rinsed at the indicated times (Figure 5.1a). The samples were analyzed by fluorescence microscopy before and after treatment with cDNA. After analysis, the samples were treated with more cDNA and reanalyzed. The results of this assay suggest that the 60 min incubation time used in most of these experiments is sufficient to saturate the membrane with cDNA (Figure 5.1).

Additionally, the hybridization was directly monitored by performing FCCS and fluorescence lifetime analysis on samples during incubation of low concentrations (10-20 fold lower than the concentration typically used for hybridization) of fluorescent cDNA (Figure 5.1b). FCCS analysis suggests that binding of both strands saturates after 1000-1500 s incubation. The decrease in lifetime from Förster Resonance Energy Transfer (FRET) of Alexa Fluor (AF) 488 to AF555 occurs more rapidly than the increase in cross-correlation, suggesting that the sequence on arm 2 binds more quickly than that on arm 1. The maximum FRET efficiency measured in this experiment is consistent with a distance of nearly 8 nm (from the number of base pairs, the expected distance is at least 6.8 nm), based on the Förster radius of the fluorophore pair provided by the manufacturer (7 nm).

Finally, the presence of solid phase synthesis truncation products was evaluated by dena-

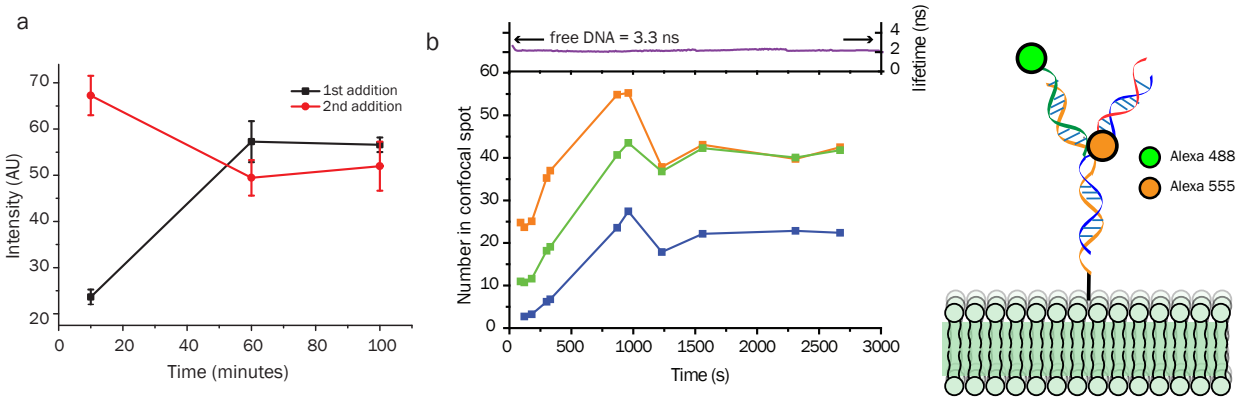

Figure 5.1: Optimization of the hybridization time for fluorescent DNA. (a) Incubation of fluorescent cDNA with DNA functionalized membranes at various times. To determine the saturated intensity for each membrane, additional fluorescent DNA was added and incubated for additional time. The error bars represent the standard error of the mean for multiple images and sample preparations. (b) Real time monitoring of assembly of Y-dimer shown in Figure 5.2. The Y-axis represents the average number of species diffusing in the confocal detection volume extracted from fitting the correlation functions (30 s acquisition time) at each point to a model of free 2-D diffusion. Lifetime measurements were performed during data collection with 10 s acquisition times. Arrows indicate the lifetime measurements of AF488 DNA in a no-FRET state, with no acceptor on the membrane.

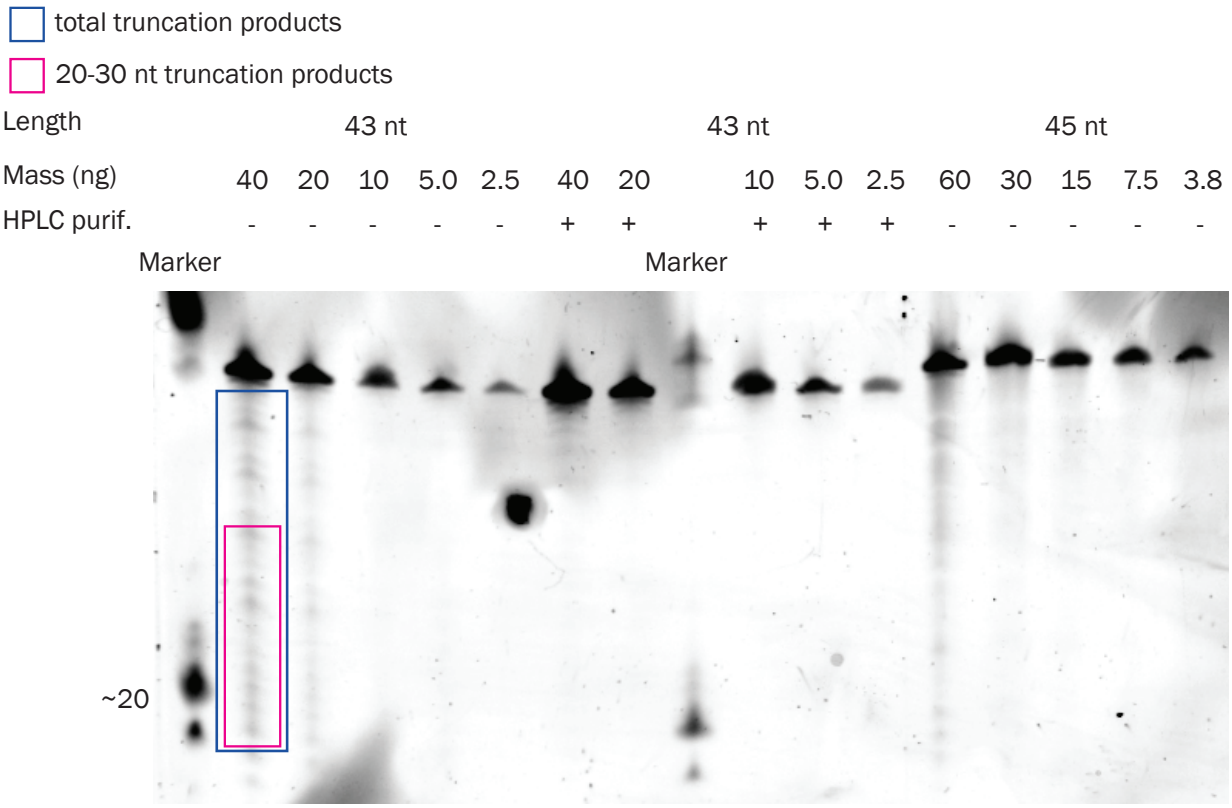

Figure 5.2: Denaturing PAGE analysis of oligonucleotides for capturing targets on arm 1 (right samples) and arm 2 (left and center samples). Marker is run on the far right and in the center of the gel, as indicated. Boxes show ranges of integration for determining total and "especially damaging" truncation products. While the width of the integration region used for analysis was identical, the boxes are sized differently for clarity.

turing PAGE. Commercially prepared oligonucleotides are synthesized from the 3' end using standard DNA synthesis techniques. This is especially damaging to truncations of the blue strand (Figure 5.1) since they would prevent hybridization with the fluorescent cDNA target, but still be competent to bind the membrane anchored DNA. Densitometry analysis of the gel shown in Figure 5.2 suggests that truncation products compose 34% of the cross-linking DNA (and a similar amount of the thiol DNA in the rightmost 5 lanes of the gel, but these are not expected contain thiol groups). This analysis also suggests that 22% of the DNA consists of truncation products between 20-30 nt in length. These strands are long enough to bind the membrane DNA, but would have truncated domains for target binding that do not form stable duplexes. HPLC purified DNA still contains some truncation products, but considerably less (24% of total), and a lower proportion of 20-30 nt products (10%).

The presence of these products helps explain the yield of heterodimer formation presented in Chapter 2. Other factors may also contribute to lower yield, but most seem unlikely. Unbinding of DNA is expected to be prohibitively slow, based on kinetic parameters of similar strands reported the literature.[1] Secondary structure cannot be ruled out, but little is predicted by simulation.[2] Alternatively, the FCCS measurement may underestimate the yield. These possibilities cannot be excluded, and additional characterization experiments may provide

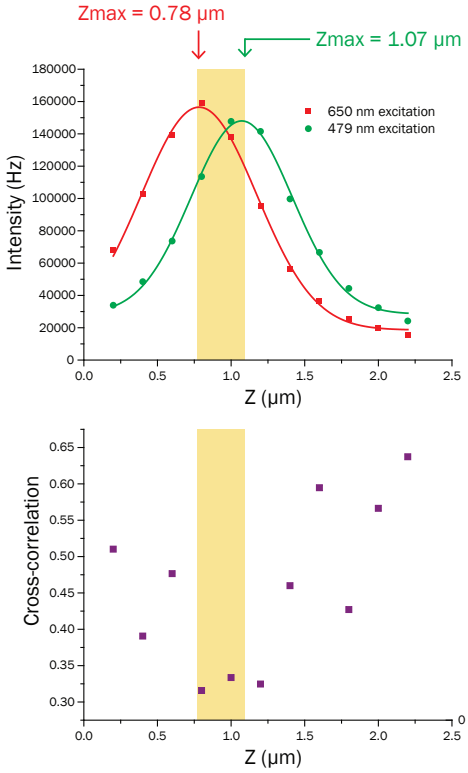

Figure 5.3: Measurement of the intensity profile normal to coverslip on the FCCS instrument used in chapter 2. At each point, cross-correlation functions were measured and fitted. Despite the 300 nm offset between the maximum intensity points for the two beams, the amount of cross-correlation measured was relatively constant over this range, suggesting that the measurement is not heavily affected by slight changes in the focus position. Many of the cross-correlation measurements outside this range are scattered due to the low signal to noise.

clues to allow further optimization.

Section 5.2: Discussion of cross-correlation analysis and excitation/emission volume overlap

Precise measurement of many of the degree of cross-correlation is difficult, due to certain technical issues that arise specifically in dual-color fluorescence cross-correlation.[3–5] Most importantly, because of the difference in wavelength of the two lasers used, both the excitation areas and the light collection areas are differently sized, even if they are aligned perfectly. Additional offset of these volumes significantly decreases the observed cross-correlation amplitude as suggested by both empirical measurements[3,4] and simulation.[5] The analysis described in Chapter 2 corrects for these factors by analyzing a sample that is labeled with both fluorophores. This correction only empirically corrects the relative cross-correlation. Here we discuss briefly the possibility that this offset affects measured cross-correlation due to inconsistent focusing between samples, which would not be corrected by this analysis.

Examination of the combined excitation and emission displacement in our experimental setup by performing a Z-scan of intensity through a supported membrane revealed that the detected intensity maximum of the two channels was offset by approximately 300 nm (Figure 5.3a). This shift, however, has little effect on the measured cross-correlation between the two maxima, (shaded area in Figure 5.3b) suggesting that this measurement is not particularly sensitive to user error in focusing between samples.

Section 5.3: Discussion of membrane receptor heterooligomer formation and future directions

The experiments described in Figures 3.7 and 3.8 demonstrate the ability to alter the composition of signaling clusters in cell membranes, since these data suggest that both ligands in the heterodimer, ephrinA1 and EGF, are competent to bind their cognate receptors. Still, some aspects of signal transduction may not be affected by such a macroscopic change, and may require both ligands in a given heterodimer to bind their target on the cell membrane, forcing the receptors to dimerize.

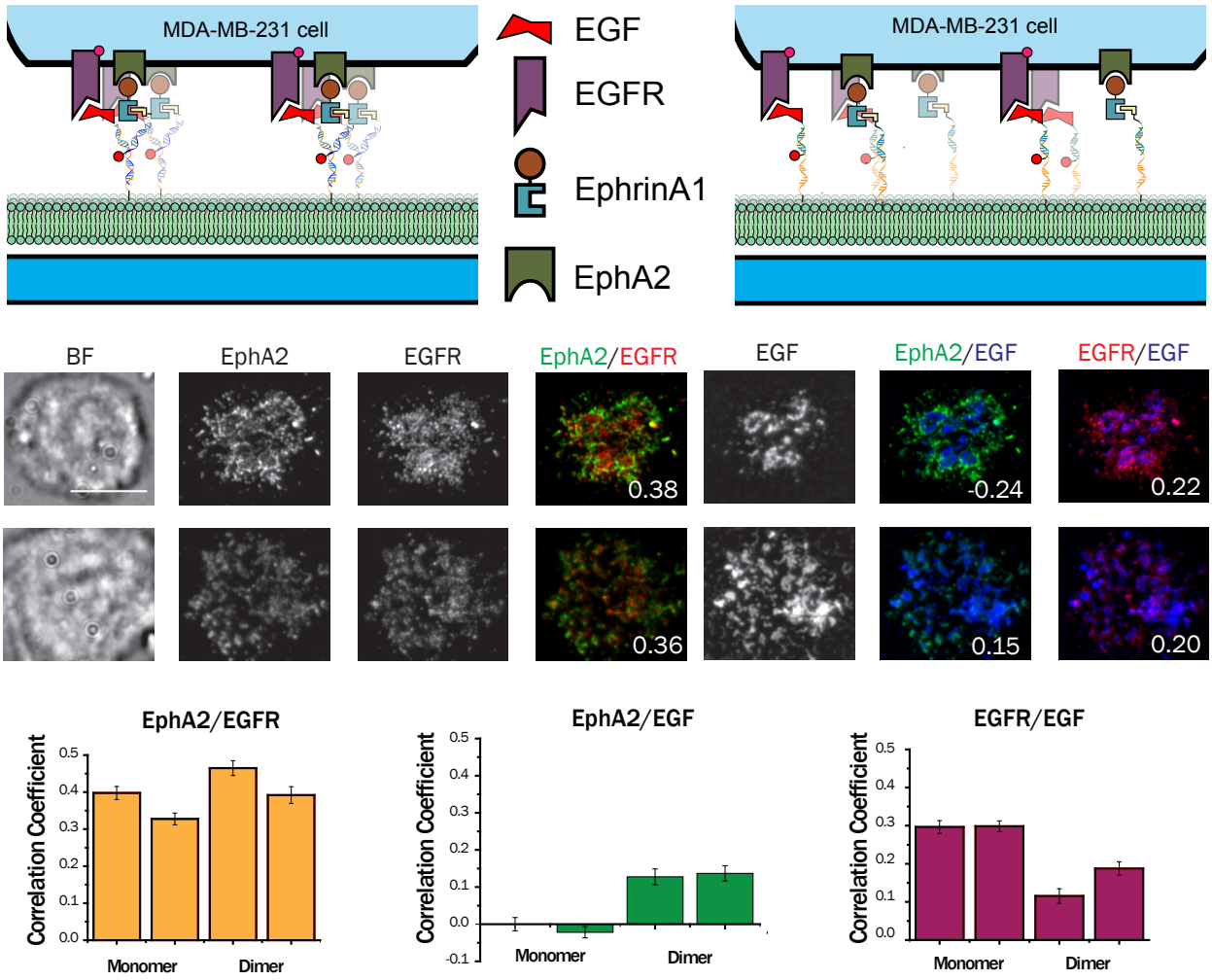

Figure 5.4: Assay for receptor dimerization. Cells were presented with heterodimers of unlabeled ephrinA1 and Cy5 labeled EGF in a similar manner to that described in chapter 3. Cells were then fixed, permeablized and stained for both EphA2 and EGFR. Correlation coefficients were measured as described in chapter 3.

An attempt to adapt the assay used in Figures 3.7 and 3.8 to measure colocalization of receptors in the cell membrane gave inconclusive results (Figure 5.4). In this experiment, ephrinA1 was left unlabeled to allow observation of both EphA2 and EGFR. Analysis (see Chapter 3) revealed that EGF-EphA2 colocalization depended strongly on the oligomerization state of the ligand, consistent with the experiment described in Figure 3.8. Additionally, correlation analysis of EGF-EGFR showed the opposite trend, with higher correlation observed in the cells presented with monomeric ligand. This suggests that EGF in the heterodimer is less able to bind its receptor. EGFR-EphA2 colocalization did not show a clear trend. Furthermore, visual examination of the images (Figure 5.4) did not show the striking difference in colcalization that was clearly visible in Figures 3.7 and 3.8.

These results suggest that heterodimerized ligands on the membrane bind to receptors in a mutually exclusive manner. Still, they also suggest that the Pearson's correlation assay is unlikely to answer this question definitively. Future optimization could be performed using a FRET assay between membrane receptors fused to fluorescent proteins. This assay can be

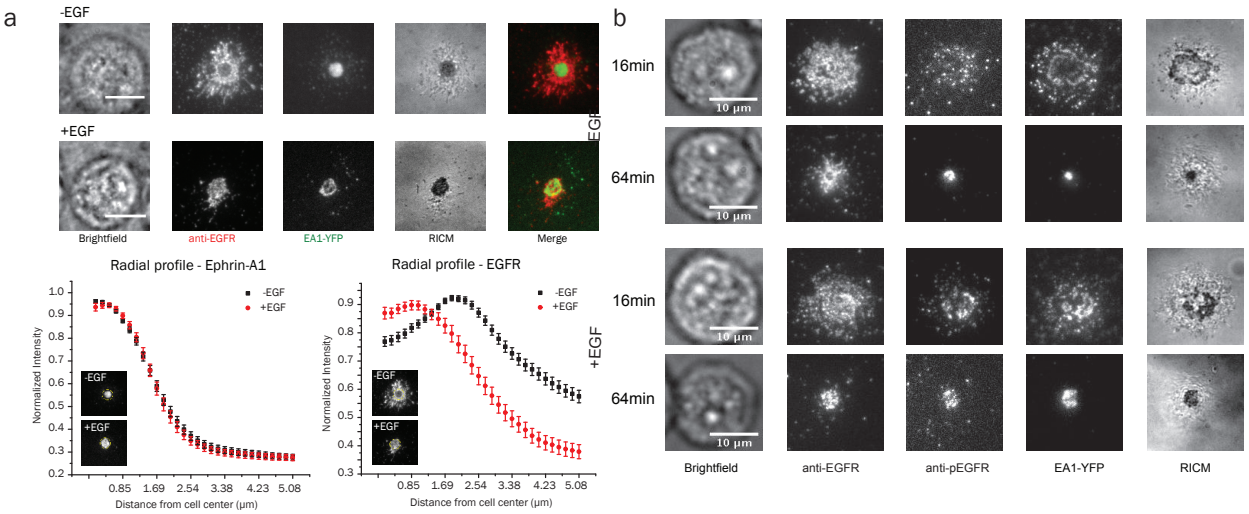

Figure 5.5: EGF dependent sorting of EGFR and EphA2 in MDA-MB-231 cells. (a) Cells were stimulated with an ephrinA1-YFP-His_{10} functionalized membrane either in the presence or absence of EGF. Radial profiles over a population demonstrate the depletion of EGFR at the large, micro-scale clustered region of ephrinA1. (b) Staining for pTyr-EGFR shows that it colocalizes with ephrinA1 in both stimulated and unstimulated cells.

done with live cells and should be sensitive to differences in colocalization at the 2-10 nm scale.

Section 5.4: Observations on intrinsic EphA2/EGFR colocalization in MDA-MB-231 cells

Note: the following experiments were performed with Qian Xu, and are likely also described in her thesis. At the time of writing, her thesis is not, to my knowledge, available online, so a specific citation cannot be provided.

EGFR and EphA2 receptor tyrosine kinases are upregulated in many cancers and are both important therapeutic targets.[6–9] Recent evidence suggests that these two signaling pathways interact. EphA2 expression, for example, is upregulated in response to EGFR stimulation and Erk activation.[10,11] This results in a negative feedback loop since stimulation of EphA2 with ephrinA1 has been shown to downregulate EGF-induced Erk phosphorylation) upstream of Ras.[10]

We were interested in examining and directing interactions between EGFR and EphA2 in MDA-MB-231 cells. These cells express both EGFR and EphA2. Since, EphA2 has been shown to be clustered upon stimulation with ligand (see Chapter 1),[12,13] we investigated whether EGFR was potentially enriched or excluded from EphA2 clusters. Cells were stimulated with membrane bound ephrinA1[13] and treated with or without EGF. Cells treated without EGF were found have excluded EGFR staining at sites of ephrinA1 clustering, while ephrinA1 and EGFR colocalized in cells treated with EGF, as shown by radial intensity profile analysis (Figure 5.5). Staining for pTyr-EGFR revealed similar localization in both EGF stimulated and unstimulated cells.

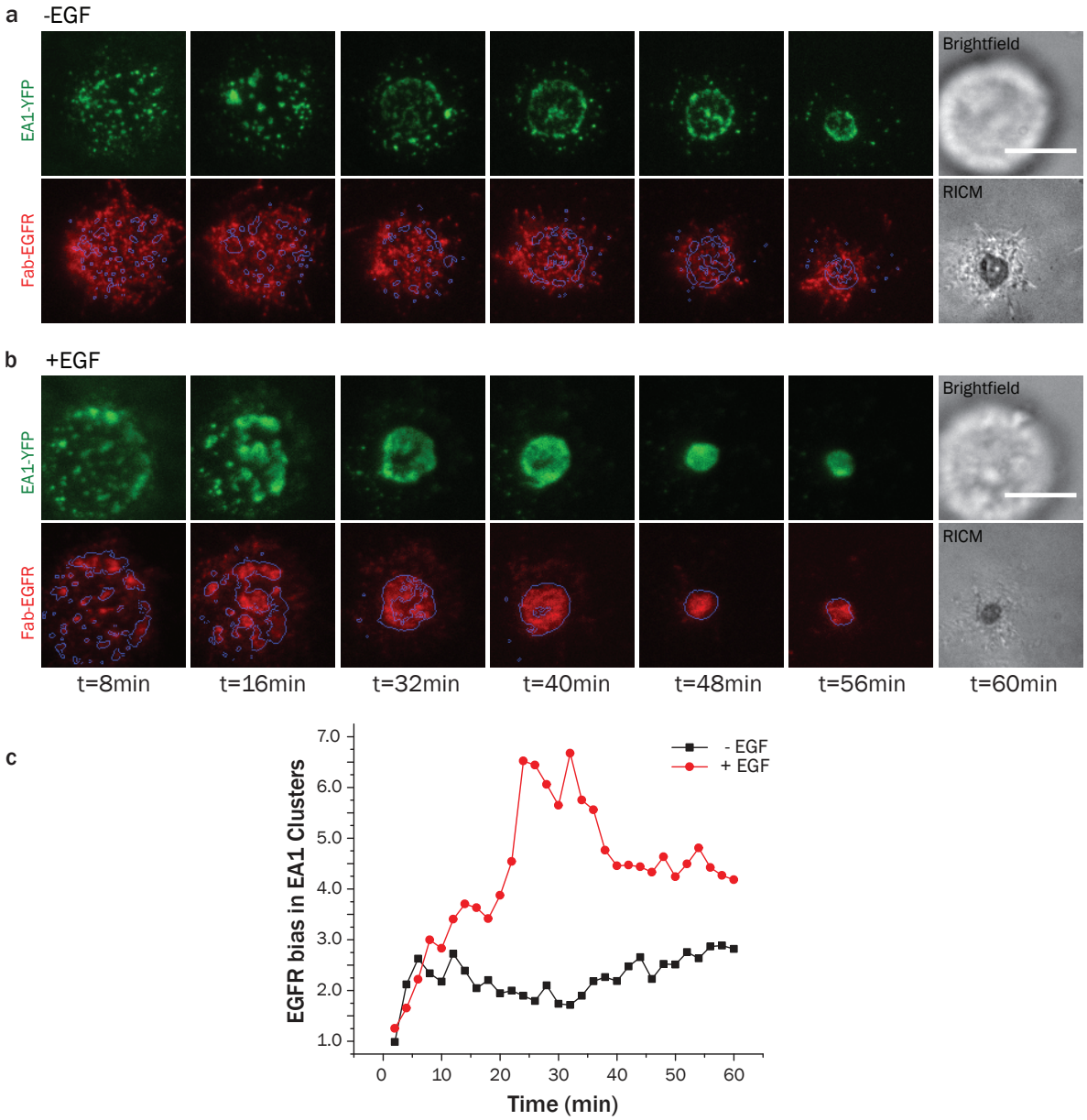

Figure 5.6: Live cell tracking of EGFR and ephrinA1 during stimulation. (a) TIRF imaging of Fab labeled EGFR and ephrinA1-YFP shows EGF dependent colocalization and transport. (b) Enrichment of EGFR in ephrinA1 clusters (fold over background) is considerably higher in EGF stimulated cells.

To investigate the dynamics of this process in live cells, EGFR on MDA-MB-231 cell membranes was labeled with a Fab fragment that has been shown neither to activate EGFR nor to prevent ligand stimulation.[14] After staining, cells were deposited on a membrane functionalized with ephrinA1-YFP-His_{10} and imaged with TIRF microscopy (Figure 5.6). Ligand stimulated samples showed high colocalization, as measured by the correlated probability of EGFR intensity within ephrinA1 clusters. The regions of high ephrinA1-YFP fluorescence intensity are outlined with a blue line in the EGFR image.

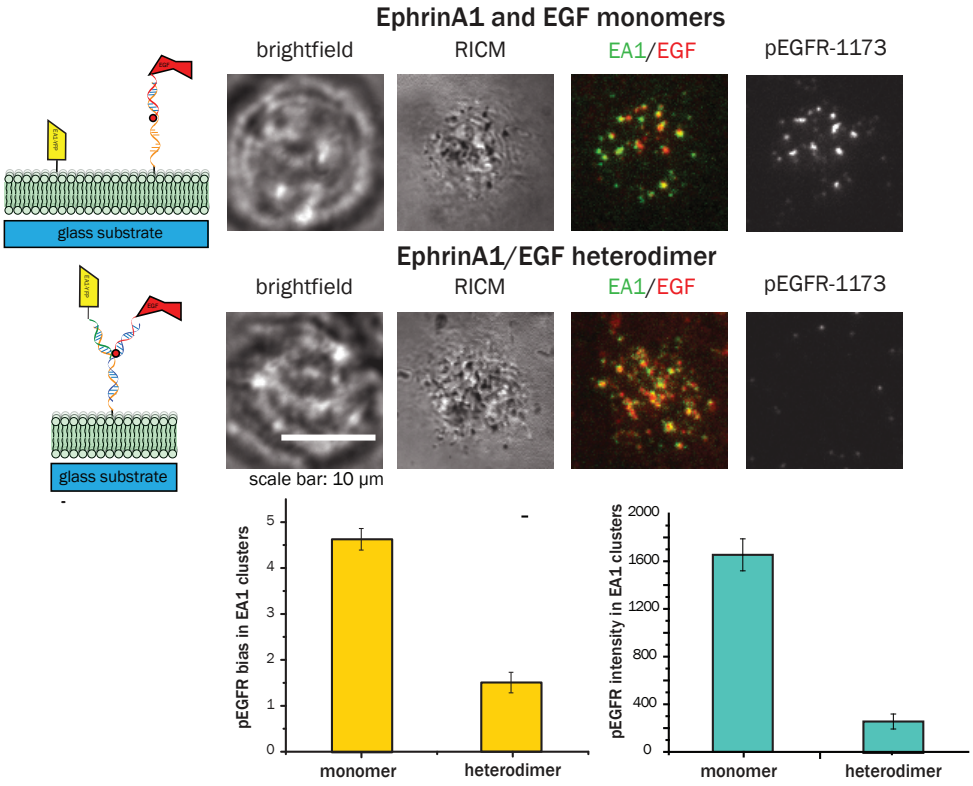

Figure 5.7: Induced dimerization of EGF and ephrinA1. Measurement of pTyr-EGFR in cells presented with either monomeric ligands or a heterodimer suggests inhibition of phosphorylation in cells presented with heterodimeric ligand. This could result from a variety of factors and is discussed in more detail in the text.

This led us to ask whether EGFR association had any direct effect on signal transduction. EphA2 is known to interfere with EGFR signal propagation through the Ras/MAPK pathway and upstream of Ras. To determine the effect of colocalization of EphA2 and EGFR on EGFR phosphorylation, membranes containing a Fab against EGFR and EphrinA1 ligand were prepared.

Preliminary evidence supported this hypothesis. An ephrinA1-EGF heterodimer appeared to decrease receptor activation in MDA-MB-231 cells, measured either by the fluorescence intensity of phosphotyrosine EGFR staining or by the ratio of phosphotyrosine EGFR in ephrinA1 clusters, compared to that outside the clusters (Figure 5.7). These results should be cautiously interpreted. We have not verified that receptor binding from a single heterodimer (one EGF/EphrinA1 complex) is not mutually exclusive between the members of a given pair (discussed above and in Chapter 3). Additionally, we observed that the surface density of ephrinA1 conjugated to DNA via Ni^{2+} chelation was relatively unpredictable.

When repeating the experiment, we found little effect of heterodimerization at an extremely low surface density (Figure 5.8a). This observation is not inconsistent with those reported in Figure 5.7, but does indicate that better control of the surface density might be critical for precise measurement of cellular phenomenon. Using the conjugation scheme described in Chapter 3, which allows purification of the covalent ephrinA1-DNA conjugate, allowed for bet-

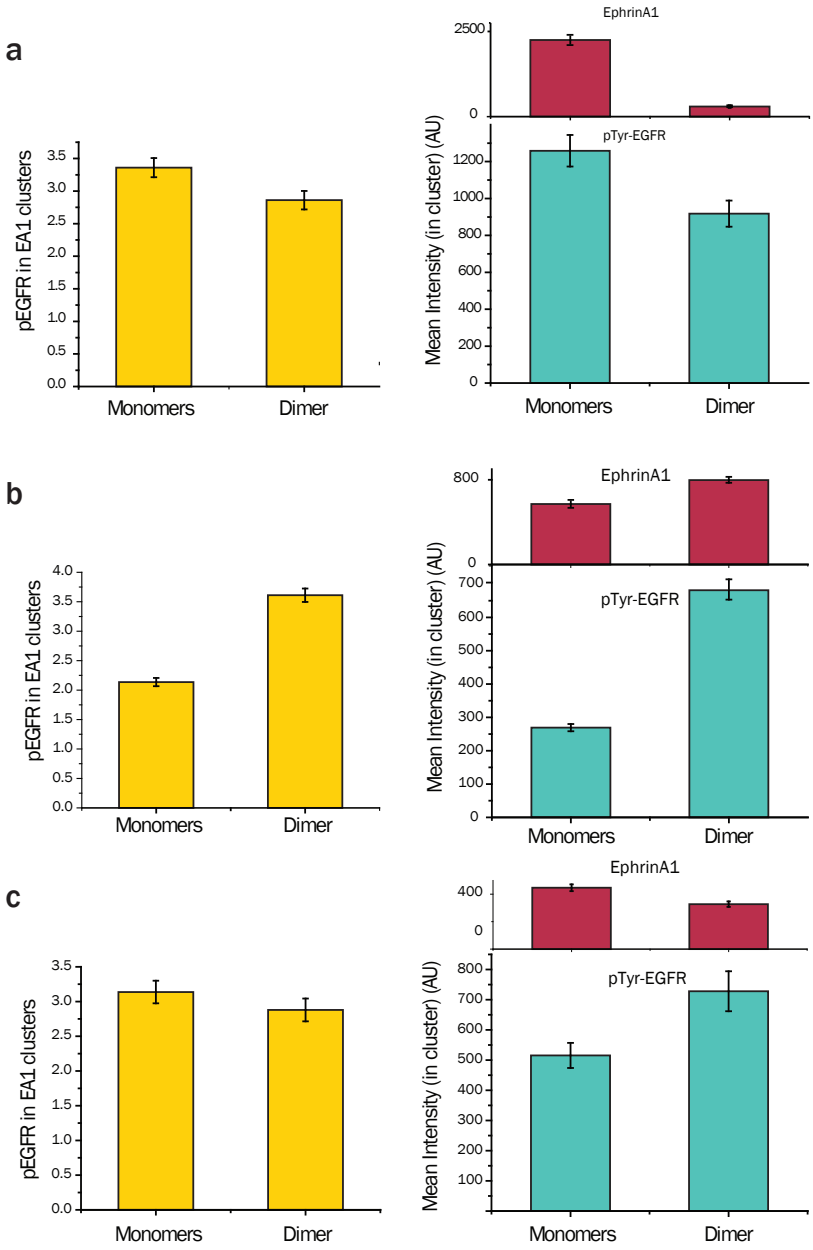

Figure 5.8: Inconsistencies in the measurement of pTyr-EGFR levels in cells presented with heterodimeric ligands. (a) Repetition of the experiment with the metal chelated ephrinA1-DNA conjugate shows the inconsistency in surface density that results from use of this technique. (b) Analysis used in Figure 5.7 performed on cells shown earlier in Figure 3.7 suggests that pTyr-EGFR is actually higher when cells are presented with heterodimeric ligand, which is inconsistent with Figure 5.7. (c) This experiment was also performed with serum starved MDA-MB-231 cells, and gave similar results, but ones that differed from the observation in Figure 5.7.

ter control of the surface density. However, performing the same analysis on the data shown in Figure 3.7, we observe the opposite trend for cells treated with heterodimeric ligands (Figure 5.8b). It should be noted, however, that these cells were not serum starved. Even when using serum starved cells (Figure 5.8c), a trend similar to that in Figure 5.8b is observed, which is inconsistent with the earlier observations in Figure 5.7. These observations suggest that some factors involved in heterodimer assembly or analysis of the data from these experiments may still need to be investigated and optimized. Future work will focus on live cell assays with higher labeling efficiencies (such as transfected fluorescent proteins) and higher resolution (FRET).

Section 5.5: Conclusions

My graduate work has focused on addressing the need for methods to control the assembly of proteins in cell membranes into signaling clusters. The DNA based method presented in this work allows protein-DNA conjugates to be anchored on supported membranes at a range of surface densities and allows them to be assembled into functional heterodimers. Additionally, we have demonstrated the use of various bioconjugation techniques for linking DNA to cell binding proteins that will be useful in studying cell signaling and in other applications that require nanoscale organization of proteins.

Section 5.6: Chapter 5 experimental

DNA hybridization time screening

Supported membranes with anchored DNA were prepared as described in the other chapters. AF488 labeled fluorescent DNA (1 μM) incubated for the indicated times, then washed with excess buffer. The same amount of DNA was added for the second incubation.

Analysis of two fluorophores binding was performed by preparing bilayers in 8-well chamber slides (Nunc) cleaned with 1hr 0.5M NaOH treatment. These were functionalized with 45 nt and then treated with the HPLC-purified cross-linking strand (blue in Figure 5.1 and 5.2) at 100 nM for 2 hr. After rinsing, the membranes were treated with 10 nM of both AF488 DNA and AF555 DNA. PIE-FCCS was performed as indicated in chapter 2, but the 568 nm line of the KrAr laser was used instead of the 647 nm line. Lifetime fitting was performed as described in chapter 5 using Matlab.

Antibody staining

Experiments were performed as described in chapter 3. EphA2 was stained with a 1:100 dilution of mouse monoclonal α-EphA2 (clone D7, Millipore) for 40 min in PBS with 1% BSA. EGFR was stained with a 1:250 dilution of rabbit monoclonal α-EGFR (clone EP38Y, Abcam) using the same procedure.

EGFR staining in section 5.3 was performed with mouse monoclonal anti-EGFR (clone 528, Calbiochem). Fab fragments for live cell imaging were produced by labeling the EGFR Ab-11 antibody (clone 199.12, ThermoFisher) with AF594 and digestion with a Fab digestion kit (Pierce).

EphrinA1 DNA conjugation

EphrinA1-DNA conjugates were prepared as in chapter 3, but using non-fluorescent DNA. The conjugate behaved similarly to that shown in chapter 3 in size exclusion chromatography and SDS-PAGE characterization assays.

Denaturing polyacrylamide gel electrophoresis

Polyacrylamide gels (12.5%) for analysis of oligonucleotides were prepared by tetramethylethylenediamine (1/10000 volume of gel) and ammonium persulfate (.01 % w/v) initated polymerization of a 29:1 mixture of acrylamide/bis-acrylamide (Fisher) with 0.5X tris-borate-EDTA (TBE) buffer and 7 M urea. Gels were stained with SyBr Gold (Invitrogen) at approximately a 1:50,000 dilution in 0.5X TBE buffer for 5-10 min.

Other methods

Protocols regarding ephrinA1-YFP-His_{10} expression, purification, characterization, and other associated methods are described in Xu, *et al* 2011.

Section 5.7: Chapter 5 references

(1) Morrison, L. E.; Stols, L. M. *Biochemistry* **1993**, *32*, 3095–3104.
(2) Zadeh, J. N.; Steenberg, C. D.; Bois, J. S.; Wolfe, B. R.; Pierce, M. B.; Khan, A. R.; Dirks, R. M.; Pierce, N. A. *Journal of computational chemistry* **2011**, *32*, 170–3.
(3) Bacia, K.; Schwille, P. *Nature protocols* **2007**, *2*, 2842–56.
(4) Foo, Y. H.; Naredi-Rainer, N.; Lamb, D. C.; Ahmed, S.; Wohland, T. *Biophysical journal* **2012**, *102*, 1174–83.
(5) Weidemann, T.; Wachsmuth, M. *Single Molecules* **2002**, *3*, 49–61.
(6) Petty, A.; Myshkin, E.; Qin, H.; Guo, H.; Miao, H.; Tochtrop, G. P.; Hsieh, J.-T.; Page, P.; Liu, L.; Lindner, D. J.; Acharya, C.; Mackerell, A. D.; Ficker, E.; Song, J.; Wang, B. *PLoS ONE* **2012**, *7*, e42120.
(7) Carles-Kinch, K.; Kilpatrick, K. E.; Stewart, J. C.; Kinch, M. S. *Cancer Res.* **2002**, *62*, 2840–2847.
(8) Reichert, J. M.; Valge-Archer, V. E. *Nature reviews. Drug discovery* **2007**, *6*, 349–56.
(9) Shawver, L. K.; Slamon, D.; Ullrich, A. *Cancer Cell* **2002**, *1*, 117–123.
(10) Macrae, M.; Neve, R. M.; Rodriguez-Viciana, P.; Haqq, C.; Yeh, J.; Chen, C.; Gray, J. W.; McCormick, F. *Cancer cell* **2005**, *8*, 111–8.
(11) Larsen, A. B.; Pedersen, M. W.; Stockhausen, M.-T.; Grandal, M. V.; Van Deurs, B.; Poulsen, H. S. *Molecular cancer research* **2007**, *5*, 283–93.
(12) Salaita, K.; Nair, P. M.; Petit, R. S.; Neve, R. M.; Das, D.; Gray, J. W.; Groves, J. T. *Science* **2010**, *327*, 1380–5.
(13) Xu, Q.; Lin, W.-C.; Petit, R. S.; Groves, J. T. *Biophysical journal* **2011**, *101*, 2731–9.
(14) Chung, I.; Akita, R.; Vandlen, R.; Toomre, D.; Schlessinger, J.; Mellman, I. *Nature* **2010**, *464*, 783–787.